Western University
Scholarship@Western

Digitized Theses | Digitized Special Collections

2011

POROUS NANOMATERIALS AS CONTROLLED DRUG DELIVERY SYSTEMS

Jeffrey Kenneth Gordon

Follow this and additional works at: https://ir.lib.uwo.ca/digitizedtheses

Recommended Citation
Gordon, Jeffrey Kenneth, "POROUS NANOMATERIALS AS CONTROLLED DRUG DELIVERY SYSTEMS" (2011). *Digitized Theses*. 3473.
https://ir.lib.uwo.ca/digitizedtheses/3473

This Thesis is brought to you for free and open access by the Digitized Special Collections at Scholarship@Western. It has been accepted for inclusion in Digitized Theses by an authorized administrator of Scholarship@Western. For more information, please contact wlswadmin@uwo.ca.

POROUS NANOMATERIALS AS CONTROLLED DRUG DELIVERY SYSTEMS

(Spine Title: Porous nanomaterials as controlled drug delivery systems)

(Thesis Format: Integrated Article)

By:

Jeffrey Kenneth Gordon

Graduate program in Engineering Science

Department of Chemical and Biochemical Engineering

A thesis submitted in partial fulfillment
of the requirements for the degree of
Master of Engineering Science

School of Graduate and Postdoctoral Studies
The University of Western Ontario
London, Ontario, Canada

© Jeffrey Kenneth Gordon 2011

Abstract

MIL-53(Fe) was synthesized by conventional electric (CE) heating, and by ultrasound (UTS) and microwave (MW) irradiation to develop rapid and energy efficient synthesis techniques. MW and UTS conditions rapidly produced small and highly crystalline materials in 10 and 7 minutes, respectively. The energy consumption of UTS and MW irradiation were less than CE heating, confirming that these two technologies are quicker, more efficient and greener alternatives to conventional synthesis methods. The use of MIL-53(Fe), MIL-101, and SBA-15 as matrices for the adsorption and *in vitro* drug delivery of acetaminophen, progesterone, and stavudine was studied. An initial burst release from both MIL-53(Fe) and MIL-101 was followed by a slow diffusion-controlled release, which occurred for up to 6 and 5 days, respectively. Complete release from SBA-15 occured in as quickly as 30 minutes as a result of rapid drug dissolution and diffusion out of the pores.

Keywords: metal-organic frameworks, microwave irradiation, ultrasound, crystallization, rapid synthesis, silica-based ordered mesoporous material, incipient wetness, drug delivery, MIL-53(Fe), MIL-101, SBA-15

Statement of Co-Authorship

Chapter 3: The original draft of this chapter was prepared by the author, and reviewed by Dr. Sohrab Rohani, who provided a series of revisions and recommendations which were incorporated into the chapter by the author. A version of this chapter is being reviewed for possible publication.

Chapter 4: The original draft of this chapter was prepared by the author, and reviewed by Dr. Sohrab Rohani, who provided a series of revisions and recommendations which were incorporated into the chapter by the author. A version of this chapter is being reviewed for possible publication.

Acknowledgments

I would sincerely like to thank my supervisor, Dr. Sohrab Rohani for the talented guidance, insight, and support he has provided me throughout all stages of this research. I am very grateful to have had the opportunity to work under his supervision.

I am also thankful to Dr. Hossein Kazemian for the guidance and assistance that he has provided me. I am deeply indebted to him for his tireless support in all areas of this research.

It is my pleasure to have worked with many colleagues during my time at the Control and Crystallization of Pharmaceuticals Laboratory (CCPL), and at the Zeolitic and Nano Materials Laboratory (ZNML). I would like to convey my gratitude to them for their contributions, support, and friendship that have made my studies an enjoyable and meaningful experience.

Special thanks are given to my parents and my brother for their support, encouragement, and guidance which have been the key to my successes in all areas of my life.

Table of Contents

Certificate of Examination ii

Abstract iii

Statement of Co-Authorship iv

Acknowledgments v

Table of Contents vi

List of Tables ix

List of Figures xii

Nomenclature/Glossary xiv

1. Introduction 1

1.1. Introduction 2

1.2. Porous Solids 3

1.3. Model Drugs 4

1.4. Thesis Objectives 6

1.5. References 6

2. Literature Review 8

2.1. Drug Delivery 9

2.1.1. Background 9

2.1.2. Particle Size and Cellular Uptake 10

2.1.3. Passive/Active Targeting 14

2.2. Metal-Organic Frameworks 17

2.2.1. Background 17

2.2.2. Synthetic Approaches 23

2.2.3. Applications 27

2.3. Mesoporous Silica Materials 30

2.3.1. Background 30

2.3.2. Synthetic Approaches 32

2.3.3. Applications 37

2.4. Conclusions 42

2.5. References 43

3. Rapid and efficient crystallization of MIL-53(Fe) by ultrasound and microwave irradiation 47

3.1. Introduction 48

3.2. Experimental Section 51

3.2.1. MIL-53(Fe) Synthesis 51

3.2.2. Experimental Design 54

3.3. Results and Discussion 56

3.4. Conclusions 64

3.5. References 65

4. MIL-53(Fe), MIL-101, and SBA-15 as potential platforms for drug delivery 68

4.1. Introduction 69

4.2. Model Drugs 74

4.3. Experimental Section 75

4.3.1. Synthesis of Materials 75

4.3.2. Drug Loading 78

4.3.3. Physicochemical Characterization 78

4.3.4. *In Vitro* Drug Release 79

4.4. Results and Discussion 80

4.5. Conclusions 91

4.6. References 92

5. Conclusions and Recommendations 94

5.1. Conclusions 95

5.1.1. Overview 95

5.1.2. Rapid and efficient crystallization of MIL-53(Fe) by ultrasound and microwave irradiation 95

5.1.3. MIL-53(Fe), MIL-101, and SBA-15 as potential platforms for drug delivery 96

5.2. Recommendations 97

5.3. References 98

Appendices 99

Appendix A 100

Appendix B 104

Curriculum Vitae 118

List of Tables

Table 3-1. Experimental design for MIL-53(Fe) synthesized by CE heating. 52

Table 3-2. Experimental design for MIL-53(Fe) synthesized by MW irradiation. 52

Table 3-3. Experimental design for MIL-53(Fe) synthesized by UTS irradiation. 53

Table 3-4. Summary of the ANOVA of the model equation for the product crystallinity as a function of MW irradiation. 54

Table 3-5. Summary of the ANOVA of the model equation for the product crystallinity as a function of CE heating. 55

Table 3-6. Summary of the ANOVA of the model equation for the product crystallinity as a function of UTS irradiation. 55

Table 3-7. Summary of the ANOVA of the model equation for the product yield as a function of MW irradiation. 55

Table 3-8. Summary of the ANOVA of the model equation for the product yield as a function of UTS irradiation. 55

Table 3-9. Summary of the ANOVA of the model equation for the product yield as a function of CE heating. 56

Table 3-10. Final model equations for product crystallinity from CE heating, MW and UTS irradiation. 60

Table 3-11. Final model equations for product yield from CE heating, MW and UTS irradiation. 60

Table 4-1. Structural formulas of the model drugs, the wavelengths used for quantification and the media used for *in vitro* drug release experiments. 75

Table 4-2. BET surface area (S_{BET}), mesopore volume (V_{mes}) and drug loading information of drug-free and drug-loaded MIL-53(Fe), MIL-101 and SBA-15 samples. 81

Table B-1. UV absorbance measurements and sample data used to determine the cumulative release (%) of acetaminophen from MIL-53(Fe) after each time interval (trial #1). 106

Table B-2. UV absorbance measurements and sample data used to determine the cumulative release (%) of acetaminophen from MIL-53(Fe) after each time interval (trial #2). 107

Table B-3. UV absorbance measurements and sample data used to determine the cumulative release (%) of progesterone from MIL-53(Fe) after each time interval (trial #1). 108

Table B-4. UV absorbance measurements and sample data used to determine the cumulative release (%) of progesterone from MIL-53(Fe) after each time interval (trial #2). 109

Table B-5. UV absorbance measurements and sample data used to determine the cumulative release (%) of stavudine from MIL-53(Fe) after each time interval (trial #1). 110

Table B-6. UV absorbance measurements and sample data used to determine the cumulative release (%) of progesterone from MIL-53(Fe) after each time interval (trial #2). 111

Table B-7. UV absorbance measurements and sample data used to determine the cumulative release (%) of acetaminophen from MIL-101 after each time interval (trial #1). 111

Table B-8. UV absorbance measurements and sample data used to determine the cumulative release (%) of acetaminophen from MIL-101 after each time interval (trial #2). 112

Table B-9. UV absorbance measurements and sample data used to determine the cumulative release (%) of progesterone from MIL-101 after each time interval (trial #1). 112

Table B-10. UV absorbance measurements and sample data used to determine the cumulative release (%) of progesterone from MIL-101 after each time interval (trial #2). 113

Table B-11. UV absorbance measurements and sample data used to determine the cumulative release (%) of stavudine from MIL-101 after each time interval (trial #1). 113

Table B-12. UV absorbance measurements and sample data used to determine the cumulative release (%) of stavudine from MIL-101 after each time interval (trial #2). 114

Table B-13. UV absorbance measurements and sample data used to determine the cumulative release (%) of acetaminophen from SBA-15 after each time interval (trial #1). 114

Table B-14. UV absorbance measurements and sample data used to determine the cumulative release (%) of acetaminophen from SBA-15 after each time interval (trial #2). 115

Table B-15. UV absorbance measurements and sample data used to determine the cumulative release (%) of progesterone from SBA-15 after each time interval (trial #1)..... 115

Table B-16. UV absorbance measurements and sample data used to determine the cumulative release (%) of progesterone from SBA-15 after each time interval (trial #2)..... 116

Table B-17. UV absorbance measurements and sample data used to determine the cumulative release (%) of stavudine from SBA-15 after each time interval (trial #1)..... 116

Table B-18. UV absorbance measurements and sample data used to determine the cumulative release (%) of stavudine from SBA-15 after each time interval (trial #2)..... 117

List of Figures

Figure 1-1. Molecular structure of stavudine. 5

Figure 1-2. Molecular structure of acetaminophen. 5

Figure 1-3. Molecular structure of progesterone. 6

Figure 2-1. Schematic of the known pathways for intracellular uptake of nanoparticles. 14

Figure 2-2. Schematic representation of different mechanisms by which nanocarriers can deliver drugs to tumours. Polymeric nanoparticles are shown as representative nanocarriers (circles). 15

Figure 2-3. Classes of porous structures based on spatial dimensions. 18

Figure 2-4. The MOF-5 structure and its topology. 21

Figure 2-5. Example of SBUs from carboxylate MOFs. 22

Figure 2-6. Formation of mesoporous materials by structure-directing agents: a) true liquid-crystal template mechanism, b) cooperative liquid-crystal template mechanism. 34

Figure 2-7. Interactions between the inorganic species and the head group of the surfactant with consideration of the possible synthetic pathway in acidic, basic, or neutral media. Electrostatic: S^+I^-, $S^+X^-I^+$, $S^-M^+I^-$, S^-I^+; through hydrogen bonds: S^0I^0/N^0I^0, $S^0(XI)^0$. 37

Figure 3-1. Typical XRPD patterns of fully crystallized MIL-53(Fe) synthesized by a) CE for 18 h at 150°C, b) MW for 30 min at 150°C, and c) UTS for 15 min at 60% power. 57

Figure 3-2. Typical SEM images of fully crystallized MIL-53(Fe) synthesized by a) CE for 18 h at 150°C (25 μm scale), b) MW for 30 min at 150°C (5 μm scale), and c) UTS for 15 min at 60% power (10 μm scale). 58

Figure 3-3. SEM image of MIL-53(Fe) synthesized by UTS for 7 min at 40% power. 62

Figure 3-4. XRPD patterns of MIL-53(Fe) synthesized by a) UTS for 7 min at 40% power, and b) MW for 10 min at 150°C. 62

Figure 4-1. DSC thermograms of acetaminophen, progesterone, and stavudine in their crystallized forms and of drug-loaded MIL-53(Fe), MIL-101, and SBA-15 materials. 83

Figure 4-2. XRPD patterns of drug-free and drug-loaded MIL-53(Fe), MIL-101, and SBA-15 materials. 85

Figure 4-3. Cumulative release of acetaminophen, progesterone, and stavudine from MIL-53(Fe) in PBS at 37°C. The depicted results are mean values (*n* = *2*). 87

Figure 4-4. Cumulative release of acetaminophen, progesterone, and stavudine from MIL-101 in PBS at 37°C. The depicted results are mean values (*n* = *2*). 87

Figure 4-5. Cumulative release of acetaminophen, progesterone, and stavudine from SBA-15 in PBS + 0.5% SDS at 37°C. The depicted results are mean values (*n* = *2*). 88

Figure A-1. XRPD pattern of acetaminophen. 100

Figure A-2. XRPD pattern of progesterone. 101

Figure A-3. XRPD pattern of stavudine. 101

Figure A-4. Nitrogen adsorption isotherm of MIL-53(Fe) at 77 K, degassed at 323 K. 102

Figure A-5. Nitrogen adsorption isotherm of MIL-101 at 77 K, degassed at 323 K. 102

Figure A-6. Nitrogen adsorption isotherm of SBA-15 at 77 K, degassed at 323 K. 103

Figure B-1. Calibration curve of acetaminophen (λ = 244 nm) in PBS solution. The depicted results are mean values (*n* = *3*). 104

Figure B-2. Calibration curve of progesterone (λ = 245 nm) in PBS + 0.5% SDS solution. The depicted results are mean values (*n* = *3*). 105

Figure B-3. Calibration curve of stavudine (λ = 266 nm) in PBS solution. The depicted results are mean values (*n* = *3*). 105

Nomenclature/Glossary

0D	Zero-Dimensional
1D	One-Dimensional
2D	Two-Dimensional
3D	Three-Dimensional
A	Ampere
AIDS	Acquired Immunodeficiency Syndrome
ANOVA	Analysis of Variance
AZT-TP	Azidothymidine Triphosphate
BET	Brunauer, Emmett, and Teller
CE	Conventional Electric
CMC	Critical Micelle-Concentration
CSA	Co-Operative Self-Assembly
CTAB	Cetyltrimethylammoniumbromide
DDS	Drug Delivery System
DFT	Density Functional Theory
DMF	*N,N*-Dimethylformamide
DSC	Differential Scanning Calorimetry
E	Energy (J)
EGF	Epidermal Growth Factor
EO	Ethylene Oxide
EPR	Enhanced Permeability and Retention
FDA	Food and Drug Administration
FR	Folate Receptor
H_2BDC	1,4-Benzenedicarboxylic Acid

HF	Hydrofluoric Acid
HIV	Human Immunodeficiency Virus
I	Current (A)
IRMOF-1	An isoreticular MOF
J	Joule
kJ	Kilojoule
LCT	Liquid Crystal Templating
LED	Light-Emitting Diode
MCM	Mobil Crystalline Material
MCM-41	A highly ordered Silica-Based Ordered Mesoporous Material
MDR	Multi-Drug Resistance
MIL	Materials of Institute Lavoisier
MIL-101	A rigid mesoporous Metal-Organic Framework
MIL-53(Fe)	A flexible microporous Metal-Organic Framework
MOF	Metal-Organic Framework
M-O-M	Metal-Organic-Metal
MW	Microwave
NRTI	Nucleoside Reverse Transcriptase Inhibitor
P	Power (W)
P-123	Pluronic 123
PBS	Phosphate Buffered Saline
PEG	Polyethylene Glycol
PEO	Polyethylene Oxide
PLGA	Poly(DL-lactide-co-glycolide)acid
PPO	Polypropylene Oxide

PTFE	Polytetrafluoroethylene
RC	Relative Crystallinity
RES	Reticuloendothelial System
RME	Receptor-Mediated Endocytosis
SBA	Santa Barbara Amorphous
SBA-15	A highly ordered SMM
SBU	Secondary Building Unit
SDA	Structure-Directing Agent
SDS	Sodium Dodecyl Sulphate
SEM	Scanning Electron Microscopy
SGF	Simulated Gastric Fluid
SMM	Silica-Based Ordered Mesoporous Material
t	Time (s)
TEOS	Tetraethyl Orthosilicate
TfR	Transferrin Receptor
TGA	Thermogravimetric Analysis
TMAOH	Tetramethylammonium Hydroxide
USP	US Pharmacopeia
UTS	Ultrasound
UV	Ultraviolet
V	Voltage
VOC	Volatile Organic Compound
W	Watt
XRPD	X-Ray Powder Diffraction
λ	Wavelength

1. Introduction

1.1. Introduction

In the 1990s there was a significant increase in the number of new drugs having larger molecular sizes, higher dose sensitivities, and poorer stabilities in biological environments.[1] The difficulties associated with conventional drug administration has resulted in a push towards the development of efficient encapsulation and controlled-release technologies, capable of improving clinical efficacy and patient compliance, decreasing the frequency and cost of administering drugs, and extending product life. Drug delivery now represents one of the fastest growing segments in the pharmaceutical industry, with approximately 10% annual growth.[1]

Drug delivery is achieved by encapsulating pharmaceuticals within a porous compound. Three types of porous materials exist, including organic, inorganic, and coordination polymers.[2] Extensive research has been dedicated towards using various types of organic nanoparticles as drug delivery systems (DDSs). Although these systems have several advantages and represent the majority of DDSs now approved for use by the Food and Drug Administration (FDA), several limitations affect their applicability as DDSs. Liposomes and micelles suffer from poor stability that limits both their route of administration and shelf life. It is also very difficult to develop micelles and liposomes that release therapeutic agents in a controlled and sustained manner. The degradation by-products of synthetic polymers pose toxicity problems, and the lack of control over monomer purity for natural polymers, such as chitosan, leads to a lack of reproducibility in their release profiles. Dendrimers suffer from low blood stability, and are quickly eliminated from the body by the kidneys and liver.[1]

These limitations have led researchers to search for alternative systems with longer half-lives and higher therapeutic efficacies. Recent research on metal-organic framework (MOF) materials and inorganic silica-based ordered mesoporous materials (SMMs) has revealed that these two classes of materials are very promising in the field of drug delivery. Their high porosities and surface areas have afforded these materials applications not only in the field of controlled drug delivery, but in many other areas of potential economic and environmental importance as well.

1.2. Porous Solids

In this study, two MOF materials and an SMM were synthesized, characterized, and investigated as DDSs. The two MOF materials that were studied are MIL-53(Fe) and MIL-101 (MIL = Materials of Institute Lavoisier). MIL-53(Fe) is a microporous iron(III) benzenedicarboxylate MOF, which was selected because of its flexible structure. It is capable of opening and closing its pores to maximize host-guest molecule interactions, thus prolonging drug delivery. MIL-53 has the formula $M^{III}(OH)\bullet(O_2C\text{-}C_6H_4\text{-}CO_2)\bullet H_2O$ ($M = Al^{3+}$, Cr^{3+} or Fe^{3+}).[5] MIL-101 was selected because of its high drug loadings. MIL-101 is a rigid chromium benzenedicarboxylate MOF, possessing large mesoporous cages (~29 and 34 Å). MIL-101 has the formula $Cr_3OX(H_2O)_2[(O_2C)\text{-}C_6H_4\text{-}(CO_2)]_3\cdot nH_2O$ (where X = F,OH and n is ~25).[6] The SMM that was selected in this study is SBA-15 (SBA = Santa Barbara Amorphous). It has a hexagonally-ordered array of tunable pores which can range in diameter from 5 to 30 nm. It has a high surface area, a large pore

volume, and a silanol-containing surface capable of being functionalized, thus enabling high drug loadings and release profiles which can be highly modified.[7]

1.3. Model Drugs

The drug release from each of these materials was investigated using three drug molecules: stavudine, acetaminophen, and progesterone. These molecules were selected because of their different physicochemical properties. Stavudine is a nucleoside reverse transcriptase inhibitor (NRTI) used for the treatment of human immunodeficiency virus (HIV) (Figure 1-1). It was approved for use by the FDA in 1994. Ever since acquired immunodeficiency syndrome (AIDS) was discovered in 1981, it has remained one of the greatest public health challenges. Every year more than 2.5 million people become infected with human immunodeficiency virus (HIV), resulting in the number of people living with this virus continuing to grow. Seven NRTIs have been approved for use, but in general they have limited stabilities and poor bioavailabilities. The bioavailability of an orally administered drug can be affected by incomplete absorption and first-pass metabolism. As an NRTI, stavudine has a reasonably high bioavailability of about 80%. However, its half-life in systemic circulation is about 1 to 1.6 hours, necessitating frequent doses which results in severe dose-dependent side effects.[8] For this reason, stavudine is an ideal candidate for sustained drug release.

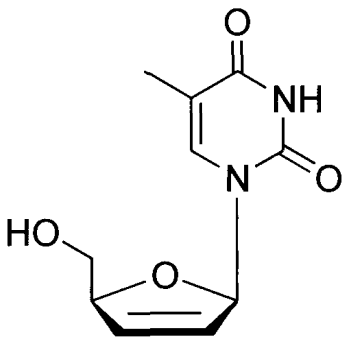

Figure 1-1. Molecular structure of stavudine.

Acetaminophen (also known as paracetamol) is an analgesic which distributes rapidly and evenly throughout most tissues (Figure 1-2). Like stavudine, it is orally administered, and has a bioavailability ranging from 70 to 90% and a short plasma half-life ranging from 1.9 to 2.5 hours.[9]

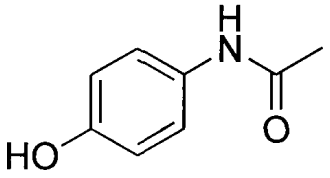

Figure 1-2. Molecular structure of acetaminophen.

Progesterone is a steroid hormone belonging to the progestogen class that naturally occurs in both males and females (Figure 1-3). It is administered to individuals with a long-term decline of natural levels in the body, as well as to patients with acute situations. Like all steroid hormones it is hydrophobic, therefore, when taken orally it has a poor bioavailability and a half-life upwards of 50 hours.[10]

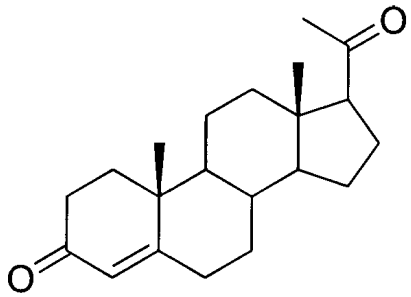

Figure 1-3. Molecular structure of progesterone.

1.4. Thesis Objectives

This thesis in general aims to investigate the drug release profiles of three important porous solids: MIL-53(Fe), MIL-101, and SBA-15. The objective will be to optimize the drug incorporation into each of these materials and obtain controlled, sustained release of stavudine, acetaminophen, and progesterone. The release profiles of each of the materials, as well as each of the drugs will be compared. MIL-53(Fe) will also be synthesized by three different methods, and the operating conditions of each method will be varied in an attempt to optimize the reaction conditions to produce small and homogeneous crystals while minimizing energy consumption.

1.5. References

(1) Barbe, C.; Bartlett, J.; Kong, L. G.; Finnie, K.; Lin, H. Q.; Larkin, M.; Calleja, S.; Bush, A.; Calleja, G. *Adv. Mater.* **2004**, *16*, 1959-1966.

(2) Kitagawa, S.; Kitaura, R.; Noro, S. *Angew. Chem. Int. Ed.* **2004**, *43*, 2334-2375.

(3) Meek, S. T.; Greathouse, J. A.; Allendorf, M. D. *Adv. Mater.* **2011**, *23*, 249-267.

(4) Hoffmann, F.; Cornelius, M.; Morell, J.; Fröba, M. *Angew. Chem. Int. Ed.* **2006**, *45*, 3216-3251.

(5) Horcajada, P.; Serre, C.; Maurin, G.; Ramsahye, N. A.; Balas, F.; Vallet-Regí, M.; Sebban, M.; Taulelle, F.; Férey, G. *J. Am. Chem. Soc.* **2008**, *130*, 6774-6780.

(6) Férey, C.; Mellot-Draznieks, C.; Serre, C.; Millange, F.; Dutour, J.; Surblé, S.; Margiolaki, I. *Science* **2005**, *309*, 2040-2042.

(7) Selvam, P.; Krishna, N. V.; Viswanathan, B. *J. Indian Inst. Sci.* **2010**, *90*, 271-285.

(8) Khalil, N. M.; Carraro, E.; Cotica, L. F.; Mainardes, R. M. *Expert Opin. Drug Deliv.* **2011**, *8*, 95-112.

(9) Forrest, J. A. H.; Clements, J. A.; Prescott, L. F. *Clin. Pharmacokinet.* **1982**, *7*, 93-107.

(10) Pike, M. C.; Spicer, D. V.; Dahmoush, L.; Press, M. F. *Epidemiol. Rev.* **1993**, *15*, 17-35.

2. Literature Review

2.1. Drug Delivery

2.1.1. Background

Since liposomes were first described in the 1960s and proposed as carriers of drugs and proteins for treating disease, there has been a significant development in the utilization of drug carriers for delivery.[1] So far, over two dozen nanotechnology-based therapeutic products have been approved by the FDA for clinical use, and more are currently in clinical trials. The pursuit of drug delivery systems (DDSs) can be justified by their ability to improve the therapeutic and pharmacological properties of conventional free drugs.[2] These systems are designed to alter the pharmacokinetics and biodistribution of drugs, and/or to function as sustained release systems. The ultimate goal is to improve the therapeutic effect of the entrapped drug by enhancing its delivery to, or uptake by, target cells and/or reducing the toxicity of the drug to healthy tissue.[3] Problems exhibited by free drugs that can be improved by these systems include (1) poor solubility, (2) tissue damage on extravasation, (3) rapid breakdown of the drug (4) rapid drug clearance, and (5) lack of selectivity for target tissues.[2] The first problem is explained by the inherent difficulty of achieving convenient pharmaceutical formats. Hydrophobic drugs suffer from poor dissolution in aqueous media, and the use of solubilizers as excipients are associated with side effects. Certain DDSs such as lipid micelles, liposomes, and MOFs provide both hydrophobic and hydrophilic environments, enhancing solubility. Just as importantly, drug levels are continuously maintained in a therapeutically desirable range, reducing adverse side effects. The second problem - tissue damage caused by inadvertent extravasation of cytotoxic drugs - can be reduced or eliminated by regulated drug release from the DDS. The third and fourth problems of conventional therapy require that higher

doses be administered, which may cause side effects if the drug suffers from a lack of selectivity for the target tissue. DDSs protect drugs from premature degradation under physiological pH, thus, lowering the required dose. DDSs can also substantially alter the pharmacokinetics of drugs and reduce clearance by the kidneys, especially for small molecules. By decreasing the number of required dosages and possibly implementing less invasive dosing, patient compliance becomes improved resulting in a higher therapeutic effect. Finally, the distribution of drugs not only to diseased tissue but also to normal tissues leads to side effects that reduce the amount of drug that can be administered. However, limiting the dosage to prevent side effects also results in lower concentrations in target tissues, lowering the therapeutic effect. By site-specific targeting, DDSs can increase drug concentrations in diseased tissues, improving drug specificity and decreasing harmful side effects.[2]

2.1.2. Particle Size and Cellular Uptake

Nanomaterials have been used for a number of applications, including catalysis, gas adsorption/separation/storage, electronics, lithographic techniques, materials engineering, and biomedicine. Their applications in the field of biomedicine include drug delivery, gene delivery, cancer therapy, and as biosensors.[4] Their attractiveness for biomedicine is based on their unique properties, including large specific surface areas, crystallinity, surface chemistry, quantum properties, ability to adsorb and carry other compounds, and size.[3] Particle size is an extremely important factor controlling the performance and function of DDSs. Smaller particles have increased dissolution rates due to their greater

surface area-to-volume ratios, enabling them to overcome solubility-limited bioavailability. They also have a greater cellular uptake, reducing the risk of being rapidly cleared from the body by the liver or spleen and minimizing their uptake by the reticuloendothelial system (RES). In fact, 100 nm size particles exhibit 15-250-fold greater uptake efficiencies than small microparticles (1-10 μm). The bioavailability and blood circulation time are also strongly dependent on size. Particles with diameters less than 10 nm are rapidly cleared from the body through extravasation of capillary fenestrations and by the kidneys;[5] particles with diameters ranging from 10 to 70 nm are able to enter into very small capillaries;[6] particles with diameters ranging from 70 to 200 nm have the longest circulation times;[7] and particles with diameters greater than 200 nm are typically sequestered by the spleen, resulting in eventual removal by phagocytes.[8]

However, many challenges must be overcome if the application of nanotechnology in the field of drug delivery is to result in improved therapies. A critically important process for nanoparticles to become effective in their therapeutic functions is that they can easily enter target cells. Yet, this inherent requirement is also a cause of major concern that may lead to potential toxic effects. Compared to traditional medicines, nanoparticles easily enter cells, however this could produce adverse effects due to the small size, large surface area, and/or high reactivity of some nanoparticles.[4] Biodegradable and biocompatible DDSs are needed to ensure that (1) the drug is released when the formulation enters the cell, and (2) the nanoparticle degradation products are not toxic to the cell. The Royal Society and Royal Academy of Engineering 2004, has proposed that only particles with sizes $\leq$ 100 nm can be defined as nanoparticles.[3] Nanoparticles this small can readily translocate among different cells, tissues, and organs, potentially posing a great risk to

human health.[4] Thus, a fundamental understanding of the mechanisms governing cellular uptake is an important step towards understanding the biological fate of nanoparticles.

Cell membranes are somewhat permeable, allowing only small molecules to pass through into the cell. Oxygen, carbon dioxide, water, and small hydrophobic or nonpolar molecules are driven by their concentration gradients to freely diffuse through the membrane. Ions and amino acids are actively transported across the membrane by integral membrane protein pumps or ion channels.[4] DDSs, on the other hand, must be shuttled across the cell membrane by a process called endocytosis. Typically, larger DDSs will remain outside cells where they release their payloads to create high extracellular drug concentrations, while smaller systems will be endocytosed directly. In this process the cell internalizes objects by enclosing a portion of the plasma membrane around the object, which pinches off from the rest of the membrane to form a vesicle. Subsequent to their uptake, DDSs are transported from early endosomes to sorting endosomes where they are either exported from the cell or transported to secondary endosomes/lysosomes. From here the DDSs will have one of two fates: either they are degraded and the activity of the encapsulated drug is diminished, or they escape into the cytoplasm and release their payloads to produce their desired therapeutic effect.[9]

Several different endocytotic processes exist, including phagocytosis, pinocytosis, receptor-mediated endocytsis, and caveolae-dependent or clathrin-mediated endocytosis (Figure 2-1). Particles with diameters >750 nm are internalized by phagocytosis, a process mainly conducted by specialized cells such as monocytes, macrophages, and neutrophils. Almost all cell types can perform pinocytosis or macropinocytosis to internalize particles ranging from a few to several hundred nanometers in diameter. In

clathrin-mediated endocytosis the particles are deposited in small vesicles (usually <100 nm in diameter) which eventually fuse with early endosomes in the cytosol. The most important cellular uptake process for nanoparticles by endothelial cells is caveolae-mediated endocytosis, in which vesicles 50 to 80 nm in size are formed.[4] Each type of nanoparticle has a preferred type of entry into the cell, which is dependent on such factors as size, shape, surface charge and functionalization. For example, Edetsberger at al.[10] showed that nanoparticles about 20 nm in diameter were sufficiently small that endocytosis did not contribute to cellular uptake. In another study, poly(DL-lactide-co-glycolide)acid (PLGA) nanoparticles were ingested by endocytosis and released into the cytosol intact, resulting in cytoplasmic delivery of the encapsulated drug.[11, 12] The escape from the endosomes was attributed to a change in surface charge of the PLGA nanoparticles from negative to positive. This hypothesis was supported by data obtained with negatively charged polystyrene nanoparticles, which did not escape from the endosomes.[3]

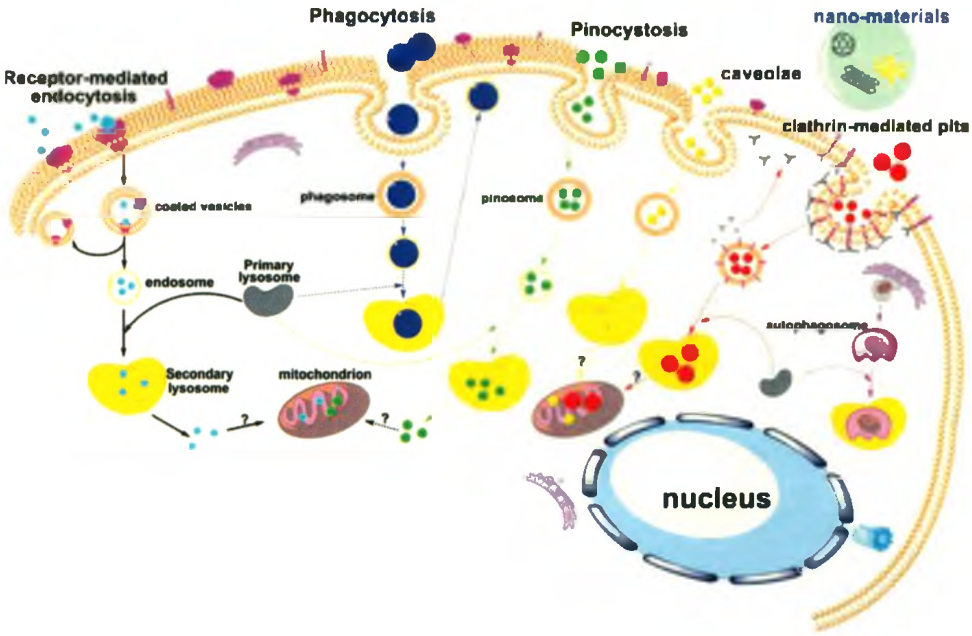

Figure 2-1. Schematic of the known pathways for intracellular uptake of nanoparticles.[4]

2.1.3. Passive/Active Targeting

In the domain of drug delivery, DDSs can be designed to either passively or actively target the diseased site. Passive targeting relies on the extravasation of the particles into the diseased tissue by the enhanced permeability and retention (EPR) effect. The escape of DDSs from blood circulation is restricted to sites where the capillaries have open fenestrations.[13] In certain pathological conditions the endothelial barrier may become perturbed, increasing the permeability of the tissue vasculature and allowing DDSs (which are normally excluded) to extravasate and accumulate in the tissue interstitial space. In particular, DDSs can enter into tumour tissues and localize there by the EPR effect as a result of leaky blood vessels, which may form gaps as large as 600 to 800 nm between adjacent endothelial cells. This common feature of tumours is a result of angiogenesis, which is a process involving the recruitment of new blood vessels to the

tumour to meet its growing demands of oxygen and nutrients. Tumours also have impaired lymphatic drainage, so the accumulated DDSs are retained (Figure 2-2).[2]

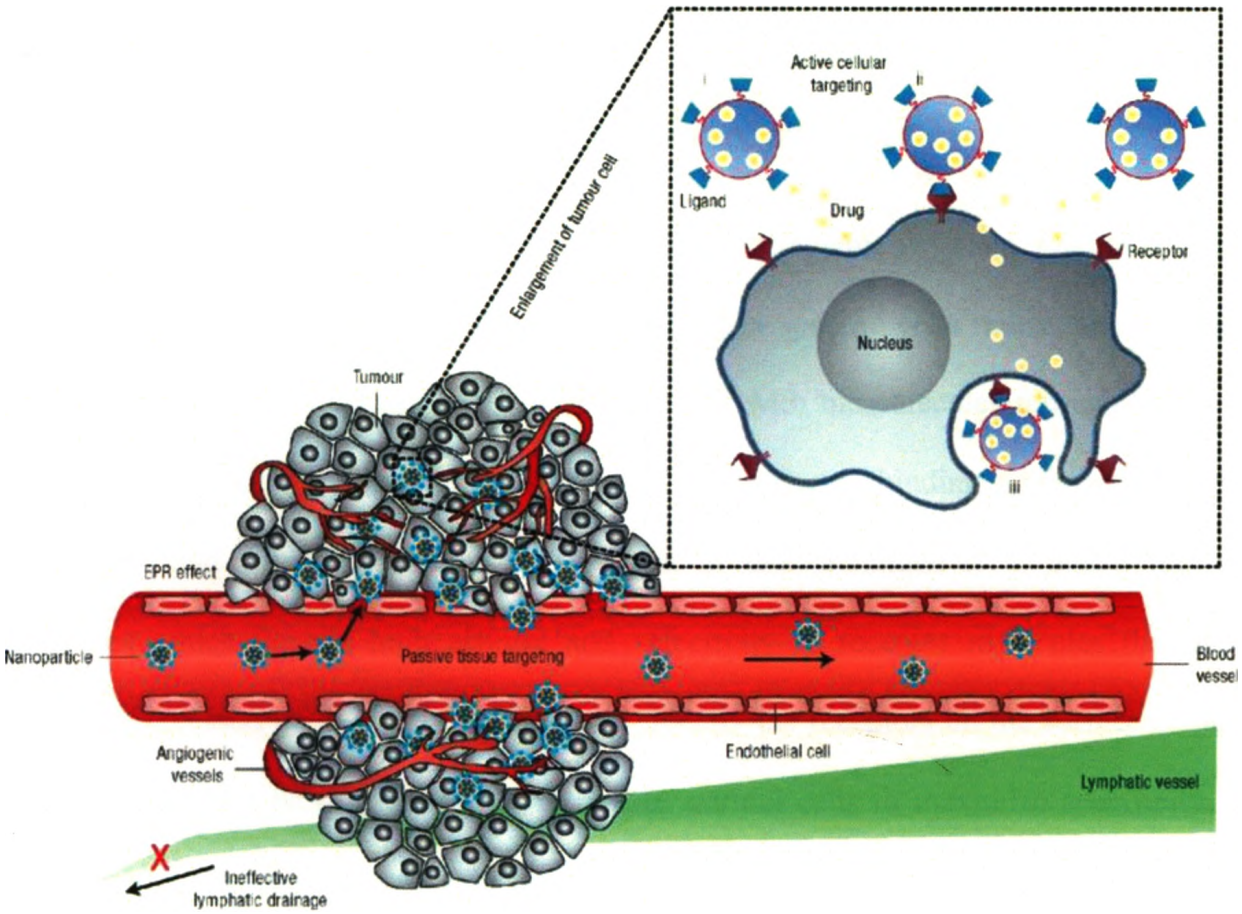

Figure 2-2. Schematic representation of different mechanisms by which nanocarriers can deliver drugs to tumours. Polymeric nanoparticles are shown as representative nanocarriers (circles).[14]

DDSs relying on the EPR effect require long half-lives for optimal accumulation of the drug in the diseased tissue. Once the DDS has accumulated then the drug must be released at a rate that maintains the concentration within the therapeutic range for sufficient periods of time. In tumours, for example, the drug concentration should be maintained within the therapeutic range for a period of at least several hours.[2] Although

passive targeting is the conventional therapeutic approach for treating disease, it suffers from several limitations. Especially in the case of chemotherapy, the lack of control of this process may induce multiple-drug resistance (MDR) whereby cancer cells become resistant to one or more drugs. Furthermore, the EPR effect may not be exhibited by all tumours, and the permeability of vessels may vary significantly throughout a single tumour, limiting the ability of DDSs to extravasate into the tissue.[14]

Active targeting can overcome these limitations. As the name suggests, this process is characterized by the ability of DDSs to actively target specific cells rather than tissues. This is accomplished by functionalizing the surface with biomolecules through various techniques, including physical adsorption, electrostatic binding, complementary recognition and covalent coupling.[9] The idea of this technique is to attach ligand molecules which have a high affinity and selectivity to receptor molecules that are uniquely expressed on the target cell surface. Ideally the receptors on the surface of the target cells should be overexpressed relative to normal cells to maximize specificity.[14] The nanoparticles can either release their contents in close proximity to the target cells, attach to the membrane of the cell through ligand-receptor interactions and act as an extracellular sustained-release drug depot, or internalize into the cell by receptor-mediated endocytosis (RME) (Figure 2-2 inset).[14]

Internalization leads to higher intracellular drug concentrations and increased therapeutic activity. DDSs can even be modified to target specific organelles within the cell. For example, anionic particles will usually remain in lysosomes, while cationic particles will concentrate in the cytoplasm and within mitochondria.[9] There are many different types of molecules that can be used as targeting ligands, including antibodies, aptamers, growth

factors or vitamins, and peptides. Cancer cells are most commonly targeted by growth factor or vitamin interactions, since they overexpress receptors for nutrition to maintain their fast-growing metabolism. An example of receptors which are overexpressed on the surface of some cancer cells which have been used for targeting include the epidermal growth factor (EGF) receptor, the folate receptor (FR), and the transferrin receptor (TfR). Functionalization of DDS surfaces with EGF, folate, and Tf has improved intracellular delivery of encapsulated drugs and therapeutic outcome in animal models.[14]

2.2. Metal-Organic Frameworks

2.2.1. Background

Since this class of porous solids emerged as a new domain of research in the early 1990s, remarkable advancements have been made in their chemistries. Before becoming known as MOFs they were more generally referred to as coordination polymers. This term correctly identifies that these materials contain small clusters of inorganic polyhedra which are connected together by ligand monomers through coordination bonds, however it is a somewhat simplistic definition that does not consider the final structure or morphology of the materials. The discovery that these hybrid solids contain a large dimensionality, forming either chains (1D), layers (2D) or frameworks (3D) led to their classification as MOFs.[15] This classification defines them as materials with strong bonding and a high degree of robustness, linking units that are available for modification, and geometrically well-defined structures.[16]

In general, the porosity of every type of porous structure belongs to one of the following four categories: 0D cavities, 1D channels, 2D layers, or 3D intersecting channels (Figure 2-3). 0D cavities (dots) are completely enclosed by surrounding wall molecules, preventing entrapped guest molecules from escaping. MOFs can be designed to have channels, layers, or intersecting channels, each of which can accommodate and exchange guest molecules.[17]

a) Dots (0D cavity)

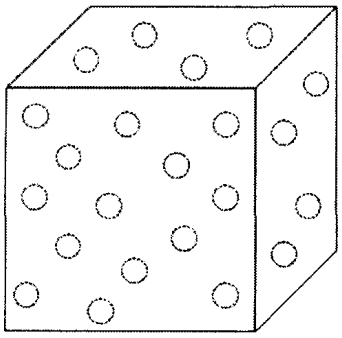

b) Channels (1D space)

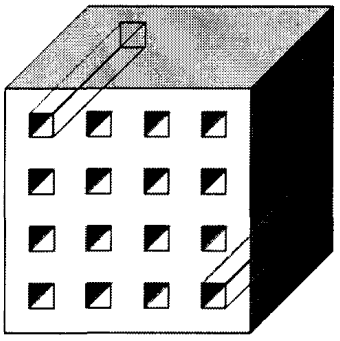

c) Layers (2D space)

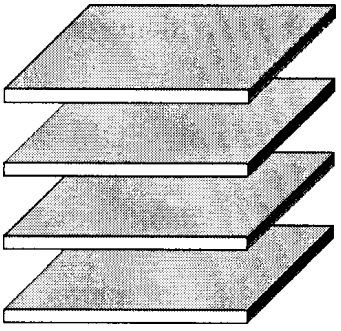

d) Intersecting channels (3D space)

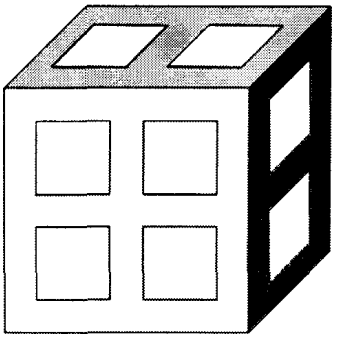

Figure 2-3. Classes of porous structures based on spatial dimensions.[17]

This chemical versatility that MOFs provide is the sole reason why they continue to receive so much interest from various domains in the scientific community, including physics, chemistry and materials science. Before they were discovered, there existed two types of porous materials – organic and inorganic materials. MOFs combine both organic and inorganic groups within their structures, thus they represent a new type of porous material referred to as hybrid solids. The two largest subclasses of inorganic solids are the aluminophosphates and aluminosilicates. Zeolites are members of the aluminosilicate subclass, whose structures are composed of interconnected tunnels or cages within which water molecules or metal ions are inserted. Their porosity is provided by the elimination of these species from the pores. The aluminophosphates are composed of tetrahedral Al^{3+} and P^{5+} ions linked by corner-sharing oxygen atoms.[17] Structurally, MOFs are very similar to inorganic porous solids in that both of their three-dimensional skeletons are composed of secondary building units (SBUs). In place of the inorganic tetrahedral species found in the structure of inorganic porous solids, though, MOFs contain organic linker molecules. The properties of MOFs also resemble those of zeolites, such as the adsorption of gases and shape-selective catalysis of both materials. However, MOFs offer a much wider range of structures and properties such as high porosity, pore dimensionality, and functionality of metal ions and organic linkers.[18]

The MOF structure contains two central components – inorganic metal centers and organic linkers. The two characteristics of the metal centers and linkers which are important for defining the final structure of the framework are the number and orientation of their binding sites (coordination numbers and coordination geometries). MOFs can be constructed from a great variety of transition metal ions, with coordination numbers

ranging from two to seven. Many different coordination geometries may be formed as a result of this large selection of metals, including linear, T- or Y-shaped, tetrahedral, square-planar, square-pyramidal, trigonal-bipyramidal, octahedral, trigonal-prismatic, and pentagonal-bipyramidal.[17] Furthermore, considering the large number of organic linkers which can be associated with the metals and the different possible linkages, binding strength and directionality, the number of possible combinations is seemingly infinite. Consequently, many different MOF framework topologies exist, forming either microporous (pore diameter $\leq$2 nm) or mesoporous (pore diameter between 2-50 nm) channels. The existence of organic and inorganic species in the MOF structure also presents an opportunity to incorporate both hydrophilic and hydrophobic parts within the pores, thus allowing for control over the adsorption properties.[15]

Owing to the infinite number of possible combinations between inorganic and organic parts, soon after the discovery of MOFs a rationalization became necessary for organizing the structures into classes. The inorganic clusters that are linked to the organic component were observed to resemble the shapes of simple geometric figures (diamonds, sodalites, etc.). These became known as secondary building units (SBUs) which, by sharing of vertices through the organic linkers, build up the final solid.[15] The majority of MOFs, including the MIL family (MIL = Materials of Institute Lavoisier), incorporate a carboxylate functionality to chelate the metal ions and lock them into rigid metal-oxygen-carbon clusters. The first carboxylate MOFs designed to resemble this structure were MOF-2 and MOF-5. The MOF-5 structure is composed of octahedral SBUs, each of which is formed by four ZnO_4 tetrahedra. These SBUs are joined together by benzene

dicarboxylate linkers to give an extended 3D cubic framework (Figure 2-4) with an exceptionally high porosity and stability.[19]

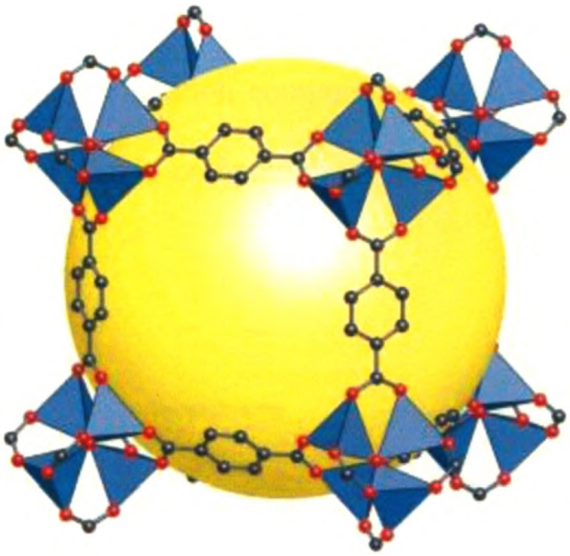

Figure 2-4. The MOF-5 structure and its topology.[19]

Figure 2-5 shows some of the SBUs that are formed in carboxylate MOFs. The inorganic units are defined by metal-oxygen polyhedra (such as the ZnO_4 tetrahedra in MOF-5). The carboxylate atoms that are bound to these polyhedra define the vertices of the SBUs, which are held together by the organic linkers (such as the benzene dicarboxylate linkers in MOF-5).[19]

Porous coordination compounds in general can be further classified into three categories, called generations. First generation compounds have a microporous framework held together only by guest molecules, and which collapse irreversibly upon guest removal. Second generation compounds have stable and robust porous frameworks which exhibit permanent porosity when guest molecules are evacuated from the pores. Third generation

compounds have flexible frameworks which respond to external stimuli (light, temperature, pressure, electric or magnetic field, guest molecules, etc.) and change their structures reversibly. The stimulus can induce either an expansion or a contraction of the cell volume and induce movements larger than 10 Å. Most inorganic porous solids fall under the category of second generation compounds. MOFs on the other hand, can be rigid and robust second generation compounds as well as highly flexible and dynamic third generation compounds.[17]

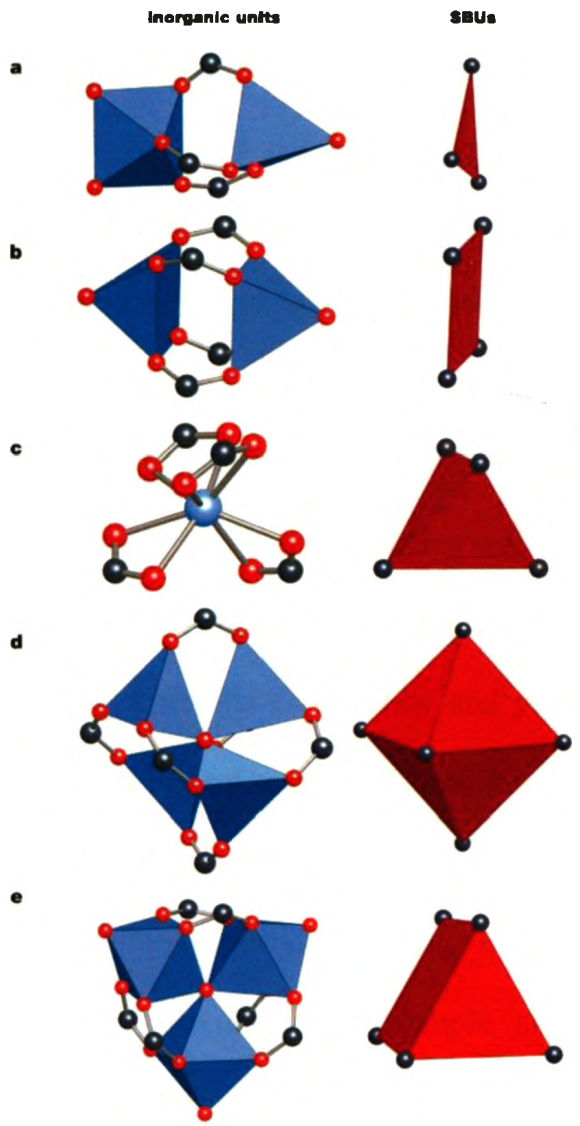

Figure 2-5. Examples of SBUs from carboxylate MOFs.[19]

2.2.2. Synthetic Approaches

Successful synthesis of an MOF requires the reaction of a bridging ligand with a metal ion having more than one vacant or labile site.[20] Syntheses are typically carried out under solvothermal conditions (> 100°C) from a mixture containing the ligand and metal salt for 12-48 h.[21] Most commonly used solvents include water, alcohols, dialkyl formamides, and pyridine.[15] Some of the more labile metal ions which are most often used include Cu^{+}, Cu^{2+}, Ag^{+}, Cd^{2+}, Zn^{2+}, Co^{2+} and Ni^{2+}. However, one of the difficulties in using labile metal ions is that they do not have a strong preference for a given geometry, leading to a lack of control and predictability over the structure of the network obtained. Flexibility in a bridging ligand having a number of possible conformations can also contribute to this problem. Another difficulty is that a single metal coordination geometry can propagate into more than one type of framework topology.[20] For example, more than 100 different topologies are possible for linking tetrahedral building blocks together.[19] Of course, during synthesis there are other important structure-determining factors affecting product crystallinity and yield, including the pH, concentration, solvent polarity, and temperature. It has been shown that only subtle changes in these parameters can lead to significant changes in product crystallinity and yields, or the formation of entirely new phases.[16] Therefore, a careful selection of reaction conditions is important. Temperature is an especially important factor. Under solvothermal conditions the dielectric properties of the solution change, leading to weakened intermolecular interactions between the solvent molecules. For example, at 180°C the pH of water becomes 5.5, thus, an extrapolation of the conditions applied at room temperature is not valid since the chemistry of the solution is not the same at elevated temperatures. An

excellent example of the temperature influence was demonstrated by the synthesis of cobalt(II) succinates between room temperature and 250°C. Over this temperature range seven different materials were synthesized. As the temperature increased the number of coordinated water molecules per cobalt atom decreased (when $T \leq 100°C$), the edge-sharing connectivity for the Co^{2+} octahedra increased, the coordination numbers for carboxylate groups increased, and above 100°C hydroxide groups were incorporated into the phases. The dimensionality of the structures was also changed. One-dimensional structures were isolated at 60°C (with isolated octahedral for the inorganic part) and at 100°C (with isolated inorganic trimers). The framework became two-dimensional at 150°C in which 14-membered rings of corner-sharing Co^{2+} octahedra were obtained. The frameworks were three-dimensional above 190°C and 250°C and the inorganic subnetwork was always 2D, but the connectivity of the M-O-M bonds was higher at the higher temperature.[15]

The nature of the metallic salt also greatly influences the nature of the final products. Owing to their own redox characteristics, counter ions of metal salts can influence the reaction conditions. The Zn^{2+}/1,4-benzenedicarboxylic acid/solvent reaction system resulted in the synthesis of MOF-5 with NO_3^-, $CH_3CO_2^-$, and O_2^- as the counter ion of the salt, however, when SO_4^- was used an unknown phase was synthesized.[22]

Recently, significant steps have been taken in developing more efficient methods of MOF synthesis. The conventional solvothermal method can yield high quality crystals, but it suffers from long reaction times and can be difficult to scale above ~1 g. There is a huge potential for industrial applications of MOFs, therefore researchers have been investigating new and efficient alternative synthesis techniques capable of reducing

production costs by decreasing reaction times and improving energy efficiency. These techniques include electrochemical methods, microwave, sonochemical, and solvent-free mechanochemical syntheses.[21]

Microwave heating is a method that has already been applied to inorganic porous compounds as a means of accelerating their reaction rates. Crystallization of these materials using conventional solvothermal synthesis methods usually requires several days as a result of slow heat transfer. Microwave heating has proven to be a much more efficient synthesis technique, resulting in rapid crystallization, homogeneous nucleation, vast reductions in particle size/size distribution, higher yields, and allowing for facile morphology control and efficient evaluation of process variables.[23] The rate enhancements under microwave irradiation are thought to be a consequence of the intense localized heating that can rapidly be attained in the microwave field. This is referred to as the thermal/kinetic effect, but "specific microwave effects" are also responsible for the accelerations which cannot be achieved by conventional heating. There have also been suggestions of the existence of "non-thermal microwave effects" which result from a direct interaction of the electric field with dipolar molecules in the reaction medium.[24]

Of the few studies that have investigated microwave heating for MOF synthesis, the results appear to be very promising. Conventional synthesis methods of MIL-100 and MIL-101 require heating for 96 h at 220°C. However, Chang and co-workers[25] have shown that under microwave irradiation these MOFs can be formed in less than 1 h. Another study demonstrated the accelerated reactions of a cubic nickel glutarate, MIL-77, which previously required several hours or days depending on the reaction temperature. Microwave irradiation produced the more stable tetragonal nickel glutarate within a few

minutes.[26] Recently, our group demonstrated a novel hybrid synthesis technique involving initial UTS irradiation followed by MW irradiation for rapid synthesis of IRMOF-1. Compared with IRMOF-1 synthesized by means of CE heating, crystallites synthesized using this approach were more cubic shaped, much smaller (size reduction by a magnitude of approximately 10), had a narrower particle size distribution (5-15 μm), and had similar high surface areas (~2470 m^2/g).[27] Finally, Morris et al.[28] have reported the synthesis of an anionic MOF by conventional and microwave conditions using an ionic liquid 1-ethyl-3-methylimidazolium bromide, as the solvent and template. Their results indicate that microwave irradiation produces MOFs that are purer in phase and have a higher crystallinity.

Another method that accelerates reactions and produces small and homogeneous crystals is sonochemical synthesis. There have only been a few investigations using this method, but the results are promising. The accelerated reactions under ultrasound conditions are a result of a phenomenon termed "acoustic cavitation". This process involves the formation, growth, and implosive collapse of cavitation bubbles generated in the liquid by the ultrasound wave. Extremely high local temperatures (> 5000 K), pressure (> 2000 atm), and heating and cooling rates (> 10^{11} K/s) are generated as a result.[23] MOF-177 and a Zn-2,2'-bipyridine-5,5'-dicarboxylate MOF synthesized by ultrasonic irradiation produced crystals very similar to those obtained from conventional heating and microwave irradiation. In the case of MOF-177, crystals had superior properties to those synthesized by microwave irradiation.[21] Furthermore, synthesis of $Zn_3(BTC)_2 \cdot 12H_2O$ by this method allowed for a control of the crystal size from 50-900 nm depending on the

reaction time.[29] Despite these results the beneficial effects of MOF sonochemical synthesis have yet to be fully explored.

2.2.3. Applications

For a long time inorganic porous solids have had applications in petrochemistry, catalysis and selective separation as a result of their porosity, high thermal stability and surface area. However, up until the discovery of mesoporous materials, an important limitation of these materials was the relatively small size of the pores. MOFs provided a breakthrough, since they have potentially unlimited porosities and surface areas, including all the desired properties of inorganic solids. Currently, we are living in a time when energy problems must be addressed by the development of sustainable and "greener" alternatives to existing technologies. Owing to the tunability of their structures and the increasingly efficient and greener synthesis techniques, MOFs can have many applications in these areas. MOFs have electronic, optical and magnetic applications, as well as applications in the areas of catalysis, gas adsorption/separation/storage, and drug adsorption/delivery.[15]

In the field of catalysis, the advantage of MOF catalysts over other nanoporous materials like zeolites and activated carbon stem from their inorganic-organic hybrid nature and the tunability of their structures. Not only may the organic linker provide catalytic sites in addition to the metal catalytic sites, but it may also be used as a scaffold to bind catalytic complexes. The synthetic flexibility of MOFs allows for a greater control of the pore size and environment, allowing for a higher selectivity.[21] MOF catalysis mainly includes

cyanosilylation, the Diels–Alder reaction, hydrogenation, esterification, and CO oxidation, however, many others exist.[15] MOFs have also been used as templates for nanoparticles in the area of guest-based catalysis. Much of this work has focussed on MOF-5, which has been encapsulated with Pd, Cu, Ru, Cu, ZnO, and Au nanoparticles by various methods to catalyze such reactions as cyclooctene hydrogenation, methanol production from synthesis gas and the oxidation of 1-phenylethanol.[21] Based on previous results from inorganic mesoporous materials, the surface functionalization of MOF pores should also be a promising research area for catalytic applications, however, this area has yet to be explored.

The domain of gas adsorption/separation/storage has become increasingly important as worldwide fossil fuel reserves continue to decrease. MOFs may provide a solution to this problem for their capacity to adsorb high amounts of important gases like CO_2, H_2, O_2, CH_4, CO, and NO_x in their pores. The ease of evacuating solvents from the pores of MOFs, coupled with their high surface areas and tunable pore sizes makes them particularly attractive in this field. So far, the use of MOFs in the separation of mixtures of gases has been confined primarily to capturing H_2, CH_4 and CO_2.[15] However, progress has also been made in the removal of other toxic and environmentally hazardous gases as well. Weireld and coworkers[30] investigated the hydrogen sulphide (H_2S) adsorption properties of several MOFs. H_2S is known to be a very challenging adsorbate due to the adsorbent decomposition and difficult regeneration that usually occur upon uptake. However, this group observed both that MIL-47(V) and MIL-53(Al, Cr) display little degradation and reversible uptake, and that MIL-53 materials displayed step-wise adsorption, making them attractive materials for the purification of natural gases. Yaghi

and coworkers[31] recently compared the adsorption of various harmful gases by several MOF materials to an activated carbon material, Calgon BPL carbon. For each gas, at least one of the MOFs studied exceeded the adsorption potential of BPL carbon. For ammonium, the MOFs displayed a 6-105 fold adsorption enhancement. Another group showed that the zinc clusters in MOF-5 actually coordinate to ammonia, thus not only increasing the adsorption capacity but also serving as a degradation pathway.[32] Collectively, these results are an indication that MOFs are promising adsorbents for harmful gases and with further research may have applications in large-scale industrial processes.

In the field of drug adsorption/delivery the size of the pores becomes very important. The main drawback of organic porous solids is that their pore sizes are too small to allow for a successful incorporation of most organic molecules. With their tunable porosities MOFs are able to provide a solution to this problem. Horcajada and coworkers[33] showed that the rigid mesoporous MOFs, MIL-100 and MIL-101, were able to achieve both a high drug loading and a controlled release. MIL-100 and MIL-101 both exhibited high uptake (0.35 g and 1.4 g of ibuprofen per gram of MOF, respectively) and 3-6 day release times under simulated physiological conditions. Even at these high loadings there was no observed loss of crystallinity or decomposition of the frameworks.

Despite the fact that microporous solids are limited to the incorporation of small organic molecules, Horcajada et al.[34] also demonstrated the adsorption and delivery capabilities of a flexible microporous MOF, MIL-53(Fe). This material adsorbed 0.21 g ibuprofen/g MOF and completely released the drug after three weeks. The sustained release profile was attributed to the flexibility of the framework, which is able to reversibly open and

close its pores upon adsorption of guest species. This property allows MIL-53(Fe) to maximize host-guest interactions. More recently, this group investigated the delivery of nine drugs from five MIL materials. MIL-100 was able to achieve 25% loading by weight of the anticancer drug busulfan, approximately five times higher than the best system of polymer nanoparticles (5-6 wt%). Studies on human leukaemia and human multiple myeloma cells in culture showed that busulfan-loaded MIL-100 exhibited very similar cytotoxic activity to busulfan in its free form. Empty MIL-100 nanoparticles exhibited a complete absence of cytotoxicity in the same cell lines. *In vitro* HIV virus replication was significantly inhibited by MIL-100 loaded with the anti-HIV drug AZT-TP.[35] The MIL family is a unique candidate in the field of drug adsorption/delivery and is ready for more extensive *in vivo* testing.

2.3. Mesoporous Silica Materials

2.3.1. Background

In 1992, researchers at the Mobil Oil Company developed a new class of silica-based ordered mesoporous materials (SMMs) known as the M41S phase. At the time, zeolites were the most researched and promising porous materials. However, regardless of the great amount of work dedicated to them, their pores were restricted to a diameter of about 15 Å, limiting their applications to very small molecules. Unlike zeolites, M41S materials could be designed with very large pore sizes, ranging from approximately 2 to 10 nm.[36] Furthermore, they have very large specific surface areas (up to ca. 1500 m^2/g), high pore volumes (up to ca. 1.5 cm^3/g) and ordered pore systems with very narrow pore

size distribution.[37] In general, these materials are derived from supramolecular aggregates of ionic surfactants in aqueous media, which act as structure-directing agents (SDAs) or templates for the silica mesostructure during synthesis.[36] The removal of the surfactant by solvent extraction or calcination results in the formation of the mesoporous structure. The structure of SMMs depends on the surfactant template selected and the synthesis conditions (ie. concentration, temperature, co-solvents, additives, etc.).[38] Perhaps the best-known and most studied member of the M41S materials is the Mobil Crystalline Material, MCM-41, which has a hexagonal arrangement of mesopores. Since these first mesoporous silicas were discovered progress has been significant, leading to a vast pool of SDAs and a variety of synthetic pathways.[39] By changing the inorganic precursor, organic template, reaction conditions, and synthetic pathway a variety of different mesoporous materials are possible.[40] For example, using triblock copolymer templates under acidic conditions results in the formation of SBA mesoporous silicas. One of the better known members of this class is SBA-15, which is characterized by thick pore walls (ca. 3 nm) and a two-dimensional channel consisting of a hexagonal array of mesopores with diameters between 8 and 30 nm. This material uses the relatively cheap amphiphilic triblock copolymer Pluronic 123 as the surfactant in highly acidic media.[37] A common feature of all mesoporous silica materials is the homogeneous size of their ordered pore networks, which is an especially attractive feature in the field of drug delivery since this allows for fine control of drug load and release. In addition, they have sufficient mechanical strength, thermal and pH stability, are biocompatible and contain silanol surfaces that can be functionalized to allow for an even better control over drug delivery. Compared to the M41S family, the SBA family of materials enjoys some advantages.

Firstly, they have a larger number of silanol groups due to faster condensation, making them more suitable materials to which functional groups can be attached. They also have larger pores, in addition to the presence of micropores which connect adjacent mesopores together within the framework. These can serve to allow for better access of reagents to active sites by minimizing the likelihood of blockages within the mesopores.[40] All of these properties make the SBA family very attractive materials as drug delivery systems.

2.3.2. Synthetic Approaches

Mesoporous silica materials can be synthesized by a number of different methods. The majority of these methods involve the use of a surfactant in solution to guide the formation of the inorganic mesostructure from the inorganic precursor. Because surfactants are composed of both a hydrophilic head group and a hydrophobic tail group they will self-assemble into a conformation that minimizes contact between the incompatible ends. A significant difference among the various synthesis routes is the type of interaction that is made to occur between the surfactant and the inorganic precursor, which will greatly influence the type of mesoporous material that is formed.[41] The two most common methods include liquid crystal templating (LCT) and co-operative self-assembly (CSA).[40]

The original M41S family was synthesized by combining appropriate amounts of a silica source (e.g. tetraethylorthosilicate (TEOS), Ludox, fumed silica, sodium silicate), an alkyltrimethylammonium halide surfactant (e.g. cetyltrimethylammoniumbromide (CTAB)), a base (e.g. sodium hydroxide or tetramethlammonium hydroxide (TMAOH)),

and water. The mixtures were heated at elevated temperatures (≥100°C) for 24 to 144 hours, resulting in the formation of a solid precipitate. After filtering and washing the organic-inorganic products with water, they were calcined at about 500°C under a flowing gas to burn off the surfactant, yielding the final mesoporous material. In this method, the mesoporous structure depends on the hydrocarbon chain length of the surfactant tail group, the surfactant concentration, and the influence of organic swelling agents. The Mobil Oil researchers postulated that the formation of MCM-41 - the representative M41S material - proceeded by either one of two mechanisms. In the first scheme, now known as the LCT mechanism, they proposed that the aluminosilicate precursor species occupied the space between a pre-existing hexagonal lyotropic liquid crystal (LC) phase and deposited on the micellar rods of the LC phase (Figure 2-6). The second scheme, now known as the CSA mechanism, was proposed to involve the ordering of the surfactants into a hexagonal arrangement, mediated by the inorganic component (Figure 2-6). Although they were unsure which one of these mechanisms was actually occurring, in both, the negative charge of the inorganic component was known to preferentially interact with the positively charged ammonium head groups of the surfactant to organize and condense into an ordered framework. Subsequent removal of the surfactants, which are ordered as a hexagonal array of micellar rods embedded in the silica matrix, are removed to produce the open, mesoporous MCM-41 framework.[41]

It has now been discovered that the second mechanistic pathway was responsible for the formation of MCM-41. The first pathway did not take place because the surfactant concentrations used were far below the critical micelle concentration (CMC) required for hexagonal LC formation. The second pathway was found to proceed by way of a

cooperative self-assembly of the ammonium surfactant and the silica precursor below the CMC. Thus, at low surfactant concentration (as in the case of MCM-41) the CSA mechanism proceeds, resulting in the formation of a LC phase. The LCT pathway, on the other hand, occurs at such high surfactant concentrations that the silica precursor is not even required for the formation of the LC phase.[41]

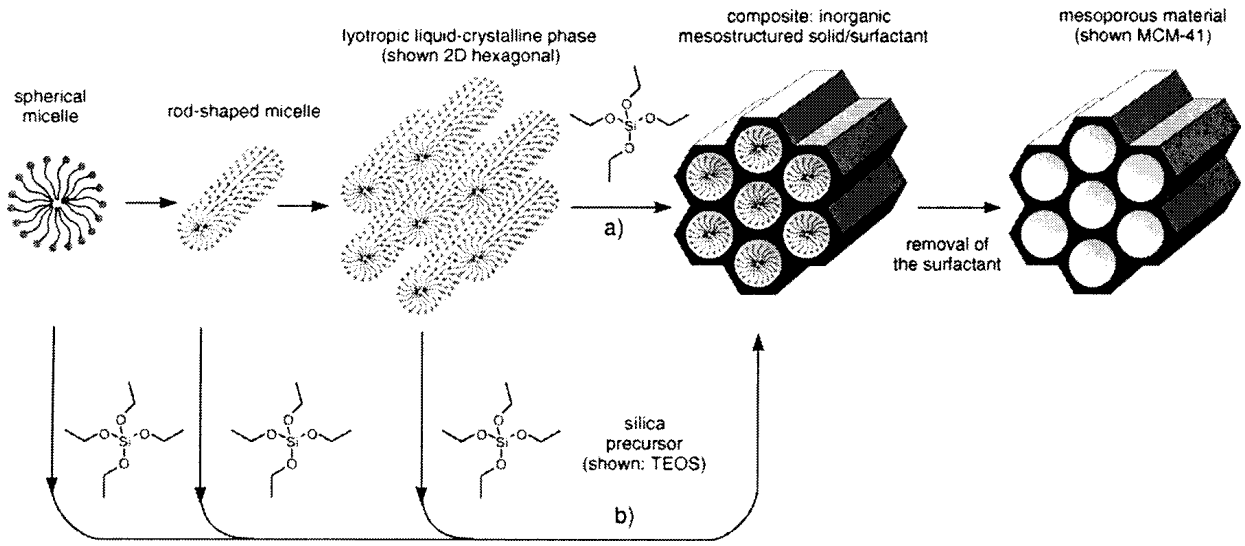

Figure 2-6. Formation of mesoporous materials by structure-directing agents: a) true liquid-crystal template mechanism, b) cooperative liquid-crystal template mechanism.[42]

The original synthesis approach that was postulated for M41S materials has been extended to at least three new routes to attain different types of structures. In addition to the basic route, there now exists the acidic, neutral, and non-ionic routes. Under acidic conditions triblock copolymer templates are used to form the SBA silica phases; the HMS/MSU family is formed under neutral conditions. A fundamental requirement for each of these routes is that there is an attractive interaction between the surfactant head

groups and the silica precursors to ensure inclusion of the SDA without phase separation taking place.[42] As proposed by Huo et al.,[43, 44] a given inorganic precursor (I) and surfactant head group (S) require an electrostatic interaction under the synthesis conditions. Based on this nomenclature, under basic conditions involving anionic silica species and cationic quaternary ammonium surfactants, the charge-interaction pathway can be categorized as S^+I^-. Preparations under acidic conditions occur below the isoelectric point (pH ≈ 2) of the inorganic silica precursors, whereby the silica species are cationic (I^+). The same ammonium surfactant S^+ can be used as in basic media, but to produce an interaction between the two it is necessary to add a mediator halide counteranion (X^-) ($S^+X^-I^+$ pathway), which buffers the repulsion between S^+ and I^+ by weak hydrogen-bonding forces. The resulting materials are referred to as acid-prepared mesostructures, or APM materials, of which the SBA family is a member. Negatively charged surfactants, such as alkyl phosphates could also be used as SDAs under acidic or basic conditions. In basic media a mediator metal cation (M^+) must be added to ensure an interaction through the $S^-M^+I^-$ pathway. In acidic media a mediator is not required (S^-I^+ pathway). The dominating interactions in these pathways are electrostatic, however when nonionic surfactants are used the attractive interactions are mediated through hydrogen bonds. The hydrogen-bonding interaction of an alkylamine (S^0) head group and hydroxylated TEOS (I^0) through the S^0I^0 pathway produces materials with thicker walls and higher thermal stability than the acidic and basic routes.[42] Another hydrogen-bonding synthesis route uses the non-ionic surfactant, triblock poly(ethylene oxide)-poly(propylene oxide)-poly(ethylene oxide - $EO_{20}PO_{70}EO_{20}$) (Pluronic 123), wherein the PEO units function as the hydrophilic head and alkyl chain and PPO units function as the core. The lengths of the head and tail groups can be adjusted, resulting in pores as large

as 58 Å in diameter. The PEO head group (N^0) is non-ionic, unlike the amine head group (S^0) which is uncharged and can be ionized. The result from this non-ionic route (N^0I^0) is materials with greater pore ordering than the neutral route (S^0I^0).[40] Each of these interactions is illustrated in Figure 2-7.

SBA-15 uses Pluronic 123 as its surfactant, however its synthesis occurs under acidic conditions (pH $\approx$ 1). It is thought that the templating of this material occurs through both electrostatic and hydrogen-bonding interactions, producing materials with pores as large as 30 nm. The orderness of its structure can be improved by decreasing the surfactant concentration, allowing for slower assembly of the silica species with surfactant molecules. As the size of the micelles increases the corresponding pore size also increases, reducing the wall thickness. Pore size can also be increased by either increasing the synthesis temperature or time during hydrothermal treatment. SBA-15 also has microporosity, which originates from penetration of EO chains in silica walls, connecting the different mesoporous cavities. The microporosity can be controlled by synthesis temperature, time, and by silica/surfactant ratio.[41]

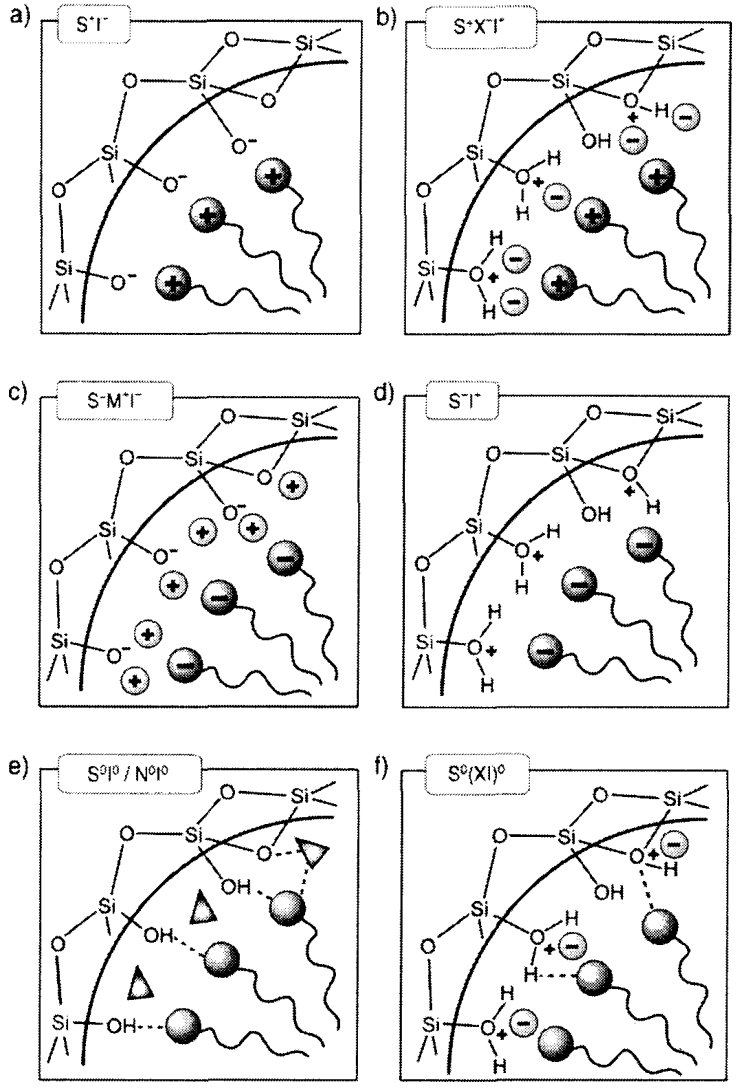

Figure 2-7. Interactions between the inorganic species and the head group of the surfactant with consideration of the possible synthetic pathway in acidic, basic, or neutral media. Electrostatic: S^+I^-, $S^+X^-I^+$, $S^-M^+I^-$, S^-I^+; through hydrogen bonds: S^0I^0/N^0I^0, $S^0(XI)^0$.[42]

2.3.3. Applications

The unique properties of SMMs have made these materials highly desirable for a number of different applications, including catalysis, gas and liquid adsorption, binding metals, and drug adsorption/delivery. Their extremely high surface areas and large pore sizes allow for high catalytic activity, fixation of large catalytically active complexes and

enables reactions involving bulky molecules. These materials have seen applications in acid/base, oxidative and chiral catalysis. Sulfonic acid derivatives were anchored to MCM-41,[45, 46] MCM-48,[45, 46] FSM-16[47] and SBA-15[48] materials, leading to good yields and selectivities in the condensation of phenol and acetone to bisphenol A.[45, 46] Additionally, high activities were reported in the acetalation of acetophenone with ethylene glycol,[47] and in the dehydration of 1-butanol to dibutyl ether.[48] Friedel-Crafts alkylation and epoxidation are also common acid-catalyzed reactions using SMMs.[41]

The majority of studies on heterogeneous oxidation catalysts have been devoted to SMMs doped with metals, metal complexes, or organometallic compounds.[42] For example, shortly after the discovery of the M41S materials, two groups simultaneously reported the synthesis of MCM-41 doped with titanium. Catalytically active titanium sites were deposited in the mesoporous matrix without significantly affecting surface area or pore size. Corma et al.[49] prepared Ti-MCM-41, which showed a higher catalytic activity than Ti-β zeolite in the epoxidation of norbornene with *tert*-butyl hydroperoxide as the oxidant. The use of MCM-41 materials as both heterogeneous base and chiral catalysts has also shown promising results.[42]

SMMs also have major potential applications in gas and liquid adsorption, and in binding metals as a result of their high porosities. Ioneva et al.[50] have shown that the adsorption of methane in MCM-41 was possible at 25°C up to 6.9 MPa, with a 75% improvement in storage capacity when the pressure was 3.45 MPa. For optimization of methane affinity, pores smaller than 20 Å are ideal. Mesoporous aluminosilica materials are also being used to adsorb volatile organic compounds (VOC) at room temperature with great capacity. Once saturated, the adsorbents are reactivated with hot air (120-150°C) and the

recovered VOCs are concentrated 3-10 times.[41] These materials have also been purposely modified to remove heavy metals from tainted water supplies. For example, Feng et al.[51] functionalized the surface of a SMM with tris(methoxy)sulfanylpropylsilane molecules with thiol terminal groups to adsorb mercury, silver, and lead ions from water. The adsorptive power of this material far exceeded that of conventional sorbents. It was also reusable, as treatment of the mercury-loaded material with HCl released the metal, yielding the intact functional adsorbent. Furthermore, the work of Liu et al.[52] showed that thiolated SBA-15 has a high affinity to mercury cations, and that amino-functionalized SBA-15 highly binds copper, zinc, chromium and nickel cations. Thus, these materials have promising applications in the removal of heavy metals from wastewaters.

Mesoporous silica materials also have very important applications in the field of drug delivery as a result of their highly ordered pores, large pore volumes and high surface areas. The well-ordered pore distribution of these materials gives them the ability to homogeneously and reproducibly adsorb and release drug molecules. Their high pore volumes and high surface areas mean that they can both host vast quantities of drugs in their pores and adsorb a large amount of molecules onto their pore walls. Additionally, a wide array of functional groups can be grafted to their silanol-containing surfaces, thus improving the adsorption and controlled release profiles of biomolecules. Finally, their pores are also highly tunable.[38]

The high density of silanol groups (SiOH) on the surface of SMMs allows for the possibility of easy chemical functionalization of the pore walls. Two methods to graft chemical groups to the pore walls of SMMs have been described in the literature. The first is direct functionalization, in which the selected functional group is present in the

reaction mixture with a trialkoxysilane during the synthesis process. The second method is post-synthesis functionalization, which involves grafting the functional group to the mesoporous material after surfactant removal. The type of chemical modification is normally selected depending on the nature of the drug molecule to be adsorbed, taking into account the desired load and release kinetics.[38]

The confinement of a number of different classes of drugs within SMMs has been described in the literature, perhaps none more than anti-inflammatory drugs, including ibuprofen. The loading of drugs within the mesoporous structures is usually performed by soaking the SMM in a highly concentrated drug solution. The loading solvent is selected based on the chemical nature of the guest molecule. Usually, the solvent that is selected is one in which the drug molecule has a very high solubility. The release process is usually performed by placing the impregnated mesoporous material into simulated body fluid (SBF) solution, which has ionic concentrations similar to those found in human plasma.[38]

The possibility of using MCM-41 as a DDS was first described in 2001 when Vallet-Regí et al.[53] performed drug loading and release studies with ibuprofen. Two MCM-41 matrices with different pore sizes - MCM-41_{16} and MCM-41_{12} (2.5 and 1.8 nm, respectively) - were synthesized using cationic surfactants with different hydrocarbon chain lengths. It has been widely reported that the pore diameter is a limiting factor in adsorption of molecules within mesoporous matrices. Ibuprofen, however, has molecular dimensions of 1.0 x 0.6 nm, so the pore diameter is not a limiting factor. The adsorption of drug molecules into SMMs is a surface phenomenon governed by the interactions of the silanol surface with the functional groups of the guest molecule. The amount of

ibuprofen adsorbed within the MCM-41 matrices was 34 wt% and 23 wt% for MCM-41_{16} and MCM-41_{12}, respectively. These different drug loadings can be attributed to the different surface areas which are 1157 and 1099 m^2/g, respectively. Thus, the chemical interactions between the functional groups of the drug and the silanol groups of the matrix are promoted by higher surface areas. This fact was also illustrated by impregnating SBA-15 (602 m^2/g) with ibuprofen, yielding a smaller drug loading of 15 wt%. Drug delivery studies with MCM-41 matrices indicated that the higher the pore size, the faster the drug release. The cumulative release of ibuprofen after 24 h from MCM-41_{16} and MCM-41_{12} was 68% and 55%, respectively. This finding was confirmed by Horcajada et al.,[54] who demonstrated this trend using several MCM-41 matrices with pore diameters ranging in size from 2.5 to 3.6 nm. These results suggest that the delivery rates of SMMs can be controlled by choosing an appropriate pore size.

One of the goals of controlled drug delivery is to achieve a site-specific controlled release pattern, which has been accomplished with SMMs by stimuli-responsive controlled release. In this approach the DDSs release the encapsulated drug molecules when desired, by responding to external stimuli. A change in pH is a stimulus that has been used to control the release from several SMMs. Certain tissues of the body are slightly more acidic than blood and normal tissue, such as tumour and inflammatory tissue.[38] For example, Yang et al.[55] studied the release of vancomycin at different pHs (2.0, 4.5 and 6.5) from a pH-responsive DDS using SBA-15. The pore entrances were modified with carboxylic acid; polycations were then adsorbed to the anionic SBA-15 closing the gates of the pores with vancomycin inside. Reducing the pH led to the carboxylic species

(COO^-) becoming protonated (COOH), resulting in the polycations moving away and opening of the gates for release of the drug.

Possibly one of the most spectacular works in the area of stimuli-sensitive mesoporous silica materials was done by Mal et al.,[56, 57] who constructed a photochemically controlled system using MCM-41. In this strategy the researchers anchored coumarin to the pore openings of an MCM-41 preparation in which the SDA was still present. This was done to ensure that coumarin reacted only with the silanol groups at the pore openings and the outer surface. After removal of the surfactant cholestane derivatives were inserted into the pores. Irradiation with UV light ($\lambda > 310$ nm) led to dimerization of the coumarin, resulting in sealing of the pore openings. Diffusion-controlled release of the enclosed active compounds was accomplished by cleaving the coumarin dimers with UV light at around 250 nm. Other stimuli-sensitive mesoporous silica release systems respond to stimuli such as temperature, light and ultrasound, each of which have the ability to improve the therapeutic efficacy of standard DDSs.[38]

2.4. Conclusions

The majority of research in the domain of metal-organic frameworks has focussed on discovering new phases and demonstrating their potential applications in various fields. Detailed investigations on the influence of reaction conditions on crystallization are the minority. The ability to carefully control drug delivery from these materials requires a fundamental understanding of the influence of synthesis conditions on their properties, such as particle size, porosity, and surface area. Optimization of the reaction conditions

also provides an opportunity to minimize energy requirements, which is essential for large scale production of MOFs.

Shortcomings of conventional therapy have justified the pursuit of drug delivery systems which are capable of improving the therapeutic and pharmacological properties of free drugs through a controlled release rate. Polymeric nanoparticles, micelles, liposomes, and microporous zeolites have been extensively researched as DDSs, but for the most part results have been unsatisfactory. The main drawback of these materials is that they either lack a well defined porosity, making a controlled release very difficult, or they have porosities that are too small to allow for a high drug loading. With their tunable host-guest properties MOFs are able to provide a solution to these problems.

2.5. References

(1) Shi, J.; Votruba, A. R.; Farokhzad, O. C.; Langer, R. *Nano Lett.* **2010**, *10*, 3223-3230.

(2) Allen, T. M.; Cullis, P. R. *Science* **2004**, *303*, 1818-1822.

(3) De Jong, W. H.; Borm, P. J. A. *Int. J. Nanomed.* **2008**, *3*, 133-149.

(4) Zhao, F.; Zhao, Y.; Liu, Y.; Chang, X.; Chen, C.; Zhao, Y. *Small* **2011**, *7*, 1322-1337.

(5) Vinogradov, S. V.; Bronich, T. K.; Kabanov, A. V. *Adv. Drug Deliv. Rev.* **2002**, *54*, 135-147.

(6) Hawley, A. E.; Davis, S. S.; Illum, L. *Adv. Drug Deliv. Rev.* **1995**, *17*, 129-148.

(7) Ishida, O.; Maruyama, K.; Sasaki, K.; Iwatsuru, M. *Int. J. Pharm.* **1999**, *190*, 49-56.

(8) Stolnik, S.; Illum, L.; Davis, S. S. *Adv. Drug Deliv. Rev.* **1995**, *16*, 195-214.

(9) Goldberg, M.; Langer, R.; Jia, X. *J. Biomater. Sci., Polym. Ed.* **2007**, *18*, 241-268.

(10) Edetsberger, M.; Gaubitzer, E.; Valic, E.; Waigmann, E.; Kohler, G. *Biochem. Biophys. Res. Commun.* **2005**, *332*, 109-116.

(11) Panyam, J.; Zhou, W. Z.; Prabha, S.; Sahoo, S. K.; Labhasetwar, V. *FASEB J.* **2002**, *16*.

(12) Konan, Y. N.; Chevallier, J.; Gurny, R.; Allemann, E. *Photochem. Photobiol.* **2003**, *77*, 638-644.

(13) Moghimi, S. M.; Hunter, A. C.; Murray, J. C. *Pharmacol. Rev.* **2001**, *53*, 283-318.

(14) Peer, D.; Karp, J. M.; Hong, S.; FaroKHzad, O. C.; Margalit, R.; Langer, R. *Nat. Nanotechnol.* **2007**, *2*, 751-760.

(15) Férey, G. *Chem. Soc. Rev.* **2008**, *37*, 191-214.

(16) Rowsell, J. L. C.; Yaghi, O. M. *Microporous Mesoporous Mater.* **2004**, *73*, 3-14.

(17) Kitagawa, S.; Kitaura, R.; Noro, S. *Angew. Chem. Int. Ed.* **2004**, *43*, 2334-2375.

(18) Hong, D.; Hwang, Y. K.; Serre, C.; Ferey, G.; Chang, J. *Adv. Funct. Mater.* **2009**, *19*, 1537-1552.

(19) Yaghi, O. M.; O'Keeffe, M.; Ockwig, N. W.; Chae, H. K.; Eddaoudi, M.; Kim, J. *Nature* **2003**, *423*, 705-714.

(20) James, S. L. *Chem. Soc. Rev.* **2003**, *32*, 276-288.

(21) Meek, S. T.; Greathouse, J. A.; Allendorf, M. D. *Adv. Mater.* **2011**, *23*, 249-267.

(22) Bauer, S.; Bein, T.; Stock, N. *Inorg. Chem.* **2005**, *44*, 5882-5889.

(23) Leonelli, C.; Mason, T. J. *Chem. Eng. Process.* **2010**, *49*, 885-900.

(24) Kappe, C. O. *Angew. Chem. Int. Ed.* **2004**, *43*, 6250-6284.

(25) Jhung, S. H.; Lee, J. H.; Chang, J. S. *Bull. Korean Chem. Soc.* **2005**, *26*, 880-881.

(26) Jhung, S. H.; Lee, J.; Forster, P. M.; Ferey, G.; Cheetham, A. K.; Chang, J. *Chem. Eur. J.* **2006**, *12*, 7899-7905.

(27) Sabouni, R.; Kazemian, H.; Rohani, S. *Chem. Eng. J.* **2010**, *165*, 966-973.

(28) Lin, Z. J.; Wragg, D. S.; Morris, R. E. *Chem. Commun.* **2006**, 2021-2023.

(29) Qiu, L.; Li, Z.; Wu, Y.; Wang, W.; Xu, T.; Jiang, X. *Chem. Commun.* **2008**, 3642-3644.

(30) Hamon, L.; Serre, C.; Devic, T.; Loiseau, T.; Millange, F.; Ferey, G.; De Weireld, G. *J. Am. Chem. Soc.* **2009**, *131*, 8775-8777.

(31) Britt, D.; Tranchemontagne, D.; Yaghi, O. M. *Proc. Natl. Acad. Sci. U. S. A.* **2008**, *105*, 11623-11627.

(32) Petit, C.; Bandosz, T. J. *Adv. Funct. Mater.* **2010**, *20*, 111-118.

(33) Horcajada, P.; Serre, C.; Vallet-Regí, M.; Sebban, M.; Taulelle, F.; Férey, G. *Angew. Chem. Int. Ed.* **2006**, *45*, 5974-5978.

(34) Horcajada, P.; Serre, C.; Maurin, G.; Ramsahye, N. A.; Balas, F.; Vallet-Regí, M.; Sebban, M.; Taulelle, F.; Férey, G. *J. Am. Chem. Soc.* **2008**, *130*, 6774-6780.

(35) Horcajada, P., et al *Nat. Mater.* **2010**, *9*, 172-178.

(36) Barbe, C.; Bartlett, J.; Kong, L. G.; Finnie, K.; Lin, H. Q.; Larkin, M.; Calleja, S.; Bush, A.; Calleja, G. *Adv. Mater.* **2004**, *16*, 1959-1966.

(37) Hartmann, M. *Chem. Mater.* **2005**, *17*, 4577-4593.

(38) Manzano, M.; Colilla, M.; Vallet-Regi, M. *Expert Opin. Drug Deliv.* **2009**, *6*, 1383-1400.

(39) Bruehwiler, D. *Nanoscale* **2010**, *2*, 887-892.

(40) Selvam, P.; Krishna, N. V.; Viswanathan, B. *J. Indian Inst. Sci.* **2010**, *90*, 271-285.

(41) Ying, J. Y.; Mehnert, C. P.; Wong, M. S. *Angew. Chem. Int. Ed.* **1999**, *38*, 56-77.

(42) Hoffmann, F.; Cornelius, M.; Morell, J.; Fröba, M. *Angew. Chem. Int. Ed.* **2006**, *45*, 3216-3251.

(43) Huo, Q. S.; Margolese, D. I.; Ciesla, U.; Feng, P. Y.; Gier, T. E.; Sieger, P.; Leon, R.; Petroff, P. M.; Schuth, F.; Stucky, G. D. *Nature* **1994**, *368*, 317-321.

(44) Huo, Q. S.; Margolese, D. I.; Ciesla, U.; Demuth, D. G.; Feng, P. Y.; Gier, T. E.; Sieger, P.; Firouzi, A.; Chmelka, B. F.; Schuth, F.; Stucky, G. D. *Chem. Mater.* **1994**, *6*, 1176-1191.

(45) Das, D.; Lee, J. F.; Cheng, S. F. *Chem. Commun.* **2001**, 2178-2179.

(46) Das, D.; Lee, J. F.; Cheng, S. F. *J. Catal.* **2004**, *223*, 152-160.

(47) Shimizu, K.; Hayashi, E.; Hatamachi, T.; Kodama, T.; Higuchi, T.; Satsuma, A.; Kitayama, Y. *J. Catal.* **2005**, *231*, 131-138.

(48) Sow, B.; Hamoudi, S.; Zahedi-Niaki, M. H.; Kaliaguine, S. *Microporous Mesoporous Mater.* **2005**, *79*, 129-136.

(49) Corma, A.; Navarro, M. T.; Pariente, J. P. *J. Chem. Soc., Chem. Commun.* **1994**, 147-148.

(50) Ioneva, M. A.; Harwell, J. H.; Mallinson, R. G.; Starling, K. E. *Abstr. Pap. Am. Chem. Soc.* **1996**, *211*, 115-COLL.

(51) Feng, X.; Fryxell, G. E.; Wang, L. Q.; Kim, A. Y.; Liu, J.; Kemner, K. M. *Science* **1997**, *276*, 923-926.

(52) Liu, A. M.; Hidajat, K.; Kawi, S.; Zhao, D. Y. *Chem. Commun.* **2000**, 1145-1146.

(53) Vallet-Regi, M.; Ramila, A.; del Real, R. P.; Perez-Pariente, J. *Chem. Mater.* **2001**, *13*, 308-311.

(54) Horcajada, P.; Ramila, A.; Perez-Pariente, J.; Vallet-Regi, M. *Microporous and Mesoporous Mater.* **2004**, *68*, 105-109.

(55) Yang, Q.; Wang, S. H.; Fan, P. W.; Wang, L. F.; Di, Y.; Lin, K. F.; Xiao, F. S. *Chem. Mater.* **2005**, *17*, 5999-6003.

(56) Mal, N. K.; Fujiwara, M.; Tanaka, Y. *Nature* **2003**, *421*, 350-353.

(57) Mal, N. K.; Fujiwara, M.; Tanaka, Y.; Taguchi, T.; Matsukata, M. *Chem. Mater.* **2003**, *15*, 3385-3394.

3. Rapid and efficient crystallization of MIL-53(Fe) by ultrasound and microwave irradiation

3.1. Introduction

Recently, inorganic-organic hybrid compounds or metal-organic frameworks (MOFs) have attracted increasing interest due to their applications in the fields of gas adsorption/storage,[1-4] catalysis,[5-7] drug storage and delivery,[8-11] electrode materials,[12-14] imaging,[10, 15] and magnetism.[16-18] They result from the assembly of organic linkers and inorganic species, exclusively by strong covalent and ionocovalent bonds.[19] The success of these materials is attributed to their remarkable porosity and the easy tunability of their pore sizes, which can be achieved by changing the organic linker and/or the inorganic moiety. As a result a huge number of three-dimensional open-framework structures are possible, with some of the highest surface areas seen for crystalline inorganic solids and porosities spanning those exhibited by microporous zeolites and mesoporous silica materials.[19] Moreover, some MOFs have a high structural flexibility and robustness, enabling them to adapt their porosity to the shape and size of hosted organic molecules.[8, 11]

To date the majority of studies on these materials have been devoted to discovering new types of MOFs and demonstrating their potential applications in various fields. However, detailed investigations about the role of reaction conditions during synthesis and scale up have been ignored. Thus far, the majority of MOFs have been synthesized by hydro- or solvothermal methods using conventional electric (CE) heating,[19] requiring reaction times as long as several days. However, because of the huge potential for industrial applications of MOFs,[20] a fundamental understanding of the synthesis of these materials is vital if they are to offer viable applications in industry. For MOF production to be scaled up to larger industrial processes it is essential to develop new and efficient alternative

synthesis techniques capable of reducing costs of the final product. To achieve this the synthesis times must be reduced and the overall energy efficiency must be improved. To this end, alternative techniques such as solvent free methods,[21] electrochemical methods,[20] ultrasound (UTS),[22-24] and microwave (MW) irradiation[22, 24-27] have been reported.

UTS and MW irradiation are particularly promising alternative techniques due to the minimisation of energy and optimization of reaction conditions with these two methods. MW irradiation is characterized by accelerated reactions, as a consequence of the intense localized heating, reducing reaction times from days and hours by classical heating to minutes and seconds.[28, 29] Since the magnitude of heating depends on the dielectric properties of the molecules, generated energy is supplied to the material directly and uniformly. This allows the whole material to be heated rapidly and simultaneously, resulting in homogeneous nucleation, fast crystallization, vast reductions in particle size and higher yields.[19, 28, 29] The remarkable effects of UTS energy (20 kHz) are attributed to "acoustic cavitation", the phenomenon involving the formation, growth, and implosive collapse of cavitation bubbles generated in a liquid by the ultrasound wave.[28] Accelerated reactions result from the violent collapse of thousands of these tiny micrometer-sized hotspots, generating extremely high temperatures (> 5000 K), pressure (> 2000 atm), and heating and cooling rates (> 10^{11} K/s).[28] In addition, UTS irradiation can lead to homogeneous nucleation. Despite these impressive capabilities, very little effort has been invested into understanding the beneficial effects of MW and UTS irradiation for MOF synthesis.

Recently, our group demonstrated a novel hybrid synthesis technique involving initial UTS irradiation followed by MW irradiation for rapid synthesis of IRMOF-1.[24]

Compared with IRMOF-1 synthesized by means of CE heating, crystallites synthesized using this approach were more cubic shaped, much smaller (size reduction by a magnitude of approximately 10), had a narrower particle size distribution (5-15 μm), and had similar high surface areas (~2470 m^2/g).[24]

Additionally, Haque et al. (2010) demonstrated the accelerated syntheses of MIL-53(Fe) by UTS and MW irradiation at relatively low temperatures, observing the crystallization rate to decrease in the order UTS > MW >> CE. These results and the findings our group has made previously suggest that syntheses performed under UTS and MW conditions may be very promising for producing MOFs.

In this work we have qualitatively analyzed the crystallization of MIL-53(Fe),[30] a structurally flexible and non-toxic iron(III) benzenedicarboxylate MOF. The main objective of this work was to develop rapid and energy efficient synthesis techniques utilizing UTS and MW irradiation. Syntheses were carried out under CE, MW and UTS conditions to gain an understanding of the effects of multiple synthesis procedures on the product yield and crystallinity. Within each reaction procedure, two-level multi-factorial designs were used to study the dependence of the two responses on each factor. The structure of MIL-53(Fe) is composed of parallel trans corner-sharing iron(III) octahedral chains, each of which are cross-linked by 1,4-benzenedicarboxylate (BDC) anions to form a one-dimensional lozenge-shaped pore channel system.[11] As mentioned elsewhere, MIL-53(Fe) only opens its pores in the presence of guest molecules, therefore, unlike other MOFs it does not have a high surface area. MIL-53 has the formula $M^{III}(OH)\bullet(O_2C\text{-}C_6H_4\text{-}CO_2)\bullet H_2O$ ($M = Al^{3+}$, Cr^{3+} or Fe^{3+}).[11]

3.2. Experimental Section

3.2.1. MIL-53(Fe) Synthesis

The MIL-53(Fe) samples were synthesized with the same batch composition reported by Horcajada et al. (2010) from a mixture of ferric chloride hexahydrate ($FeCl_3 \cdot 6H_2O$, Caledon, 97.0-102.0%), 1,4-benzenedicarboxylic acid (H_2BDC, Alfa Aesar, ≥98%), and *N,N*-dimethylformamide (DMF, Caledon, ≥99.8%) at a molar ratio of 1:1:64. All of the chemicals were used as purchased without any further purification. In the first stage of the experiment, samples were synthesized by means of an electrical oven (DKN 400, Yamato Scientific America, Inc., Santa Clara, CA) to evaluate CE heating. Each reaction mixture was prepared by dissolving 1 mmol of $FeCl_3 \cdot 6H_2O$ and 1 mmol of H_2BDC in 5 mL of DMF. The solution was then transferred either to a round bottom flask connected to a condenser or to a sealed pressurized glass vessel (Ace Glass, Inc., Vineland, NJ) and heated for a specific time (i.e. 2 h or 15 h) at a predetermined temperature (i.e. 100°C or 150°C) according to the experimental design (Table 3-1). The same batch composition and reaction vessels were used for MW irradiation (Discover, CEM Corporation, Matthews, NC). The solution was irradiated at a predetermined power (i.e. 150 W or 300 W), temperature (i.e. 100°C or 150°C) and time (i.e. 10 min or 30 min) (Table 3-2). For UTS irradiation, 10 mL of the reaction mixture was added to a vial which was placed in the probe of an ultrasonic generator (VCX 500, Sonics & Materials, Inc., Newtown, CT). These experiments were performed at a predetermined time (i.e. 7 min, 11 min or 15 min) and power (40%, 50% or 60% of maximum power) (Table 3-3), however the temperature was not controlled. After completion of each of the reactions and prior to characterization the products were cooled to room temperature before centrifugation, then

washed with DMF and dried. The high and low values used in this study for each of the reaction parameters were selected based on results from preliminary experiments.

Table 3-1. Experimental design for MIL-53(Fe) synthesized by CE heating.

Sample code	CE time (h)	CE temperature (°C)	Reaction vessel	Relative crystallinity (%)	Yield (%)
MIL-53_1	2	100	RB flask	9.9	16.9
MIL-53_2	2	150	RB flask	14.2	51.8
MIL-53_3	15	100	RB flask	23.5	58.8
MIL-53_4	15	150	RB flask	100	56.1
MIL-53_5	2	100	PG vessel	3.1	25.9
MIL-53_6	2	150	PG vessel	65.7	53.3
MIL-53_7	15	100	PG vessel	15.1	60.8
MIL-53_8	15	150	PG vessel	81.9	57.3

Table 3-2. Experimental design for MIL-53(Fe) synthesized by MW irradiation.

Sample code	MW time (min)	MW temperature (°C)	MW power (W)	Reaction vessel	Relative crystallinity (%)	Yield (%)
MIL-53_9	10	100	150	RB flask	10.2	5.1
MIL-53_10	10	100	300	RB flask	3.2	2.7
MIL-53_11	10	150	150	RB flask	15.7	41.2
MIL-53_12	10	150	300	RB flask	31.6	46.3
MIL-53_13	30	100	150	RB flask	14.5	6.3
MIL-53_14	30	100	300	RB flask	10.9	5.9
MIL-53_15	30	150	150	RB flask	36.4	36.1
MIL-53_16	30	150	300	RB flask	21.5	5.5
MIL-53_17	10	100	150	PG vessel	5.5	28.6
MIL-53_18	10	100	300	PG vessel	2.9	28.6
MIL-53_19	10	150	150	PG vessel	5.8	54.5
MIL-53_20	10	150	300	PG vessel	11.1	50.6
MIL-53_21	30	100	150	PG vessel	6.2	29.8
MIL-53_22	30	100	300	PG vessel	3.8	36.1
MIL-53_23	30	150	150	PG vessel	55.1	57.6
MIL-53_24	30	150	300	PG vessel	37.8	52.5

Table 3-3. Experimental design for MIL-53(Fe) synthesized by UTS irradiation.

Sample code	UTS time (min)	UTS amplitude	Relative crystallinity (%)	Yield (%)
MIL-53_70-1	7	40	32.9	11.8
MIL-53_70-2	7	40	39.7	11.8
MIL-53_70-3	7	40	31.9	12.2
MIL-53_71-1	15	40	34.4	18.4
MIL-53_71-2	15	40	33.1	25.1
MIL-53_71-3	15	40	35.8	27.5
MIL-53_72-1	11	50	32.6	17.3
MIL-53_72-2	11	50	35.2	17.3
MIL-53_72-3	11	50	36.8	24.5
MIL-53_72-4	11	50	33.7	25.3
MIL-53_73-1	7	60	33.5	12.5
MIL-53_73-2	7	60	38.6	17.5
MIL-53_73-3	7	60	40.8	20.4
MIL-53_74-1	15	60	34.7	20.5
MIL-53_74-2	15	60	35.7	30.2
MIL-53_74-3	15	60	37.4	30.2

overnight, yielding the as-synthesized product. Crystal morphologies of the as-synthesized products were examined with an SEM (S-2600N, Hitachi High Technologies America, Inc.). The XRPD data was collected using CuKα irradiation with a Rigaku – Miniflex powder diffractometer (Rigaku Americas Corporation, The Woodlands, TX). The particles were analyzed over the range $5° < 2\Theta < 30°$; data was processed using MDI-Jade v 7.5 software. The relative crystallinity of the products was determined by comparing the sum of the areas under two diffraction peaks ($2\Theta \approx 9.5°$ and $2\Theta \approx 19.0°$) relative to the most highly crystallized sample prepared.

3.2.2. Experimental Design

In order to optimize the synthesis of MIL-53(Fe) a statistical approach using a two level, multi factorial design was utilized. Design-Expert 7.1.5 software (StatEase, Minneapolis, USA) was used to investigate the effect of each reaction parameter on the crystallinity of the synthesized samples. CE, MW and UTS synthesis followed 2^3, 2^4 and 2^2 factorial designs, respectively. Additionally, UTS syntheses were performed in triplicate with center points incorporated. Detailed indications of the factor levels employed for each of the experimental techniques and the responses examined are summarized in Tables 3-1 to 3-3. Analysis of variance (ANOVA) was used to study which synthesis variables significantly influenced MIL-53(Fe) yield and crystallinity. Mathematical models were constructed by step-wise backward elimination of the statistically insignificant factorial terms and assigned alphabetically coded input factors (Tables 3-4 to 3-9).

Table 3-4. Summary of the ANOVA of the model equation for the product crystallinity as a function of MW irradiation.

Source	Sum of squares	Degrees of freedom	Mean square	F-value	p-value
Model	2.41	11	0.22	58.11	0.0007
A-MW time	0.41	1	0.41	107.48	0.0005
B-MW temperature	1.22	1	1.22	324.03	< 0.0001
C-MW power	0.053	1	0.053	13.99	0.0201
D-Reaction vessel	0.16	1	0.16	42.54	0.0029
AB	0.047	1	0.047	12.37	0.0245
AC	0.018	1	0.018	4.81	0.0933
AD	0.039	1	0.039	10.46	0.0318
BC	0.11	1	0.11	27.96	0.0061
BD	0.029	1	0.029	7.66	0.0504
ABC	0.12	1	0.12	32.82	0.0046
ABD	0.21	1	0.21	55.04	0.0018

Table 3-5. Summary of the ANOVA of the model equation for the product crystallinity as a function of CE heating.

Source	Sum of squares	Degrees of freedom	Mean square	F-value	p-value
Model	1.86	4	0.47	50.37	0.0044
A-CE time	0.5	1	0.5	54.5	0.0051
B-CE temperature	1.01	1	1.01	109.65	0.0019
BC	0.2	1	0.2	22	0.0183
ABC	0.14	1	0.14	15.33	0.0296

Table 3-6. Summary of the ANOVA of the model equation for the product crystallinity as a function of UTS irradiation.

Source	Sum of squares	Degrees of freedom	Mean square	F-value	p-value
Model	110.08	3	36.69	0.83	0.5043
A-UTS power	83.74	1	83.74	1.90	0.1959
B-UTS time	18.50	1	18.50	0.42	0.5308
AB	7.84	1	7.84	0.18	0.6816

Table 3-7. Summary of the ANOVA of the model equation for the product yield as a function of MW irradiation.

Source	Sum of squares	Degrees of freedom	Mean square	F-value	p-value
Model	4767.38	2	2383.69	28.19	<0.0001
B-MW temperature	2530.09	1	2530.09	29.92	0.0001
D-Reaction vessel	2237.29	1	2237.29	26.46	0.0002

Table 3-8. Summary of the ANOVA of the model equation for the product yield as a function of UTS irradiation.

Source	Sum of squares	Degrees of freedom	Mean square	F-value	p-value
Model	411.57	3	137.19	7.65	0.0049
A-UTS power	50.02	1	50.02	2.79	0.1231
B-UTS time	359.71	1	359.71	20.05	0.0009
AB	1.84	1	1.84	0.10	0.7547

Table 3-9. Summary of the ANOVA of the model equation for the product yield as a function of CE heating.

Source	Sum of squares	Degrees of freedom	Mean square	F-value	p-value
Model	1885.18	3	628.39	56.68	0.0010
A-CE time	905.25	1	905.25	81.66	0.0008
B-CE temperature	393.40	1	393.40	35.49	0.0040
AB	586.53	1	586.53	52.91	0.0019

3.3 Results and Discussion

MIL-53(Fe) crystals synthesized by means of MW and UTS irradiation were compared with those synthesized by CE heating. The XRPD patterns of the most highly crystallized as-synthesized samples (Figure 3-1) match well with those reported earlier,[8, 11, 22] confirming that the crystal phase of the products is MIL-53(Fe) as evidenced by their monoclinic symmetry (*C2/c*, No. 15). Figure 3-2 illustrates typical SEM images of crystallized MIL-53(Fe) obtained from each of the synthesis methods. Under CE conditions a bimodal distribution of particle sizes was obtained, similar to those reported earlier.[8, 22] Two different crystal morphologies can be seen coexisting - large elongated triangular prism-shaped crystals ranging in length from 25–250 μm in addition to much smaller hexagonal bipyramidal particles, approximately 2.5 μm in diameter (Figure 3-2A). Despite the wide size distribution, these phases should be MIL-53(Fe) based on the similarity of their XRPD patterns with the other synthesized samples (Figure 3-1) and with those reported earlier.[8, 11, 22] This non-uniform size distribution can likely be explained by simultaneous nucleation and crystal growth as a result of slow heat transfer and poor temperature distribution under CE heating.

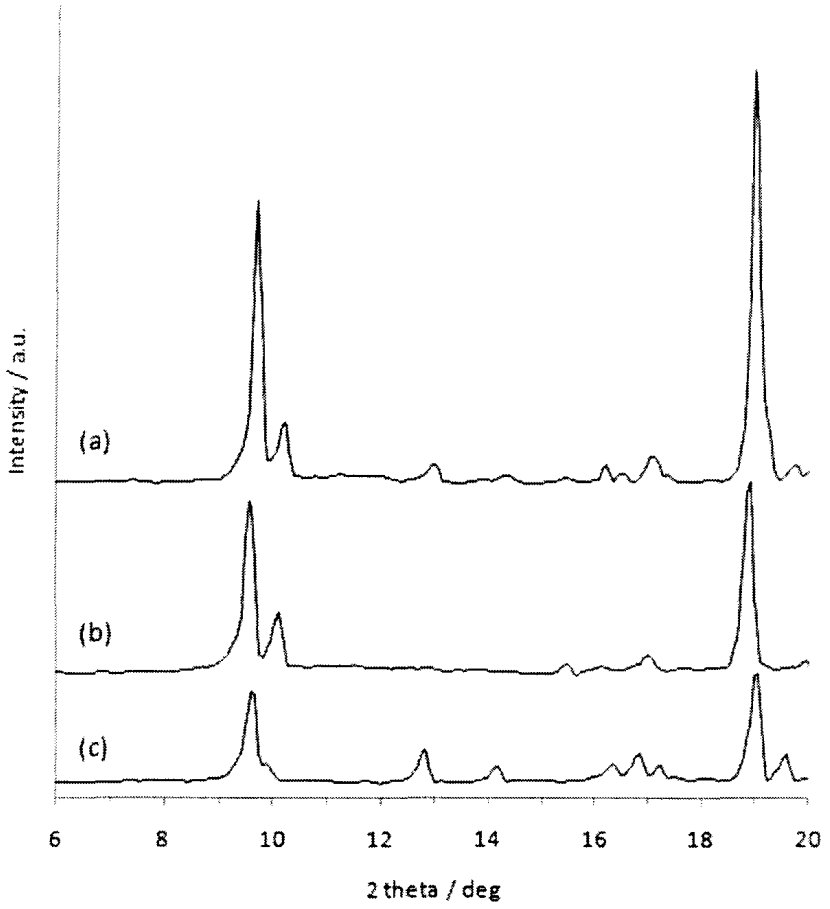

Figure 3-1. Typical XRPD patterns of fully crystallized MIL-53(Fe) synthesized by a) CE for 18 h at 150°C, b) MW for 30 min at 150°C, and c) UTS for 15 min at 60% power.

MIL-53(Fe) crystals synthesized under MW and UTS conditions produced small and homogeneous crystals, which is a clear indication of both the crystal phase purity and the efficiency of these two synthesis methods. Despite the different scales used to create the SEM images, the particles synthesized from both methods can be seen to have approximate dimensions of 0.5-1.5 μm and hexagonal bipyramidal morphologies (Figure 3-2B and Figure 3-2C). This size reduction is typical of crystals synthesized under MW or UTS conditions – a phenomenon which can be attributed to uniform and fast

nucleation. Furthermore, small MIL-53(Fe) crystals are especially effective in the fields of diffusion, catalysis, and drug adsorption/delivery.

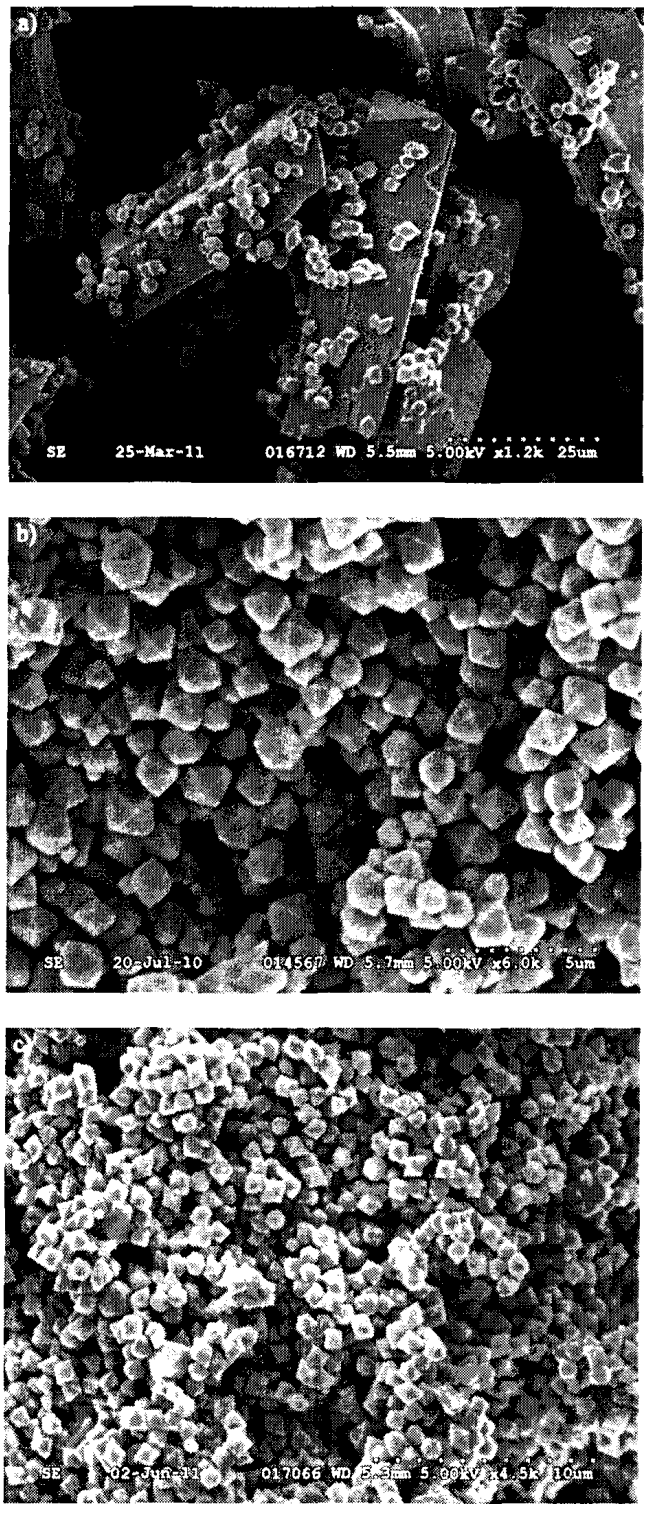

Figure 3-2. Typical SEM images of fully crystallized MIL-53(Fe) synthesized by a) CE for 18 h at 150°C (25 μm scale), b) MW for 30 min at 150°C (5 μm scale), and c) UTS for 15 min at 60% power (10 μm scale).

ANOVA was used to determine which synthesis variables significantly influenced MIL-53(Fe) yield and crystallinity utilizing models created by Design-Expert 7.1.5. According to the data in Tables 3-4 to 3-9, the only model that is not statistically significant (p-value > 0.05) is the model predicting product crystallinity from the UTS synthesis method. All of the models used for the MW and CE synthesis methods are statistically significant (p-value < 0.05). It was found that MW time (F-value = 107.48) and MW temperature (F-value = 324.03) strongly influence product crystallinity (Table 3-4). As irradiation time and temperature increase, product crystallinity increases. MW power (F-value = 13.99) and the reaction vessel (F-value = 42.54) both have a much less significant influence on product crystallinity. Likewise, for the CE synthesis method both CE time (F-value = 54.50) and CE temperature (F-value = 109.65) strongly influence product crystallinity (Table 3-5). With the UTS synthesis method, despite performing the experiments in triplicate and incorporating center points into the design, the model obtained was not significant (F-value = 0.5043) (Table 3-6). Neither the UTS time (F-value = 0.42) nor the UTS power (F-value = 1.90) were shown to have a significant influence on product crystallinity. The final model equations for each of the methods are shown in Table 3-10.

MW temperature (F-value = 29.92) and the reaction vessel (F-value = 26.46) were the factors most strongly influencing product yield (Table 3-7). Much higher yields were obtained when the temperature was 150°C and when the pressurized glass vessel was used. Under UTS irradiation, the time (F-value = 20.05) had a greater influence on product yield than power (F-value = 2.79) (Table 3-8). Longer reaction times generally resulted in higher yields. Finally, CE time (F-value = 81.66) more greatly influenced product yield than CE temperature (F-value = 35.49) (Table 3-9). Comparing the results

from each of the three synthesis methods we can see that UTS irradiation resulted in much lower yields than CE heating and MW irradiation. This is a surprising result, especially considering that higher yields are common when using MW and UTS energies instead of conventional solvothermal methods. However, this result can likely be explained by the collapse of cavitation bubbles close to or on the walls of the vial, which causes a microjet of liquid to be forced to the surface at speeds upwards of 200 m/s. Since UTS experiments were performed in an open vial much of the reaction mixture had actually escaped as mist, most likely as a result of this phenomenon. The final model equations for each of the synthesis methods are shown in Table 3-11.

Table 3-10. Final model equations for product crystallinity from CE heating, MW and UTS irradiation.

Model equations
$\log10(RC_1) = 1.37 + 0.25A_1 + 0.36B_1 + 0.16B_1C_1 - 0.13A_1B_1C_1$
$\log10(RC_2) = 1.32 + 0.16A_2 + 0.28B_2 - 0.057C_2 - 0.10D_2 + 0.054A_2B_2 - 0.034A_2C_2 + 0.050A_2D_2 + 0.081B_2C_2 + 0.043B_2D_2 - 0.088A_2B_2C_2 + 0.11A_2B_2D_2$
$RC_3 = 87.58 + 2.64A_3 - 1.24B_3 - 0.81A_3B_3$

RC_1, CE relative crystallinity; A_1, CE time; B_1, CE temperature; C_1, CE reaction vessel; RC_2, MW relative crystallinity; A_2, MW time; B_2, MW temperature; C_2, MW power; D_2, MW reaction vessel; RC_3, UTS relative crystallinity; A_3, UTS power; B_3, UTS time.

Table 3-11. Final model equations for product yield from CE heating, MW and UTS irradiation.

Model equations
$Y_1 = 47.61 + 10.64A_1 + 7.01B_1 - 8.56A_1B_1$
$Y_2 = 30.46 + 12.58B_2 + 11.82D_2$
$Y_3 = 19.84 + 2.04A_3 + 5.48B_3 - 0.39A_3B_3$

Y_1, CE yield; A_1, CE time; B_1, CE temperature; Y_2, MW yield; B_2, MW temperature; D_2, MW reaction vessel; Y_3, UTS yield; A_3, UTS power; B_3, UTS time.

Utilizing the MW synthesis method, we found that in as little as thirty seconds nucleation had occurred. The nucleation time was determined by visual observation (when the reaction mixture became cloudy). Increasing the time to ten minutes yielded highly crystalline materials; the most crystalline materials were obtained after thirty minutes. Nucleation was first observed after five minutes under UTS conditions. Since the effects of UTS time and UTS power on product crystallinity were shown to be insignificant we can conclude that after only seven minutes the products have reached their maximum crystallinity for this method. The SEM image of this product (Figure 3-3) shows crystals similar to those in Figure 3-2C, confirming the ANOVA results that time and power are insignificant. Also, the XRPD spectrum is identical to that obtained after ten minutes of MW irradiation at 150°C (Figure 3-4). To the best of the author's knowledge, these reaction times are the shortest to be reported for MIL-53(Fe) synthesis. The onset of nucleation under CE heating occurred after twenty minutes, which was forty times longer than that observed for MW irradiation. The most crystallized products were obtained after fifteen hours (30X and 128X longer than for MW and UTS irradiation, respectively), indicating that UTS and MW irradiation are quicker and more efficient alternatives to conventional electric heating.

It has generally been accepted that in the majority of cases rate enhancements under microwave conditions can be explained by the high reaction temperatures that can rapidly be attained in a microwave field.[31] This is referred to as the thermal/kinetic effect, but "specific microwave effects" caused by dielectric heating must also be considered, and these include: 1) the superheating effect, 2) the formation of microscopic hotspots, 3)

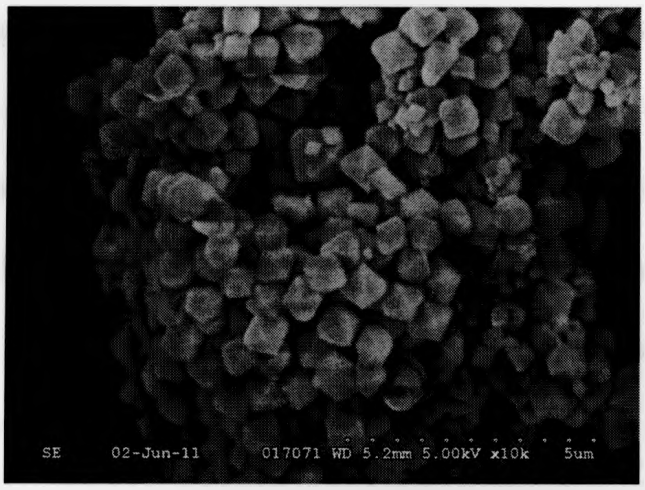

Figure 3-3. SEM image of MIL-53(Fe) synthesized by UTS for 7 min at 40% power.

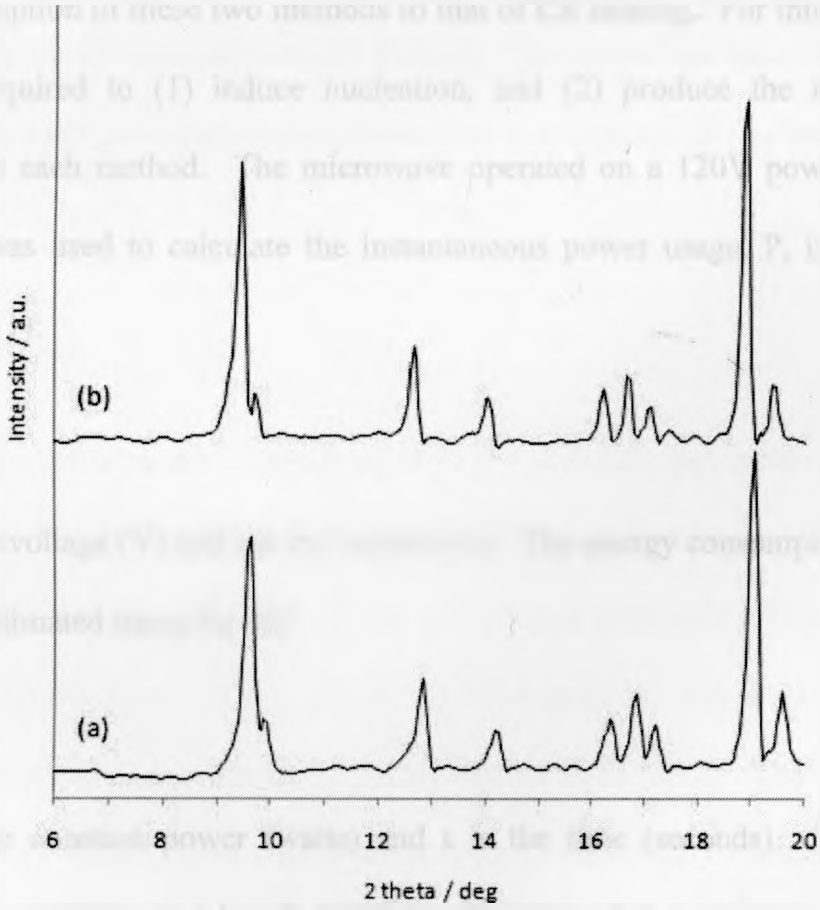

Figure 3-4. XRPD patterns of MIL-53(Fe) synthesized by a) UTS for 7 min at 40% power, and b) MW for 10 min at 150˚C.

more uniform heating, and 4) selective heating.[31] These accelerations (which are still currently the subject of considerable debate) cannot be achieved by conventional heating. There have also been suggestions of the existence of "non-thermal microwave effects" which result from a direct interaction of the electric field with dipolar molecules in the reaction medium.[31] As already mentioned, accelerated reactions seen under UTS irradiation result from "acoustic cavitation" and the implosive collapse of formed cavitation bubbles.[28]

To illustrate the efficiency of MW and UTS syntheses we compared the total energy consumption of these two methods to that of CE heating. For this we determined the energy required to (1) induce nucleation, and (2) produce the most crystalline materials from each method. The microwave operated on a 120V power source at 15 amps. This was used to calculate the instantaneous power usage, P, in watts (W), as shown by Eq. (1):

$$P = VI \tag{1}$$

where V is the voltage (V) and I is the current (A). The energy consumption, E, in joules (J) was then estimated using Eq. (2):

$$E = Pt \tag{2}$$

where P is the constant power (watts) and t is the time (seconds). The microwave required approximately 54 kJ and 3,240 kJ of energy for nucleation and maximum crystallization, respectively. As determined from ANOVA, UTS time and UTS power were not significant factors affecting product crystallinity, therefore, the method requiring the least amount of energy will be considered. The ultrasound also operated on a 120V

power source at 15 amps, which corresponded to 540 kJ and 756 kJ of consumed energy for nucleation and maximum crystallization, respectively. Compared to CE heating these energy requirements are very low. The oven operated on a 115V power source at 12 amps, and required approximately 2,500 kJ of energy to reach the temperature set point (150°C). With a power rating of 1.2 kW, an energy consumption of 4,320 kJ was required to run the oven for one hour at the set point. This corresponded to an energy consumption of 3,900 kJ and 67,000 kJ for nucleation and maximum crystallization, respectively. Considering these energy requirements, as well as the fact that both MW and UTS irradiation produced small, homogeneous crystals compared to the two populations of crystals obtained from CE heating, it is evident that these two technologies are quicker, more efficient and greener alternatives to conventional synthesis methods.

3.4. Conclusions

MIL-53(Fe), a metal-organic framework (MOF) material, has been synthesized by conventional electric (CE) heating, ultrasound (UTS) and microwave (MW) irradiation. Crystals were synthesized in as quickly as ten minutes from MW irradiation and in as little as seven minutes from UTS synthesis. To the best of the author's knowledge, these are the quickest crystallization times to be reported for MIL-53(Fe). The most crystalline materials were synthesized after fifteen hours from CE heating. Crystals produced from UTS and MW conditions were small and homogeneous, whereas those produced from CE heating had two different morphologies and sizes. The observed size reduction of crystals synthesized under UTS and MW conditions can be attributed to fast and uniform

nucleation. The non-uniform size distribution of particles produced from CE heating is likely a result of the method's inherently slow heat transfer and a poor temperature distribution within the reaction mixture. ANOVA was used to create models to determine which synthesis variables significantly influenced product yield and crystallinity. UTS irradiation resulted in much lower yields than CE heating and MW irradiation, a phenomenon that can be explained by microjets of liquid being forced to the surface of the reaction mixture during synthesis and escaping into the atmosphere. For both the MW irradiation and CE heating methods, time and temperature were shown to have a significant influence on product crystallinity. However, for the UTS method neither the time nor the power had a significant influence on crystallinity, suggesting that the products reached their maximum crystallinity for this method very shortly after nucleation. Furthermore, UTS and MW irradiation consume far less energy than CE heating, which confirms that these two technologies are quicker, more efficient and greener alternatives to conventional synthesis methods.

3.5. References

(1) Hu, Y. H.; Zhang, L. *Adv. Mater.* **2010**, *22*, E117-E130.

(2) Latroche, M.; Surblé, S.; Serre, C.; Mellot-Draznieks, C.; Llewellyn, P. L.; Lee, J. -.; Chang, J. -.; Sung, H. J.; Férey, G. *Angew. Chem. Int. Ed.* **2006**, *45*, 8227-8231.

(3) Rosi, N. L.; Eckert, J.; Eddaoudi, M.; Vodak, D. T.; Kim, J.; O'Keeffe, M.; Yaghi, O. M. *Science* **2003**, *300*, 1127-1129.

(4) Rowsell, J. L. C.; Spencer, E. C.; Eckert, J.; Howard, J. A. K.; Yaghi, O. M. *Science* **2005**, *309*, 1350-1354.

(5) Farrusseng, D.; Aguado, S.; Pinel, C. *Angew. Chem. Int. Ed.* **2009**, *48*, 7502-7513.

(6) Horcajada, P.; Surblé, S.; Serre, C.; Hong, D.; Seo, Y.; Chang, J.; Grenèche, J.; Margiolaki, I.; Férey, G. *Chem. Commun.* **2007**, 2820-2822.

(7) Lee, J.; Farha, O. K.; Roberts, J.; Scheidt, K. A.; Nguyen, S. T.; Hupp, J. T. *Chem. Soc. Rev.* **2009**, *38*, 1450-1459.

(8) Horcajada, P., et al *Nat. Mater.* **2010**, *9*, 172-178.

(9) Horcajada, P.; Serre, C.; Vallet-Regí, M.; Sebban, M.; Taulelle, F.; Férey, G. *Angew. Chem. Int. Ed.* **2006**, *45*, 5974-5978.

(10) Taylor-Pashow, K. M. L.; Della Rocca, J.; Xie, Z.; Tran, S.; Lin, W. *J. Am. Chem. Soc.* **2009**, *131*, 14261-14263.

(11) Horcajada, P.; Serre, C.; Maurin, G.; Ramsahye, N. A.; Balas, F.; Vallet-Regí, M.; Sebban, M.; Taulelle, F.; Férey, G. *J. Am. Chem. Soc.* **2008**, *130*, 6774-6780.

(12) Combelles, C.; Yahia, M. B.; Pedesseau, L.; Doublet, M. *J. Phys. Chem. C* **2010**, *114*, 9518-9527.

(13) Férey, G.; Millange, F.; Morcrette, M.; Serre, C.; Doublet, M.; Grenèche, J.; Tarascon, J. *Angew. Chem. Int. Ed.* **2007**, *46*, 3259-3263.

(14) Liu, B.; Shioyama, H.; Jiang, H.; Zhang, X.; Xu, Q. *Carbon* **2010**, *48*, 456-463.

(15) Taylor, K. M. L.; Rieter, W. J.; Lin, W. *J. Am. Chem. Soc.* **2008**, *130*, 14358-14359.

(16) Humphrey, S. M.; Angliss, T. J. P.; Aransay, M.; Cave, D.; Gerrard, L. A.; Weldon, G. F.; Wood, P. T. *Z. Anorg. Allg. Chem.* **2007**, *633*, 2342-2353.

(17) Maspoch, D.; Ruiz-Molina, D.; Veciana, J. *J. Mater. Chem.* **2004**, *14*, 2713-2723.

(18) Zhang, X.; Hao, Z.; Zhang, W.; Chen, X. *Angew. Chem. Int. Ed.* **2007**, *46*, 3456-3459.

(19) Férey, G. *Chem. Soc. Rev.* **2008**, *37*, 191-214.

(20) Mueller, U.; Schubert, M.; Teich, F.; Puetter, H.; Schierle-Arndt, K.; Pastré, J. *J. Mater. Chem.* **2006**, *16*, 626-636.

(21) Rybak, J.; Schellenberg, I.; Pöttgen, R.; Müller-Buschbaum, K. *Z. Anorg. Allg. Chem.* **2010**, *636*, 1720-1725.

(22) Haque, E.; Khan, N.; Park, H. J.; Jhung, S. H. *Chem. Eur. J.* **2010**, *16*, 1046-1052.

(23) Qiu, L.; Li, Z.; Wu, Y.; Wang, W.; Xu, T.; Jiang, X. *Chem. Commun.* **2008**, 3642-3644.

(24) Sabouni, R.; Kazemian, H.; Rohani, S. *Chem. Eng. J.* **2010**, *165*, 966-973.

(25) Jhung, S. H.; Lee, J.; Yoon, J. W.; Serre, C.; Férey, G.; Chang, J. *Adv. Mater.* **2007**, *19*, 121-124.

(26) Klinowski, J.; Almeida Paz, F. A.; Silva, P.; Rocha, J. *Dalton Trans.* **2011**, *40*, 321-330.

(27) Lin, Z.; Wragg, D. S.; Morris, R. E. *Chem. Commun.* **2006**, 2021-2023.

(28) Leonelli, C.; Mason, T. J. *Chem. Eng. Process.* **2010**, *49*, 885-900.

(29) De La Hoz, A.; Díaz-Ortiz, Á.; Moreno, A. *Chem. Soc. Rev.* **2005**, *34*, 164-178.

(30) Scherb, C.; Schödel, A.; Bein, T. *Angew. Chem. Int. Ed.* **2008**, *47*, 5777-5779.

(31) Kappe, C. O. *Angew. Chem. Int. Ed.* **2004**, *43*, 6250-6284.

4. MIL-53(Fe), MIL-101, and SBA-15 as potential platforms for drug delivery

4.1. Introduction

Despite our remarkable understanding of the biological processes responsible for many diseases, progress in their treatment has moved slowly. The use of novel drug delivery systems (DDSs) can alleviate the shortcomings of conventional therapeutics by allowing for a stability of the drug plasmatic levels through a controlled release rate. This eliminates the need for high doses, thus increasing the efficiency and decreasing the toxicity of conventional drugs. Coupled with the fact that the development of new bioactive compounds is a time-consuming, complex and costly process, the interest in nanoparticle-based therapeutics has been increasing over the last few years.[1] Currently, materials being used for delivery are classified as either organic or inorganic systems, composed of an active agent incorporated within the nanoparticle carrier. Systems that have already been extensively researched include polymeric nanoparticles, micelles, liposomes, and microporous zeolites, but are for the most part unsatisfactory. Organic systems, including biocompatible dendritic macromolecules or polymers, can be encapsulated with a wide array of drugs, however in the absence of a well-defined porosity they lack a controlled release.[2]

A third type of delivery route – the "hybrid" route – has recently been proposed.[3] Porous metal-organic frameworks (MOFs), which fall under this category, exhibit many desirable characteristics as drug carriers. They can combine exceptionally high surface areas and porosities with the presence of tunable inorganic, organic and functional groups, thus achieving both a high drug loading and a controlled release of therapeutic agents to targeted areas of the body. Their success is attributed to their remarkable porosity, biodegradability, and the tunability of their pore sizes – a result of the limitless choice of

organic bridging ligands and metal centers that make up their structures. As a result a huge number of three-dimensional open-framework structures are possible, with some of the highest surface areas seen for crystalline inorganic solids and porosities spanning those exhibited by microporous zeolites and mesoporous silica materials.[3] Not only can their connectivities be modified to accommodate the physicochemical properties of hosted drug molecules, but some MOFs have a high structural flexibility and robustness, enabling them to adapt their porosity to the shape and size of organic molecules.[4, 5]

MIL-53 is an example of such an MOF. The hydrated forms MIL-53(Al, Cr) solids exhibit a reversible pore opening which involve atomic displacements by 0.52 nm upon dehydration, corresponding to an increase in pore volume up to 45%. The dehydrated form of MIL-53(Fe), however, remains closed. This material only opens its pores during the adsorption of organic molecules, and for this reason exhibits no porosity for nitrogen at 77 K.[5] A combined XRPD/NMR/modeling study on MIL-53(Al) revealed that hydrogen bonding interactions between the hydrogens of the water molecules trapped within the channels and the carboxylate groups of the BDC linkers are responsible for contraction of the pores.[6] This reversible "breathing" effect of certain flexible MOFs has been shown to adapt the cell volumes of their structures by 50-230% without any noticeable change to their structural integrities.[5]

MIL-53(Fe) was previously used as a matrix for the adsorption and *in vitro* delivery of ibuprofen. Horcajada et al. (2008) showed that MIL-53(Fe) adsorbs 0.21 g ibuprofen/g MOF and has a very slow and complete delivery of ibuprofen in simulated body fluid at 37°C over a three week period with an unusual zero-order kinetics drug release. They attributed this slow release to the flexibility of the framework, which allows it to

maximize bonding interactions while still minimizing steric hindrance. Density functional theory (DFT) calculations revealed that the most likely interaction between the framework and the entrapped ibuprofen molecules involved a strong hydrogen bonding between the oxygen of the carboxylic group of ibuprofen and the hydroxyl group of the framework located at the surface of the pores. Weaker van der Waals and/or CH-π interactions were also found between the hydroxyl and the methyl groups of ibuprofen and the organic linker of MIL-53(Fe).[5]

However, the main drawback of using microporous (pore diameters $\leq$2 nm) MOFs such as MIL-53(Fe) is that the choice of incorporated species is restricted to relatively small drug molecules which are able to fit inside the frameworks, such as ibuprofen. To solve this problem, Ferey and co-workers[2] demonstrated drug delivery using rigid mesoporous (pore diameters between 2 and 50 nm) MOFs, MIL-100 and MIL-101, which proved suitable due to their well-defined, ordered porosity. MIL-101 has a Langmuir surface area of 5500 m^2/g, and exhibited a very high drug storage capacity of an unprecedented 1.4 g of ibuprofen per gram of MOF. The complete release of Ibuprofen was achieved under physiological conditions after six days. MIL-101 possesses large mesoporous cages (~2.9 and 3.4 nm), and large window openings of 1.2 nm and 1.6 nm for the pentagonal and hexagonal windows, respectively. As evidenced by X-ray powder diffraction (XRPD), even at these high loadings there was no apparent loss of crystallinity or decomposition of the framework structure. Taking into consideration the sustained release times and the high drug loadings, the MIL family is a unique candidate for storage and controlled release of biologically important molecules.

Long blood circulation times of MOFs are crucial for *in vivo* delivery. It is well known that particles coated with polyethylene glycol (PEG) chains on their surfaces exhibit "stealth" properties, eliminating rapid uptake by the reticuloendothelial system (RES) and short blood circulation times. A recent study showed that PEGylated single-walled carbon nanotubes (SWNTs) exhibited remarkably long blood circulation times ($t_{1/2}$ = 22.1 h) upon intravenous injection into mice, far exceeding the previous record of 5.4 h.[7] It has been roughly estimated that a circulation $t_{1/2}$ of 12-20 h in mice translates into approximately 40-60 h in humans.[8] Horcajada et al. (2010) showed that MOFs not protected by a PEG coating were rapidly sequestered from the blood by the RES and had accumulated in the spleen and liver. Thus, PEGylation of MOFs and SMMs will be an important step for prolonging *in vivo* release profiles.

The aim in this study was to evaluate to what extent reported sustained release times and high drug loadings were applicable to a series of three compounds with a high degree of physicochemical diversity. The drug loading and release behaviour of acetaminophen, stavudine and progesterone encapsulated in either MIL-53(Fe), MIL-101, or a silica-based ordered mesoporous material (SMM), SBA-15 were evaluated. SMMs are characterized by their homogeneous and ordered pore networks, mechanical strength, thermal and pH stability, biocompatibility and silanol-containing surfaces that can be functionalized to allow for a better control over drug delivery.[9, 10] SBA-15 consists of a hexagonally-ordered array of tunable pores which can range in diameter from 5 to 30 nm. It also has a high surface area ranging from 600 to 1000 m^2/g, and a large pore volume ranging from 0.8 to 1.2 cm^3/g.[11] These properties enable drug loadings upwards of 50 wt%.[12] The structure of MIL-53(Fe) is composed of parallel trans corner-sharing iron(III)

octahedral chains, each of which are cross-linked by 1,4-benzenedicarboxylate (BDC) anions to form a one-dimensional lozenge-shaped pore channel system. As previously mentioned, MIL-53(Fe) only opens its pores in the presence of guest molecules, therefore, unlike MIL-101 it does not have a high surface area. MIL-53 has the formula $M^{III}(OH)[(O_2C\text{-}C_6H_4\text{-}CO_2)]\cdot H_2O$ (where M = Al^{3+}, Cr^{3+} or Fe^{3+}) with pores of free diameter close to 1.3 nm.[5] MIL-101 is built up from trimers of chromium octahedra, which are also cross-linked by BDC, and has the formula $Cr_3OX(H_2O)_2[(O_2C)\text{-}C_6H_4\text{-}(CO_2)]_3\cdot nH_2O$ (where X = F,OH and *n* is ~25).[13]

In this study we have attempted to use an incipient wetness impregnation procedure to load the materials with the model drugs – an impregnation procedure which has not yet been reported for MOFs. In this procedure a precise amount of highly concentrated organic drug solution has been used with great success to fill the mesopores of SMMs.[11, 14, 15] This is a more convenient method than the conventional loading procedure, which involves adsorption from an organic solution followed by cumbersome and time-consuming equilibration and filtration steps to recover the loaded carrier particles.[14] Furthermore, particles can be loaded with a precisely known quantity of drug molecules using the incipient wetness procedure. In contrast, the adsorbed drug quantity in the conventional loading procedure is unknown.

As already mentioned, MIL-101 and SBA-15 have been shown to achieve drug loadings upwards of 50 wt%. However, MIL-53(Fe) previously achieved a maximum drug loading of 20 wt% for ibuprofen.[5] Thus, in this study each of the materials was impregnated with a targeted drug loading of 20 wt%. The loaded materials were

evaluated for their release profiles under simulated physiological conditions in phosphate buffered saline (PBS).

4.2. Model Drugs

Three drugs were selected based upon their diverse physicochemical properties, in order to obtain a test series with a high degree of diversity (Table 4-1). Acetaminophen is an analgesic which distributes rapidly and evenly throughout most tissues. Like stavudine, it is orally administered, and has a bioavailability ranging from 70 to 90% and a plasma half-life ranging from 1.9 to 2.5 hours.[16] Stavudine is a nucleoside reverse transcriptase inhibitor (NRTI) used for the treatment of human immunodeficiency virus (HIV). It was approved for use by the Food and Drug Administration (FDA) in 1994. Seven NRTIs have been approved for use, but in general they have limited stability and poor bioavailability. As an NRTI, stavudine has a reasonably high bioavailability of about 80%. However, its half-life in systemic circulation is about 1 to 1.6 hours, which necessitates frequent doses, as well as severe dose-dependent side effects.[17] Progesterone is a steroid hormone belonging to the progestogen class that naturally occurs in both males and females. It is administered to individuals with a long-term decline of natural levels in the body, as well as to patients with acute situations. Like all steroid hormones it is hydrophobic, therefore, when taken orally it has a poor bioavailability and a half-life upwards of 50 hours.[18] The dimensions of each drug were determined using ChemDraw. Acetaminophen (≈ 0.82 x 0.49 nm), progesterone (≈ 1.12 x 0.58 nm), and stavudine (≈ 0.85 x 0.58 nm) were all determined to have favourable dimensions for incorporation

within the pores of each nanomaterial. Acetaminophen was purchased from Sigma-Aldrich (St. Louis, MO); progesterone from Calbiochem (La Jolla, CA); stavudine was generously donated by Apotex PharmaChem Inc. (Brantford, ON).

Table 4-1. Structural formulas of the model drugs, the wavelengths used for quantification and the media used for *in vitro* drug release experiments.

Compound	Structural Formula	Wavelength for Quantification (nm)	Release Medium
Acetaminophen	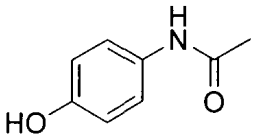	244	PBS
Progesterone	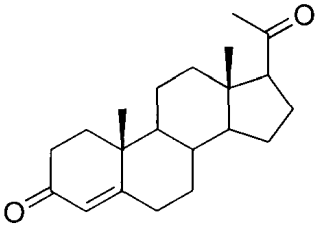	245	PBS + 0.5% SDS
Stavudine	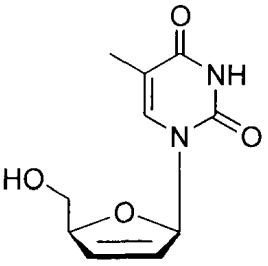	266	PBS

4.3. Experimental Section

4.3.1. Synthesis of Materials

MIL-53(Fe) was synthesized with the same batch composition reported by Horcajada et al. (2010) from a mixture of ferric chloride hexahydrate ($FeCl_3 \cdot 6H_2O$, Caledon, 97.0-102.0%), 1,4-benzenedicarboxylic acid (H_2BDC, Alfa Aesar, ≥98%), and *N,N*-

dimethylformamide (DMF, Caledon, ≥99.8%). All of the chemicals were used as purchased without any further purification. The reaction mixture was prepared in a 50 mL glass beaker by dissolving 5 mmol of $FeCl_3 \cdot 6H_2O$ and 5 mmol of H_2BDC in 25 mL of DMF. The beaker was placed in the probe of an ultrasonic generator (VCX 500, Sonics & Materials, Inc., Newtown, CT) and subjected to ultrasonic irradiation for 10 min at 70% of the maximum power; the temperature was not controlled. The as-synthesized product was prepared by centrifugation, DMF washing, and overnight drying. Prior to drug loading, the as-synthesized sample was subjected to three activation steps. To remove DMF from the pores the powder was heated for 24 h at 150°C in an oven (DKN 400, Yamato Scientific America, Inc., Santa Clara, CA) and cooled down to room temperature. To remove traces of DMF, the powder was then stirred in a large volume of deionised water and filtered. Finally, the powder was dehydrated in the oven at 150°C for 24 h to remove water from the pores.

MIL-101 was synthesized hydrothermally according to procedures previously reported[2, 13] from a mixture of chromic nitrate nonahydrate ($Cr(NO_3)_3 \cdot 9H_2O$, Caledon, ≥98.0%), 1,4-benzenedicarboxylic acid (H_2BDC, Alfa Aesar, ≥98.0%), hydrofluoric acid (HF, EMD Chemicals Inc.), and H_2O. A solution containing 3 mmol of $Cr(NO_3)_3 \cdot 9H_2O$, 3 mmol of H_2BDC, 0.1 mL of HF (52% in water), and 14.4 mL of H_2O was introduced into a 25 mL Teflon liner. The mixture was placed in a steel autoclave and heated in a furnace (Lindberg Blue M, Thermo Fisher Scientific Inc.) for 10 h at 220°C with a heating ramp of 1 h. After a cooling ramp of 3 h back down to room temperature a significant amount of free terephthalic acid remained. The reaction mixture was filtered and then washed with DMF to eliminate excess terephthalic acid, followed by a wash step with H_2O to

remove DMF. To remove the remaining terephthalic acid present inside the pores of MIL-101, a two-step process involving solvent treatments and a fluoride-anion exchange step was performed. The MIL-101 powder was added to 50 mL H_2O in a 100 mL round bottom flask and refluxed for 5 h, followed by centrifugation and drying in the oven overnight at 100°C. Next, the powder was added to 50 mL ethanol in a round bottom flask and refluxed for 3 h. Following centrifugation and a wash step with ethanol the powder was placed in the oven at 100°C overnight. The powder was then added to an aqueous mixture containing 70 mg of ammonium fluoride (NH_4F, Alfa Aeasar, ≥98.0%) dissolved in 50 mL of H_2O in a 100 mL round bottom flask. The flask was attached to a condenser and allowed to reflux for 24 h. The mixture was filtered with 1 μm retention filter paper and the powder was washed four times with 50 mL of warm water to remove traces of NH_4F. Finally, the solid was dried in a vacuum oven (Napco E Series) at 100°C overnight under reduced pressure to obtain activated, fine powdered MIL-101.

SBA-15 was synthesized according to procedures described elsewhere.[11, 14] Four grams of triblock copolymer Pluronic 123 (P-123, Sigma-Aldrich) was added to an aqueous HCl solution (2 M, 150 mL), and the resulting mixture was stirred until P-123 completely dissolved. Once P-123 had dissolved, stirring was allowed to continue while 8.6 g of tetraethyl orthosilicate (TEOS, Sigma-Aldrich, ≥99.0%) was added drop-wise during 10 min. The mixture was then transferred to a 500 mL Teflon bottle and put in the oven at 100°C for 24 h, followed by filtration and a wash step with H_2O. Finally, the silica powder was calcined at 500°C for 5 h with a 5 h heating ramp and a 5 h cooling ramp to remove P-123 from the pores.

4.3.2. Drug Loading

All model drugs were loaded onto each of the synthesized nanomaterials using an incipient wetness impregnation procedure similar to that previously reported,[11, 14, 15] in order to obtain a drug loading of 20 wt%. A concentrated solution of the drug was prepared and added to 50 mg of MIL-53(Fe), or to 100 mg of MIL-101 or SBA-15. Concentrated drug solutions were as follows: 50 mg/mL of stavudine in methanol, 30 mg/mL of acetaminophen in ethanol, and 50 mg/mL of progesterone in dichloromethane. The solvents and the concentrations used were selected based on the solubilities of the drugs. In a typical loading procedure, the drug solution was added to the powder, which was intensively mixed with a spatula until seemingly dry, and subsequently placed in the vacuum oven at 70°C under reduced pressure for 24 h to remove any residual solvent. The mass of the samples was then recorded to determine the drug loading.

4.3.3. Physicochemical Characterization

In order to study the physical state of the drugs in the porous framework, nitrogen adsorption, differential scanning calorimetry (DSC) and XRPD analyses were performed. Nitrogen adsorption measurements were recorded with a BET analyzer (Micromeritics ASAP 2010). All samples were degassed for 5 h at 40°C before analysis. The temperature was kept low to avoid degradation of the drugs. Surface area and total pore volume measurements were recorded. DSC analysis was performed with a Mettler Toledo DSC 822^{e} (Mississauga, ON). Samples were heated from 25 to 200°C at 2°C/min under nitrogen atmosphere at a flow rate of 100 mL/min. The samples were analyzed in

sealed aluminum crucibles with a small pin hole pressed through the top. The XRPD data was collected using CuKα irradiation with a Rigaku – Miniflex powder diffractometer (Rigaku Americas Corporation, The Woodlands, TX). MIL-101 and SBA-15 samples were analyzed over the range $2° < 2\Theta < 30°$; MIL-53(Fe) samples were analyzed over the range $5° < 2\Theta < 30°$. Data was processed using MDI-Jade v 7.5 software.

4.3.4. *In Vitro* Drug Release

In order to study release profiles of the drugs, approximately 5 mg of samples loaded with either stavudine or acetaminophen were suspended in 15 mL of PBS. Since progesterone is poorly soluble in aqueous media, 0.5 wt% of the surfactant sodium dodecyl sulphate (SDS) was added to PBS to maintain sink conditions. The mixtures were placed in a rotary mixer rotating at a frequency of 100 rpm and suspended in a water bath (37°C) for the duration of the experiment. Two millilitre samples were withdrawn with a syringe at predetermined time intervals, filtered through a 0.45 μm polytetrafluoroethylene (PTFE) membrane filter, and immediately replaced with 2 mL of fresh PBS. Quantification of the drug in solution was performed by UV-spectrometry with a Cary 100 UV-Visible Spectrophotometer using a quartz cuvette. The wavelengths used for quantification of the drugs were selected from the position of the absorption maximum for each of the compounds, which was 266 nm for stavudine, 244 nm for acetaminophen, and 245 nm for progesterone. Samples were diluted four-fold before their concentrations were determined by UV-spectrometry. Their concentrations were calculated by interpolation from the calibration curves using linear regression models. The stavudine and

progesterone calibration curves were linear over the concentration range of 4.6 to 20 μg/mL and were each constructed by the average of three replicates. The calibration curve for acetaminophen was constructed by the average of three replicates over the concentration range of 2.2 to 15 μg/mL, and was also linear. All drug release experiments were performed in duplicate under sink conditions, and the mean values were used to calculate the cumulative drug release after each time interval.

4.4. Results and Discussion

Prior to drug loading, the porosities of MIL-53(Fe), MIL-101 and SBA-15 were evaluated by nitrogen adsorption analyses. The porosity, surface area and drug loading measurements are presented in Table 4-2. The surface area of each material was estimated using the BET model, as shown by Eq. (1):

$$\frac{P}{v(Po-P)} = \frac{1}{vc} + \frac{c-1}{vmc}\left(\frac{P}{Po}\right) \tag{1}$$

where P and Po are the equilibrium and the saturation pressure of adsorbates at the temperature of adsorption, v is the adsorbed gas quantity, vm is the monolayer adsorbed gas quantity, and c is the BET constant.[19] As expected, the surface area of MIL-53(Fe) is very low. This is attributed to the fact that MIL-53(Fe) does not have a residual porosity. The mesopore volumes and surface areas of MIL-101 and SBA-15 were estimated to be 0.71 and 1.23 cm^3/g, and 2212 and 906 m^2/g, respectively, which are ideal for high drug loadings. Drug-loaded MIL-101 and SBA-15 materials were also characterized by nitrogen adsorption to investigate the effect on porosity and surface area compared to the

empty carriers. Each of the drug-loaded materials had significantly decreased mesopore volumes and surface areas compared to the empty carriers (Table 4-2), evidencing successful introduction of the drugs into the pores. Nitrogen adsorption analyses were not performed on drug-loaded MIL-53(Fe) samples. As seen in Table 4-2, compared to the initially intended theoretical loadings of 20 wt%, the measured loadings were very close. The ability to carefully control the drug loading is an obvious advantage of the incipient wetness loading procedure over the conventionally used solvent impregnation method. The loading time of this method is only dependent on the complete evaporation of the solvent, therefore it is much quicker than the solvent method. Additionally, a very small volume of solvent is required, so it is also a cost-effective technique.

Table 4-2. BET surface area (S_{BET}), mesopore volume (V_{mes}) and drug loading information of drug-free and drug-loaded MIL-53(Fe), MIL-101 and SBA-15 samples.

	V_{mes} (cm^3/g)	S_{BET} (m^2/g)	Drug loading (%)
MIL-53(Fe)	0	15	0
MIL-53(Fe)-aceta	-	-	19.7
MIL-53(Fe)-pro	-	-	19.6
MIL-53(Fe)-stav	-	-	20.0
MIL-101	0.71	2213	0
MIL-101-aceta	0.34	1418	19.7
MIL-101-pro	0.28	1290	20.3
MIL-101-stav	0.31	1351	20.0
SBA-15	1.23	906	0
SBA-15-aceta	0.86	420	19.6
SBA-15-pro	-	298	20.2
SBA-15-stav	0.79	402	20.2

DSC is a convenient technique to elucidate the physical state of the drug molecules in the drug-loaded samples. It has been shown that the thermodynamic properties of molecules confined to porous solids are different from those of the bulk phase, and that below a

critical pore diameter, crystallization of entrapped molecules is suppressed.[20, 21] A recent study showed that at low temperatures, ibuprofen recrystallized in MCM-41 with a pore diameter of 11.6 nm. However, when the pore diameter was decreased to 3.5 nm it existed in a glassy state, since the narrow pore size prevented the molecules from arranging themselves into a crystal lattice.[22] Crystallization inhibition is typical when organic molecules are confined to spaces that are less than 20 times larger than the molecular size.[23] DSC can detect these phase transitions, allowing us to determine the physical nature of the drug-loaded samples. Thus, we can utilize DSC to supplement the results from BET analysis, which indicated that the drug molecules had successfully been incorporated into each of MIL-101 and SBA-15. Since drug-free and drug-loaded MIL-53(Fe) samples do not contain a residual porosity, DSC is an invaluable technique to determine if the drug load had successfully been adsorbed within the microporous MIL-53(Fe) framework.

Figure 4-1 depicts the DSC thermograms of acetaminophen, progesterone and stavudine in their crystalline forms and in the drug-loaded samples. Neither at the bulk melting point of the drugs nor at elevated or depressed temperatures do the drug-loaded MIL-101 and SBA-15 thermograms show detectable signs of melting. These results can be attributed to a complete loss of crystallinity of the confined drug molecules, confirming the earlier BET results that the drugs have been successfully incorporated within the pores. Drug-loaded MIL-53(Fe) samples, however, do exhibit melting at the characteristic melting points of the respective crystalline drugs. This suggests that either a partial amount or the entire amount of each drug load deposited onto the surface of the nanomaterials. This is not surprising, since MIL-53(Fe) is a microporous material with a

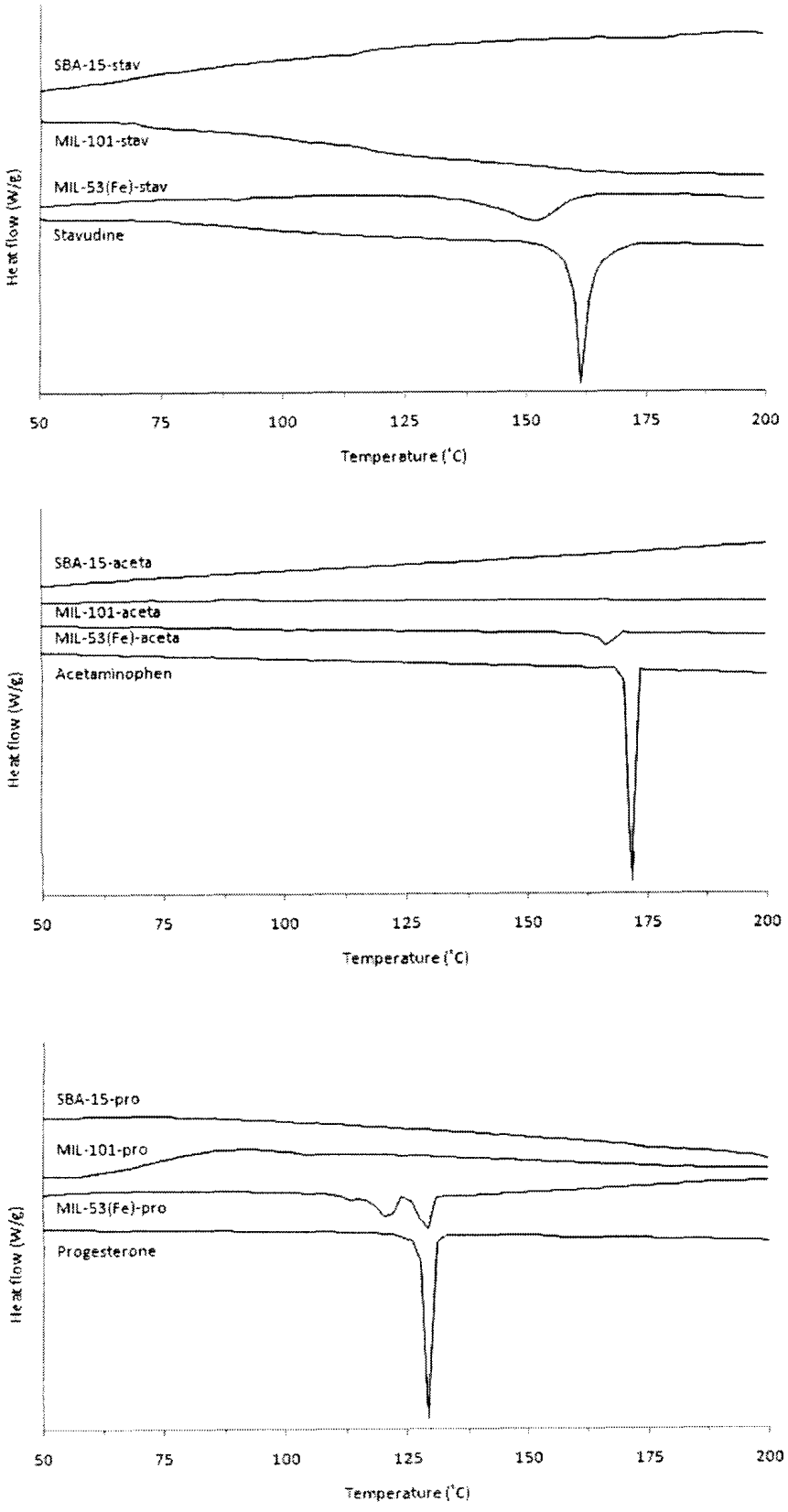

Figure 4-1. DSC thermograms of acetaminophen, progesterone and stavudine in their crystallized forms and of drug-loaded MIL-53(Fe), MIL-101 and SBA-15 materials.

much smaller pore diameter and volume than both MIL-101 and SBA-15. In its most expanded form, the pore diameter of MIL-53(Fe) is approximately 1.3 nm.[5] This is large enough to accommodate all three model drugs, which suggests that the pores are completely filled with excess molecules deposited onto the surface. The pore volume of MIL-53(Fe) is likely too small to accommodate a drug load of 20 wt%.

XRPD analyses were also performed to confirm that the structure of the materials had remained unchanged after incorporation of the drug molecules (Figure 4-2). From these spectra two conclusions can be made: (1) that the crystal structures of the materials remain unchanged, and (2) that the confined drug molecules are in an amorphous state. The diffraction peaks of the parent structures are retained in the drug-loaded samples of MIL-53(Fe) and MIL-101, indicating that there was no apparent loss of crystallinity or decomposition of the framework structure. Although the XRPD spectra of the crystallized drug molecules are not shown, we can clearly see that no new diffraction peaks were introduced into the drug-loaded samples. This is in agreement with the DSC results for MIL-101 and SBA-15, confirming that the confined drugs are in an amorphous state.

The *in vitro* release of each of the drugs from the drug-loaded materials was investigated next (Figure 4-3 to 4-5). There were two distinctive release stages for both MOF delivery systems. Initially there was a "burst" release in which a majority of the drug load was released very quickly, followed by a slow and sustained diffusion-controlled release period. Already after 30 min, the cumulative release of each of the drugs from MIL-101 had exceeded 90%. The release of progesterone from MIL-53(Fe) in the first 30 min was similar to the release from MIL-101, however, the burst release of acetaminophen and of

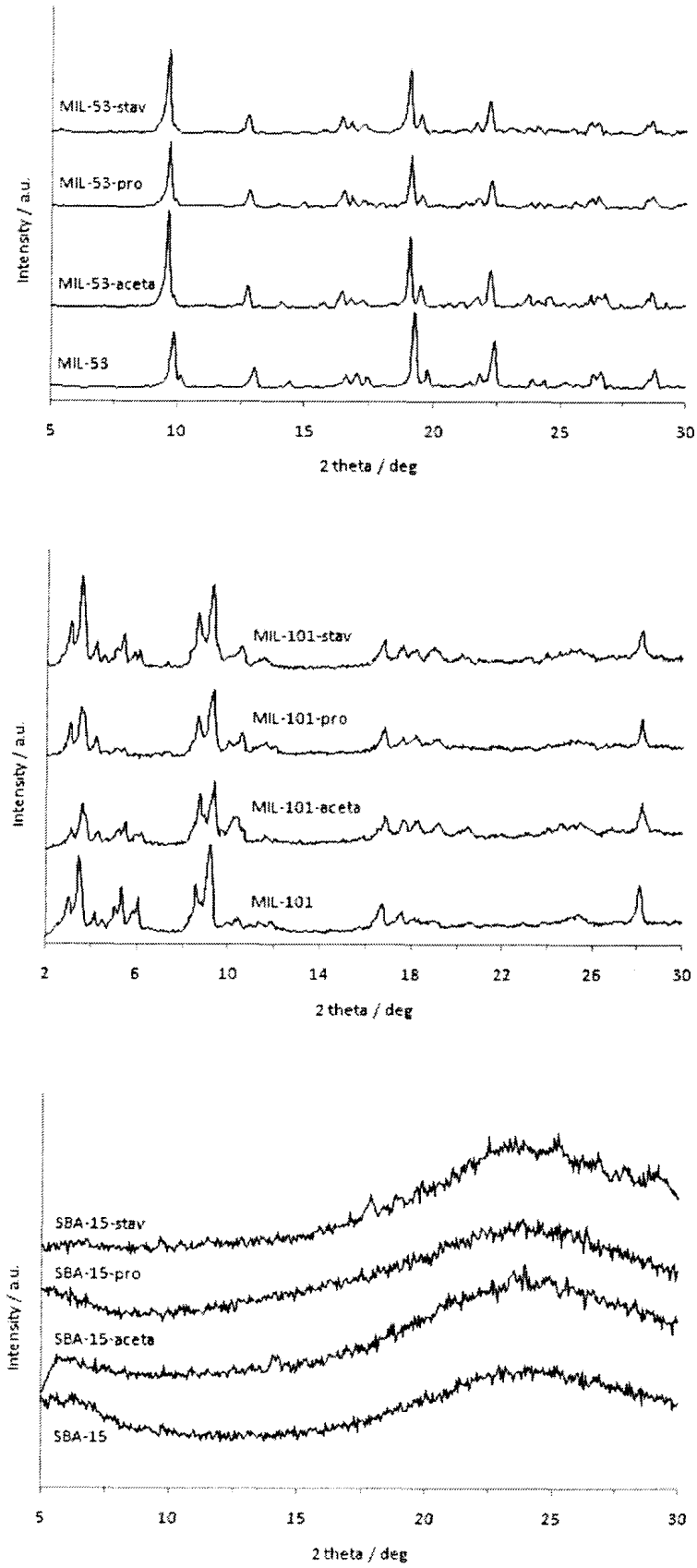

Figure 4-2. XRPD patterns of drug-free and drug-loaded MIL-53(Fe), MIL-101 and SBA-15 materials.

stavudine from MIL-53(Fe) was less. This burst release from MIL-53(Fe) suggests that the drugs had adsorbed onto the external surface of the particles, which confirms the DSC results.

The portion of the loaded drugs that had successfully been incorporated into the pores can also be estimated from the burst release amount. Approximately 80% of the total acetaminophen amount was rapidly released, suggesting that 20% of the total payload was successfully incorporated within the pores. Likewise, approximately 16% and 7% of stavudine and progesterone payloads, respectively, were successfully incorporated into MIL-53(Fe). Although these results are just an approximation, they seem to suggest that the incorporated amount is size-dependent, since the size of the model drugs increases in the order: acetaminophen < stavudine < progesterone. The approximations may also be an underestimate when considering that a portion of the successfully incorporated drug amount may have been released within these first few moments of the experiments. This amount, however, is likely very small due to the strong host-guest interactions present within the flexible MIL-53(Fe) microporous framework.

Indeed, these strong interactions are evidenced by the second release stage for each of the drug-loaded MIL-53(Fe) materials. A complete delivery of stavudine and progesterone occurred after five days; acetaminophen was completely released after six days (Figure 4-3). The release process is governed mainly by diffusion from the pores and by drug-matrix interactions. By virtue of its flexibility, MIL-53(Fe) is able to adopt a configuration in which the interactions between guest molecules and the framework are optimized. This adaptability might explain the long release times, which could result from the enhanced confinement effects and maximized host-guest interactions.[5]

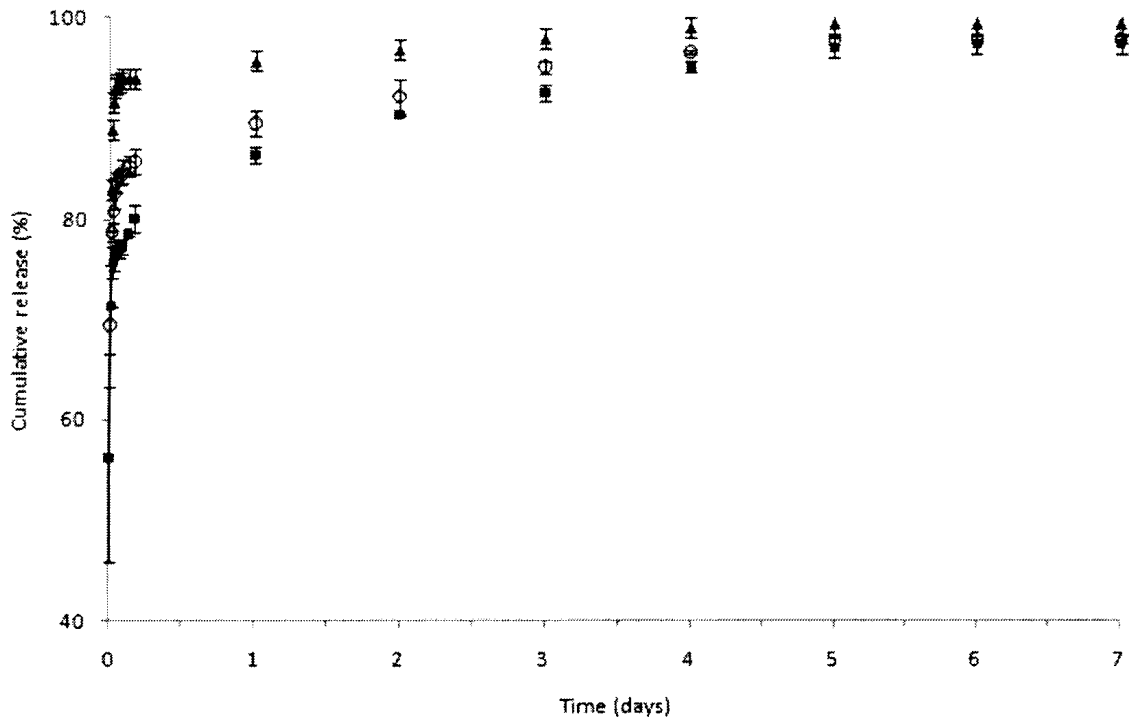

Figure 4-3. Cumulative release of acetaminophen (■), progesterone (▲), and stavudine (○) from MIL-53(Fe) in PBS at 37°C. The depicted results are mean values (*n* = *2*).

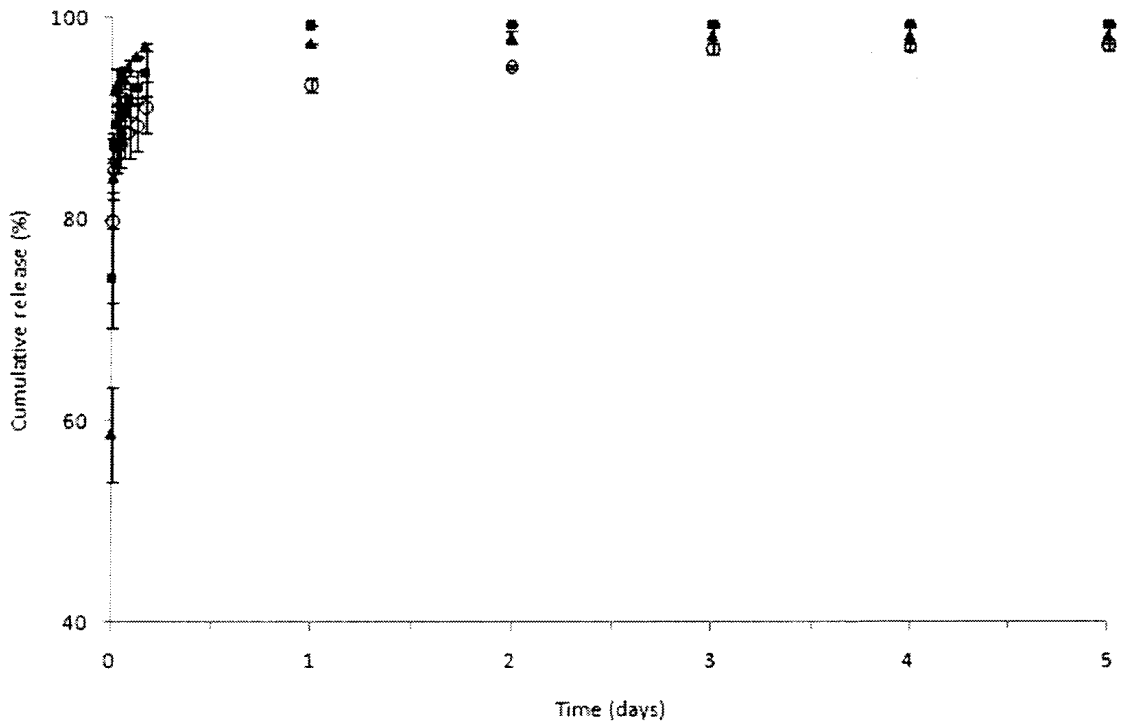

Figure 4-4. Cumulative release of acetaminophen (■), progesterone (▲), and stavudine (○) from MIL-101 in PBS at 37°C. The depicted results are mean values (*n* = *2*).

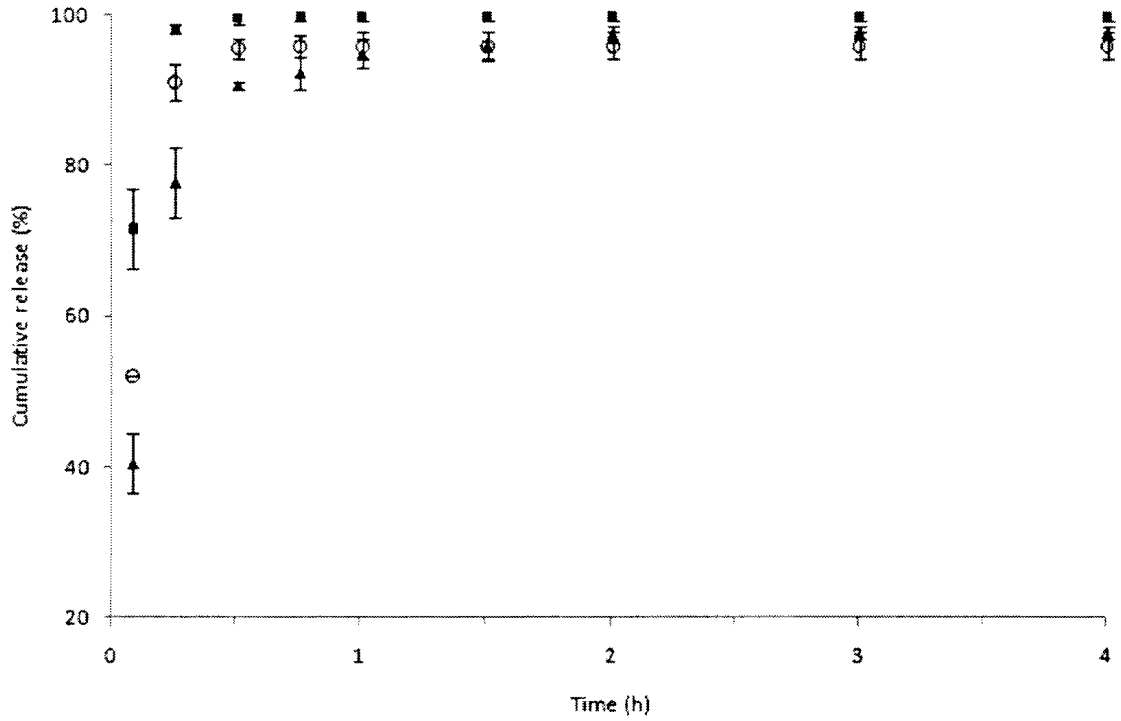

Figure 4-5. Cumulative release of acetaminophen (■), progesterone (▲), and stavudine (○) from SBA-15 in PBS + 0.5% SDS at 37°C. The depicted results are mean values (*n* = *2*).

Ibuprofen was previously reported to completely release from MIL-53(Fe) after a period of three weeks.[5] However, utilizing a three day solvent impregnation method this group successfully incorporated 20 wt% of ibuprofen within the pores, which is higher than the loadings achieved in this study. This higher drug loading is likely the reason for a longer release profile. Successive experiments will need to be conducted with MIL-53(Fe) to determine if multiple incipient wetness impregnation steps can increase the incorporated drug amount.

The burst release from MIL-101 requires a different explanation, since BET, DSC and XRPD analyses indicated that each drug-loaded sample had successfully incorporated the entire payload within the pores. The quick release likely results from a rapid dissolution, and subsequent quick diffusion from the relatively large mesopores. It is likely that the

drug fraction not directly contacting the surface of the mesopores immediately dissolved upon immersion within the release medium. Due to the large diameter of the mesopores, any resistance to diffusion out of the pores is likely very weak, resulting in rapid diffusion.

Similarly to the drug-loaded MIL-53(Fe) materials, the second release stage was prolonged, and governed by diffusion from the pores and by host-guest interactions. The complete release of stavudine from MIL-101 occurred after five days, which is comparable to the complete release of ibuprofen after six days from MIL-101 that was previously reported.[2] Progesterone was completely released after three days; acetaminophen after two days (Figure 4-4). These release kinetics are quicker than the MIL-53(Fe) kinetics, which is expected since the release is dependent on diffusion from the pores and host-guest interactions, which are likely much higher in drug-loaded MIL-53(Fe) materials. This clearly shows an influence of the flexibility of MIL-53(Fe) on the time of release.

These results suggest that very long therapies are possible using flexible MOFs for drug delivery. Stavudine suffers from a short half-life in systemic circulation, which necessitates frequent doses, causing severe dose-dependent side effects. The benefits of controlled delivery for this drug, as well as for a wide range of other pharmaceuticals with either low bioavailabilities or short circulating half-lives would include stable blood concentrations, a minimization of toxicity and adverse side effects, as well as increased patient compliance.[24]

All SBA-15 formulations released their payloads very quickly. Acetaminophen and stavudine were completely released from SBA-15 in less than an hour; 100% release of progesterone occurred after four hours (Figure 4-5). Rapid release from MIL-101 and SBA-15 materials results from fast dissolution of the confined molecules, followed by rapid diffusion from the mesopores into the release medium. Since sink conditions were installed for each of the release experiments, the slightly slower release of progesterone is a result of a slower diffusion out of the pores. Therefore, the dissolution of progesterone into the release medium cannot be considered a rate-limiting process. This indicates that the pore diameter may have been small enough to cause diffusive resistance during the release of relatively bulky progesterone molecules.

Several studies have reported that mesoporous silica materials can enhance the dissolution rates of incorporated drugs.[11, 14, 25] Van Speybroeck et al. (2009) observed that the *in vitro* release profiles of ten poorly soluble drugs from SBA-15 was faster than the dissolution of their respective crystalline counterparts. All formulations, except for one, released 80% of drug within the first 5 min of experiment, which is similar to our results for SBA-15. This enhanced dissolution has been attributed to the complete loss of crystallization of the adsorbed drug fraction, as it is well known that the high free energy associated with noncondensed states can greatly improve dissolution rates.[26] As evidenced by DSC and XRPD, each of the incorporated drugs existed in an amorphous state within the SBA-15 mesopores. An enhanced dissolution can partially account for the quick release kinetics, however, the effect was likely minimal since all release experiments were performed under sink conditions. The quick release is more likely

attributed to the large diameter of the mesopores and by adsorption competition between the drug molecules and water in favour of the latter.[14]

4.5. Conclusions

Using an incipient wetness impregnation method, three model drugs (acetaminophen, progesterone, and stavudine) were successfully loaded into MIL-53(Fe), MIL-101 and SBA-15. The MIL-101 and SBA-15 adsorbed drug fractions were found to be noncrystalline, as evidenced by DSC and XRPD analyses. DSC analysis indicated that each of the drug-loaded MIL-53(Fe) samples contained a portion of the entire drug load that had deposited onto the outer surface of the particles that had recrystallized. This is attributed to the smaller pore volume of MIL-53(Fe), which proved to be too small to accommodate a drug loading of 20 wt% for each of the model compounds. Nevertheless, the portion of the drug load that had successfully been incorporated within the MIL-53(Fe) framework was slowly released in as long as six days for acetaminophen in a diffusion-controlled process. Owing to the larger pore diameters and weaker host-guest interactions, MIL-101 release kinetics were somewhat quicker. However, release times were still prolonged, as evidenced by the complete release of stavudine which occurred after five days. Prolonging the release of stavudine and other pharmaceuticals using MOFs would alleviate many of the drawbacks encountered with conventional therapeutics. The release of the model drugs from SBA-15 was much quicker than from both MOF materials. In this study, acetaminophen and stavudine were completely released from SBA-15 in less than an hour; 100% release of progesterone occurred after

four hours. The molecules can easily diffuse into the bulk medium due to the size of the pores of the mesostructured silica. SBA-15 has proven to be very useful at enhancing the dissolution rates of poorly soluble drugs. Thus, SBA-15 is best-suited for improving drug-dissolution, which is ideal for progesterone since it is very poorly soluble due to its hydrophobic structure.

4.6. References

(1) Shi, J.; Votruba, A. R.; Farokhzad, O. C.; Langer, R. *Nano Lett.* **2010**, *10*, 3223-3230.

(2) Horcajada, P.; Serre, C.; Vallet-Regí, M.; Sebban, M.; Taulelle, F.; Férey, G. *Angew. Chem. Int. Ed.* **2006**, *45*, 5974-5978.

(3) Férey, G. *Chem. Soc. Rev.* **2008**, *37*, 191-214.

(4) Horcajada, P., et al *Nat. Mater.* **2010**, *9*, 172-178.

(5) Horcajada, P.; Serre, C.; Maurin, G.; Ramsahye, N. A.; Balas, F.; Vallet-Regí, M.; Sebban, M.; Taulelle, F.; Férey, G. *J. Am. Chem. Soc.* **2008**, *130*, 6774-6780.

(6) Loiseau, T.; Serre, C.; Huguenard, C.; Fink, G.; Taulelle, F.; Henry, M.; Bataille, T.; Ferey, G. *Chem. Eur. J.* **2004**, *10*, 1373-1382.

(7) Prencipe, G.; Tabakman, S. M.; Welsher, K.; Liu, Z.; Goodwin, A. P.; Zhang, L.; Henry, J.; Dai, H. *J. Am. Chem. Soc.* **2009**, *131*, 4783-4787.

(8) Awasthi, V.; Garcia, D.; Goins, B.; Phillips, W. *Int. J. Pharm.* **2003**, *253*, 121-132.

(9) Manzano, M.; Colilla, M.; Vallet-Regi, M. *Expert Opin. Drug Deliv.* **2009**, *6*, 1383-1400.

(10) Selvam, P.; Krishna, N. V.; Viswanathan, B. *J. Indian Inst. Sci.* **2010**, *90*, 271-285.

(11) Van Speybroeck, M.; Barillaro, V.; Do Thi, T.; Mellaerts, R.; Martens, J.; Van Humbeeck, J.; Vermant, J.; Annaert, P.; Van Den Mooter, G.; Augustijns, P. *J. Pharm. Sci.* **2009**, *98*, 2648-2658.

(12) Heikkila, T.; Salonen, J.; Tuura, J.; Kumar, N.; Salmi, T.; Murzin, D. Y.; Hamdy, M. S.; Mul, G.; Laitinen, L.; Kaukonen, A. M.; Hirvonen, J.; Lehto, V. *Drug Deliv.* **2007**, *14*, 337-347.

(13) Ferey, G. *Science* **2005**, *310*, 1119-1119.

(14) Mellaerts, R.; Jammaer, J. A. G.; Van Speybroeck, M.; Chen, H.; Van Humbeeck, J.; Augustijns, P.; Van den Mooter, G.; Martens, J. A. *Langmuir* **2008**, *24*, 8651-8659.

(15) Charnay, C.; Begu, S.; Tourne-Peteilh, C.; Nicole, L.; Lerner, D.; Devoisselle, J. *Eur. J. Pharm. Biopharm.* **2004**, *57*, 533-540.

(16) Forrest, J. A. H.; Clements, J. A.; Prescott, L. F. *Clin. Pharmacokinet.* **1982**, *7*, 93-107.

(17) Khalil, N. M.; Carraro, E.; Cotica, L. F.; Mainardes, R. M. *Expert Opin. Drug Deliv.* **2011**, *8*, 95-112.

(18) Pike, M. C.; Spicer, D. V.; Dahmoush, L.; Press, M. F. *Epidemiol. Rev.* **1993**, *15*, 17-35.

(19) Brunauer, S.; Emmett, P.H.; Teller, E. *J. Am. Chem. Soc.* **1938**, 60, 309-319.

(20) Dosseh, G.; Xia, Y.; Alba-Simionesco, C. *J. Phys. Chem. B* **2003**, *107*, 6445-6453.

(21) Morishige, K.; Kawano, K. *J. Chem. Phys.* **2000**, *112*, 11023-11029.

(22) Azais, T.; Tourne-Peteilh, C.; Aussenac, F.; Baccile, N.; Coelho, C.; Devoisselle, J.; Babonneau, F. *Chem. Mater.* **2006**, *18*, 6382-6390.

(23) Sliwinska-Bartkowiak, M.; Dudziak, G.; Sikorski, R.; Gras, R.; Radhakrishnan, R.; Gubbins, K. *J. Chem. Phys.* **2001**, *114*, 950-962.

(24) Allen, T. M.; Cullis, P. R. *Science* **2004**, *303*, 1818-1822.

(25) Mellaerts, R.; Aerts, C. A.; Van Humbeeck, J.; Augustijns, P.; Van den Mooter, G.; Martens, J. A. *Chem. Commun.* **2007**, 1375-1377.

(26) Hancock, B.; Zograf, G. *J. Pharm. Sci.* **1997**, *86*, 1-12.

5. Conclusions and Recommendations

5.1. Conclusions

5.1.1. Overview

The first stage of the experimental work was to optimize the synthesis conditions of MIL-53(Fe) to produce small and homogeneous crystals while minimizing energy consumption. Syntheses were carried out under CE, MW, and UTS conditions to gain an understanding of the effect of each synthesis procedure on the product yield and crystallinity. Within each reaction procedure, two-level multi-factorial designs were used to study the dependence of the two responses on each factor. The research carried on to investigate the drug loading and release behaviour of acetaminophen, stavudine, and progesterone impregnated in either MIL-53(Fe), MIL-101, or SBA-15. The model drugs were introduced into the pores of the materials by an incipient wetness impregnation procedure, after which drug delivery studies were performed under simulated physiological conditions.

5.1.2. Rapid and efficient crystallization of MIL-53(Fe) by ultrasound and microwave irradiation

Synthesis of MIL-53(Fe) under UTS and MW conditions is quicker, more efficient and a greener alternative to CE heating. MIL-53(Fe) was synthesized in ten minutes from MW irradiation and in seven minutes from UTS irradiation, which, to the author's knowledge, are the quickest reported crystallization times for MIL-53(Fe). The observed size reduction and homogeneity of MIL-53(Fe) crystals synthesized under UTS and MW conditions is attributed to fast and uniform nucleation, and is a clear indication of the

crystal phase purity and the efficiency of these two synthesis methods. Small MIL-53(Fe) crystals are especially effective in the fields of diffusion, catalysis, and drug adsorption/delivery. Time and temperature were the most significant factors influencing product crystallinity for both MW irradiation and CE heating. For the UTS method, neither time nor power significantly influenced product crystallinity, suggesting that the products reached their maximum crystallinity shortly after nucleation.

5.1.3. MIL-53(Fe), MIL-101, and SBA-15 as potential platforms for drug delivery

Measured drug loadings of the nanomaterials were very close to the intended theoretical loadings of 20 wt%. The advantage of the incipient wetness impregnation procedure over conventional solvent loading methods is that it requires only a very small volume of solvent, it is a much less time-consuming process, and it allows for the loaded drug amount to be carefully controlled. Drug-loaded MIL-53(Fe) materials completely released stavudine and progesterone after five days; acetaminophen was completely released after six days. The flexibility of the MIL-53(Fe) framework might explain the long release times, which could result from maximized host-guest interactions. Very long therapies are possible using flexible MOFs for drug delivery. MIL-101 completely released stavudine after five days; progesterone was completely released after three days; acetaminophen after two days. Larger pore diameters and slightly weaker host-guest interactions are responsible for moderately quicker release kinetics. Stavudine and acetaminophen were completely released from SBA-15 in less than an hour; complete release of progesterone occurred after four hours. Rapid release results from fast

dissolution of the confined molecules, followed by rapid diffusion from the mesopores into the release medium.

5.2. Recommendations

1. Optimization of MIL-53(Fe) synthesis reaction conditions using nontoxic solvents.

Synthesis of MIL-53(Fe) was conducted using a class 2 solvent (Health Canada), DMF, due to its excellent solubilizing properties. The use of a nontoxic solvent to synthesize MIL-53(Fe) may be desirable for potential large-scale production processes, however it must be considered that small changes in solvent polarity and pH can lead to poorer quality crystals, reduced yields, or the formation of entirely new phases.[1] MIL-53(Fe) has previously been synthesized in water,[2] however the crystals were very large, therefore they are not suitable for drug delivery. Thus, optimization experiments using either water and/or ethanol are recommended. Alcohols are often used to synthesize MOFs; the use of ethanol to synthesize MIL-53(Fe) may be promising since it easily dissolves H_2BDC.

2. Control of the burst release from MIL-53(Fe) and MIL-101.

The burst release of each of the three model drugs (acetaminophen, progesterone, and stavudine) from MIL-53(Fe) and MIL-101 must be controlled. Drug-loaded MIL-53(Fe) particles should be washed to remove drug molecules deposited onto the outer surface of the particles. Following this, the drug content remaining inside the pores needs to be determined before *in vitro* drug release studies are conducted. Additionally, successive incipient wetness impregnation steps should be conducted to determine if the incorporated drug amount within MIL-53(Fe) micropores can be increased. The organic

linker of MIL-53(Fe) and MIL-101 can also be functionalized to attempt to increase the affinity of the drug molecules to the framework for extended release profiles. However, this may decrease the porosity of each framework, decreasing the drug loading amount.

3. Cellular uptake studies of DDSs.

Finally, comprehensive cellular uptake studies should also be conducted. The size and surface charge of the DDSs will need to be carefully controlled to achieve high uptake efficiencies.

5.3. References

(1) Rowsell, J. L. C.; Yaghi, O. M. *Microporous Mesoporous Mater.* **2004**, *73*, 3-14.

(2) Horcajada, P., et al *Nat. Mater.* **2010**, *9*, 172-178.

Appendices

Appendix A

Characterization studies of model drugs

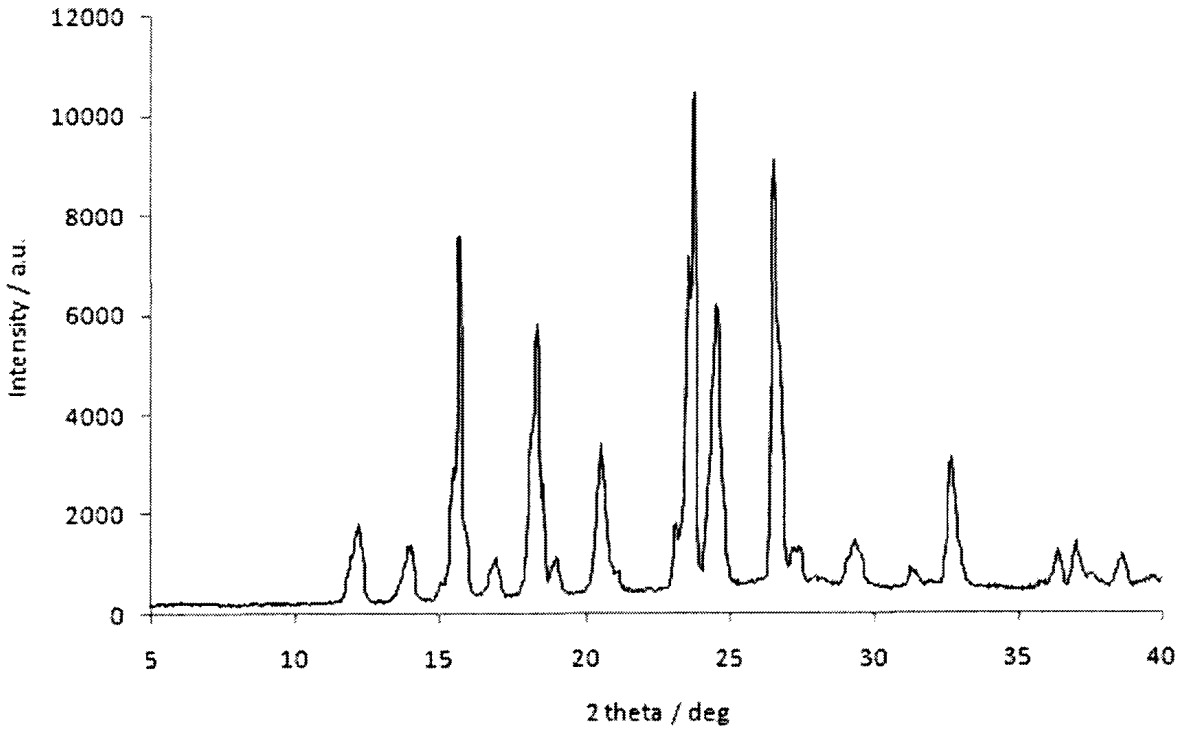

Figure A-1. XRPD pattern of acetaminophen.

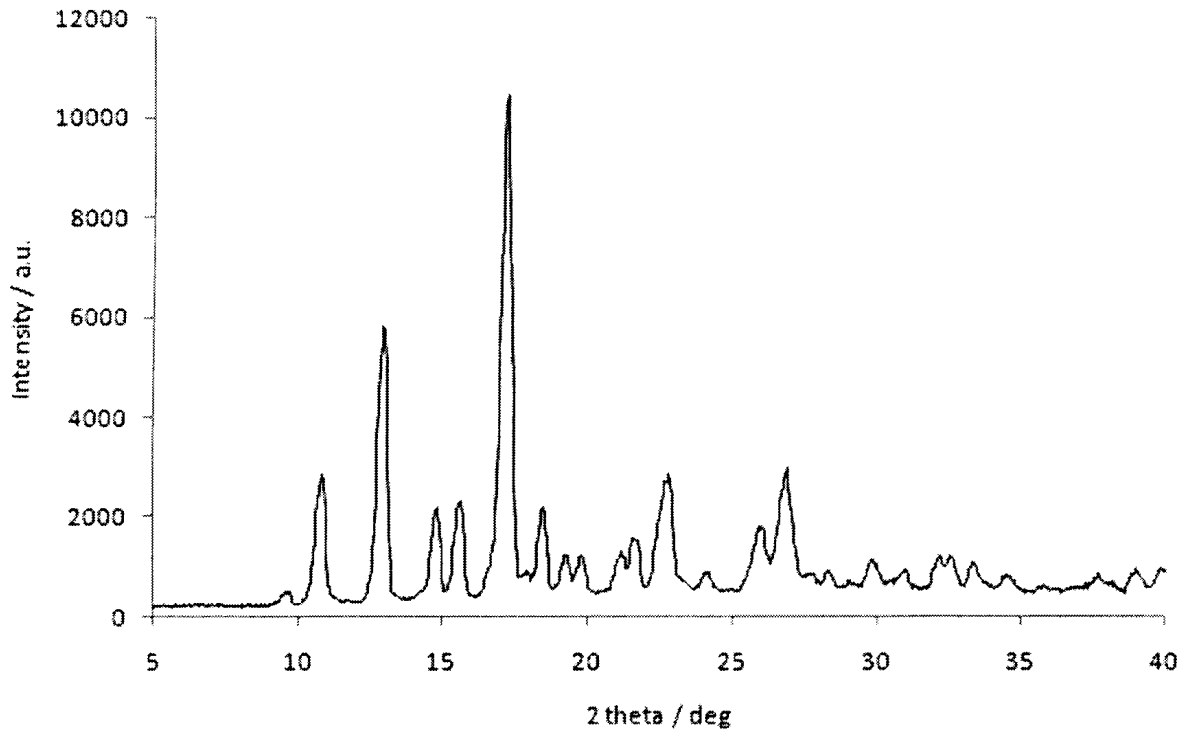

Figure A-2. XRPD pattern of progesterone.

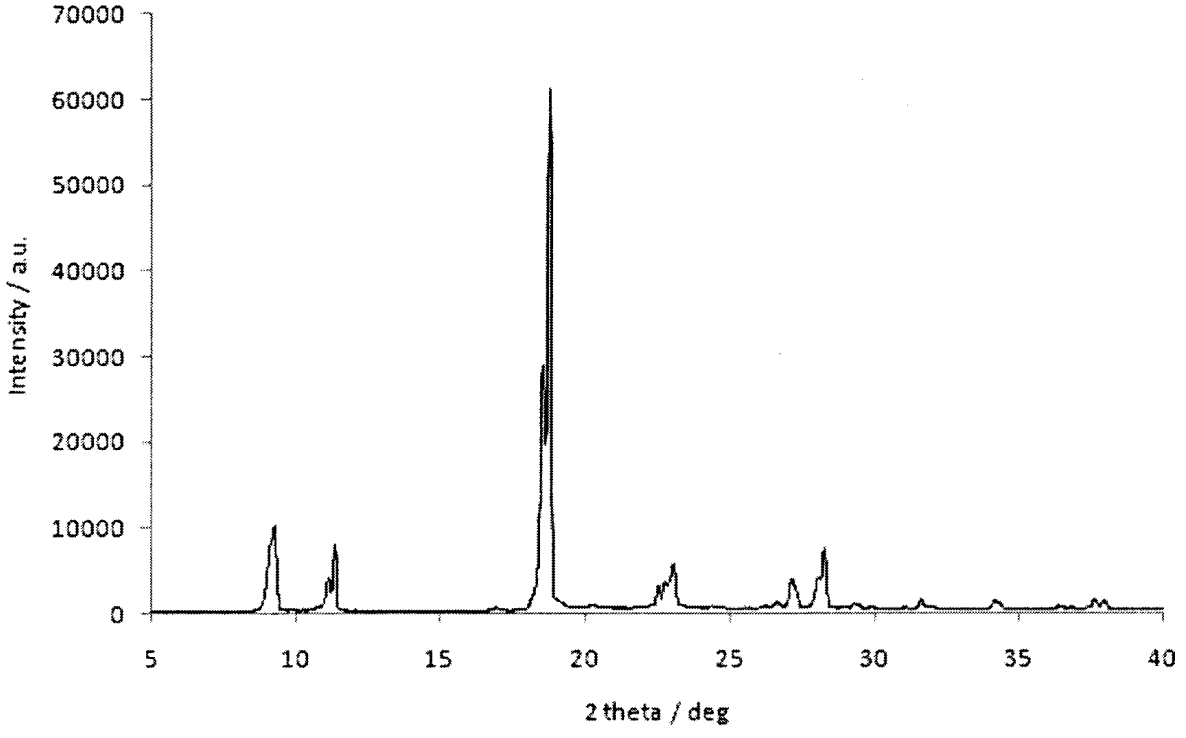

Figure A-3. XRPD pattern of stavudine.

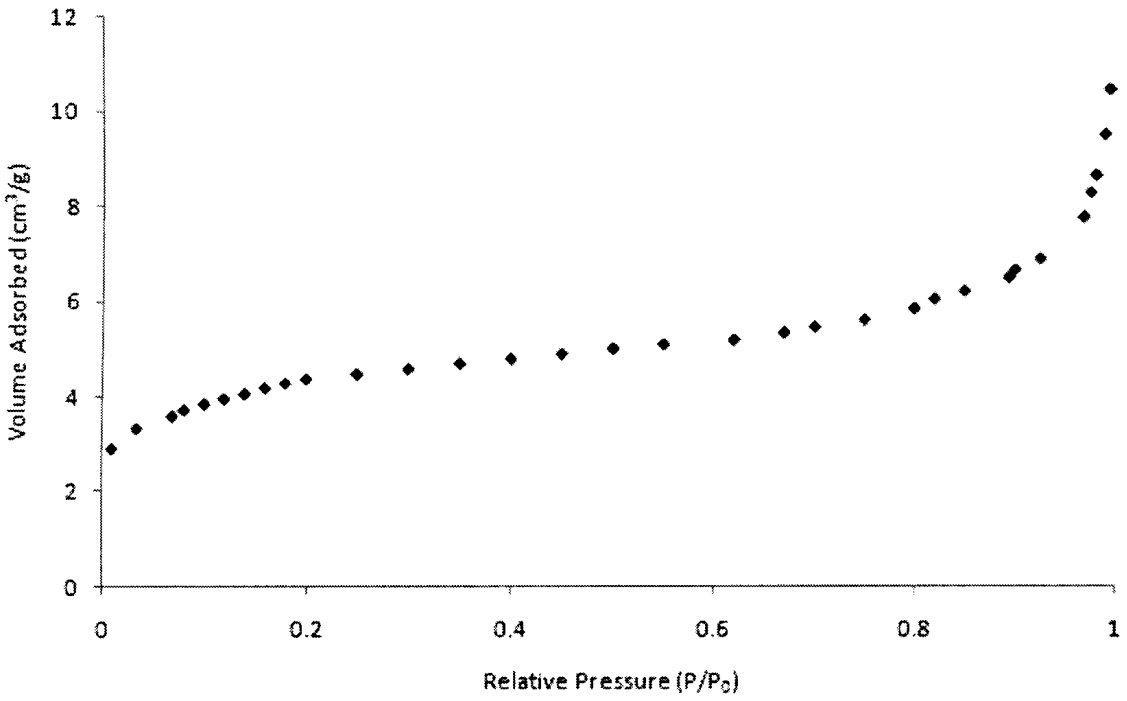

Figure A-4. Nitrogen adsorption isotherm of MIL-53(Fe) at 77 K, degassed at 323 K.

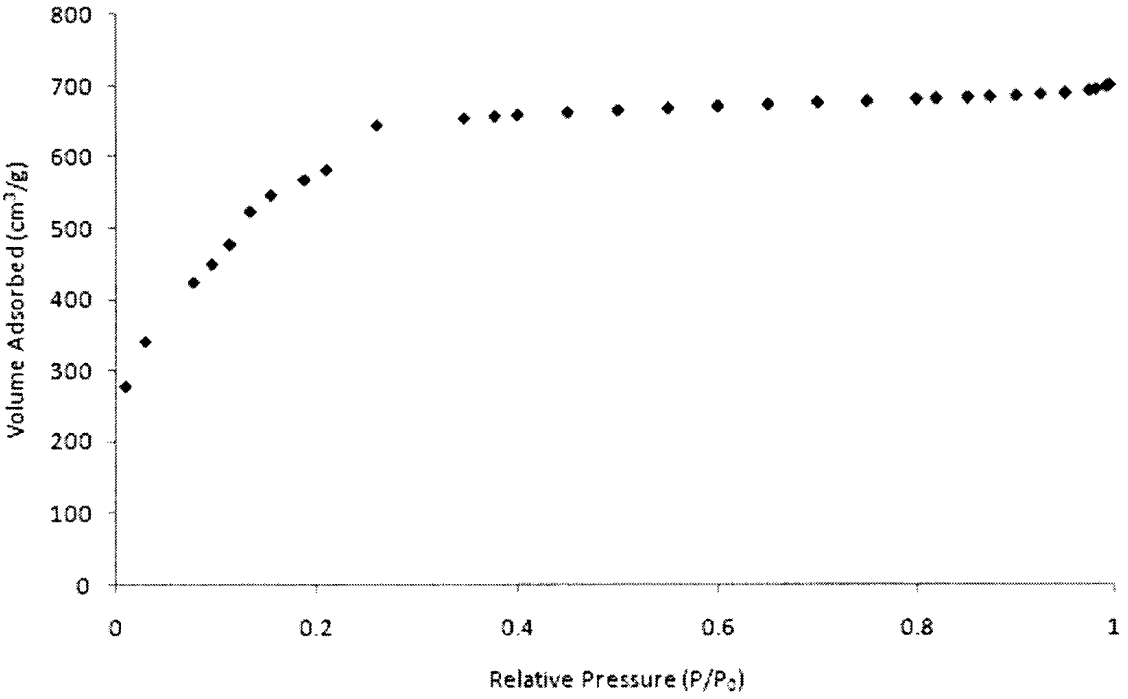

Figure A-5. Nitrogen adsorption isotherm of MIL-101 at 77 K, degassed at 323 K.

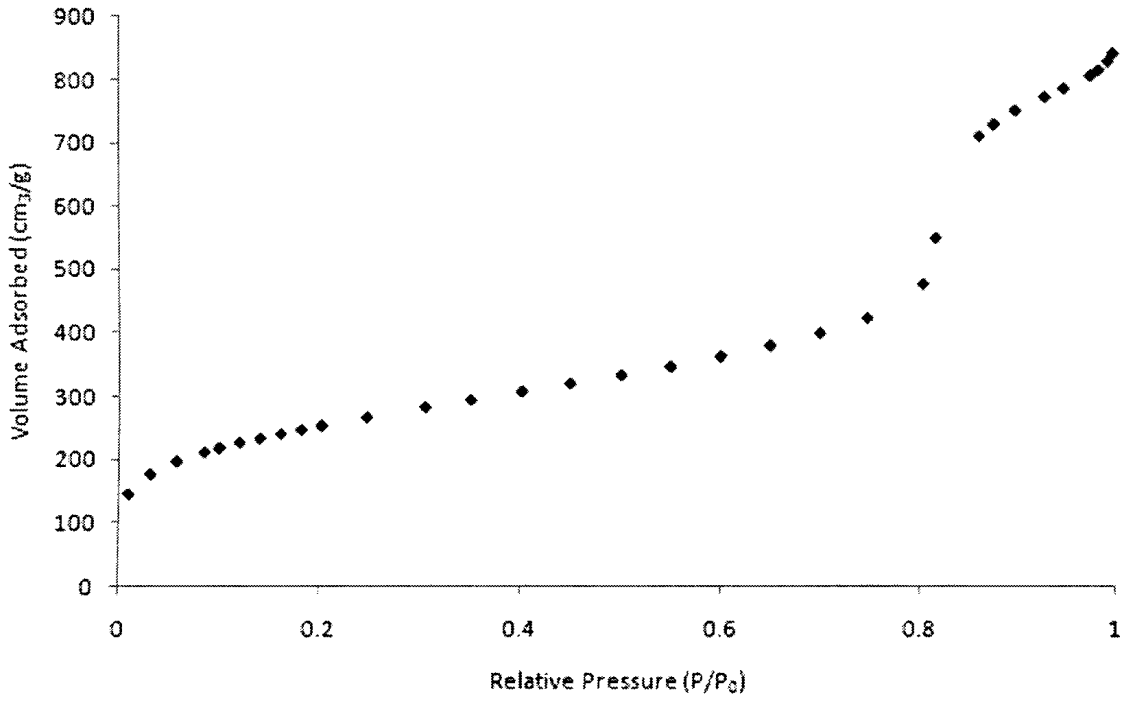

Figure A-6. Nitrogen adsorption isotherm of SBA-15 at 77 K, degassed at 323 K.

Appendix B

Calibration curves and UV absorbance data used to determine cumulative release (%) of the model drugs from MIL-53(Fe), MIL-101, and SBA-15

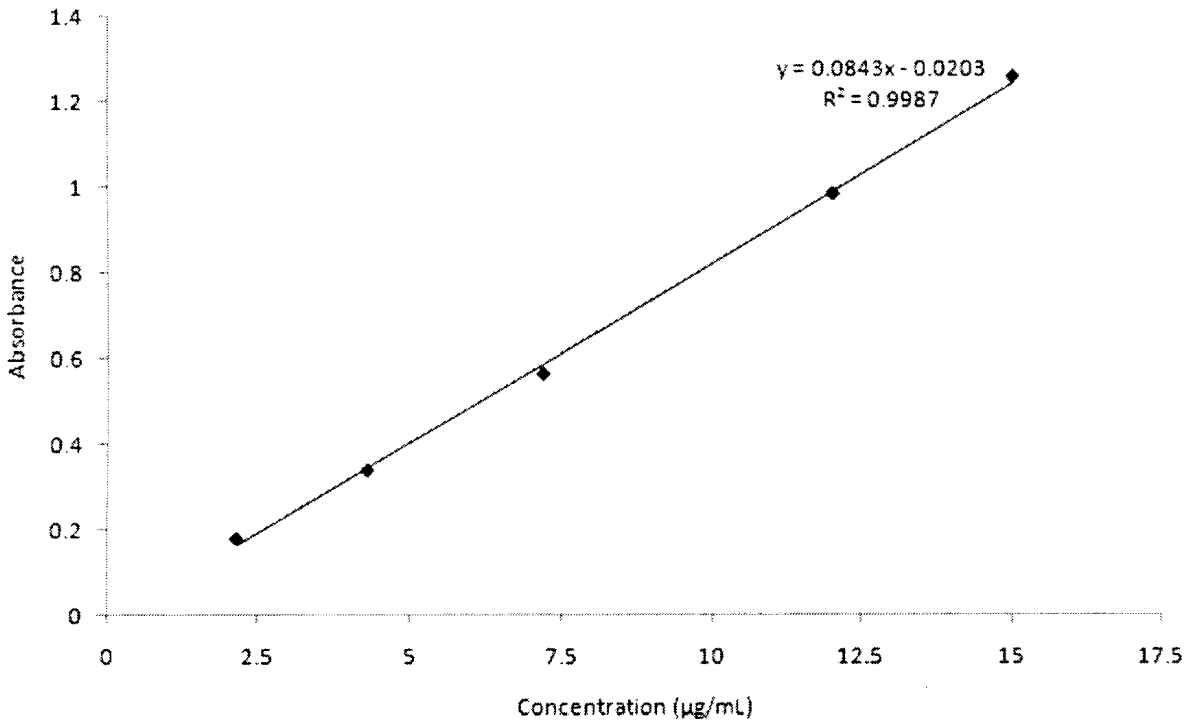

Figure B-1. Calibration curve of acetaminophen (λ = 244 nm) in PBS solution. The depicted results are mean values (*n* = *3*).

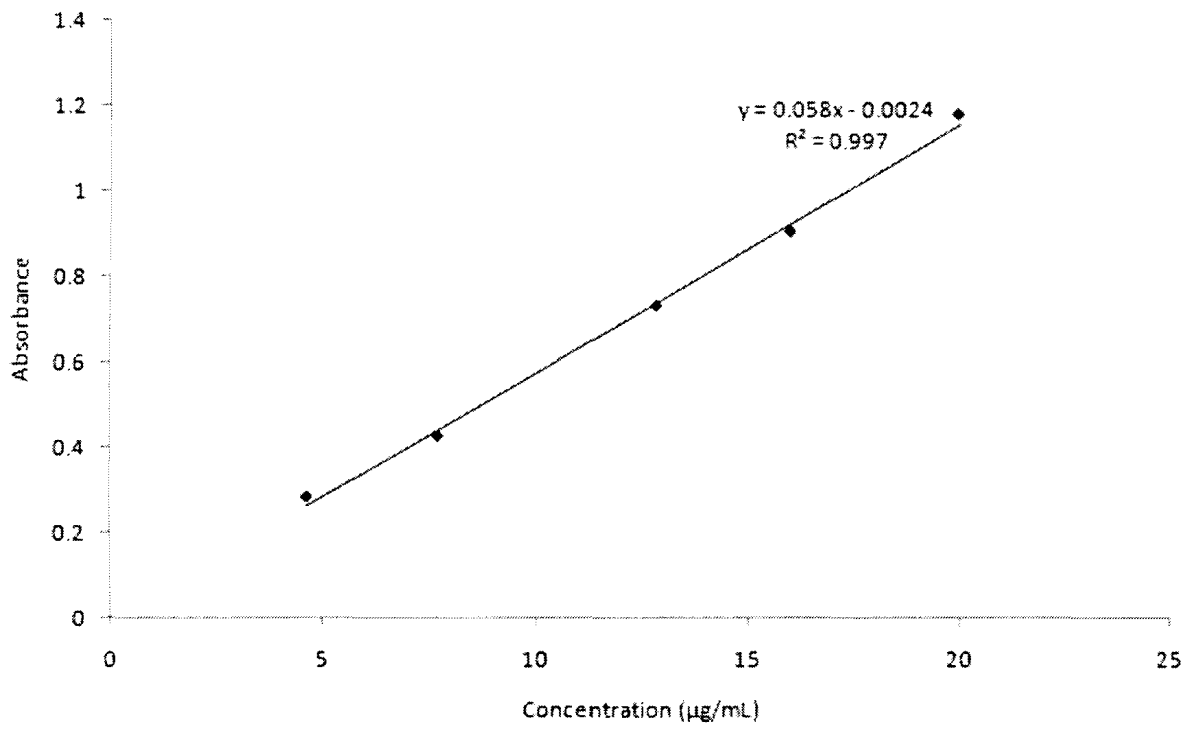

Figure B-2. Calibration curve of progesterone (λ = 245 nm) in PBS + 0.5% SDS solution. The depicted results are mean values (*n* = *3*).

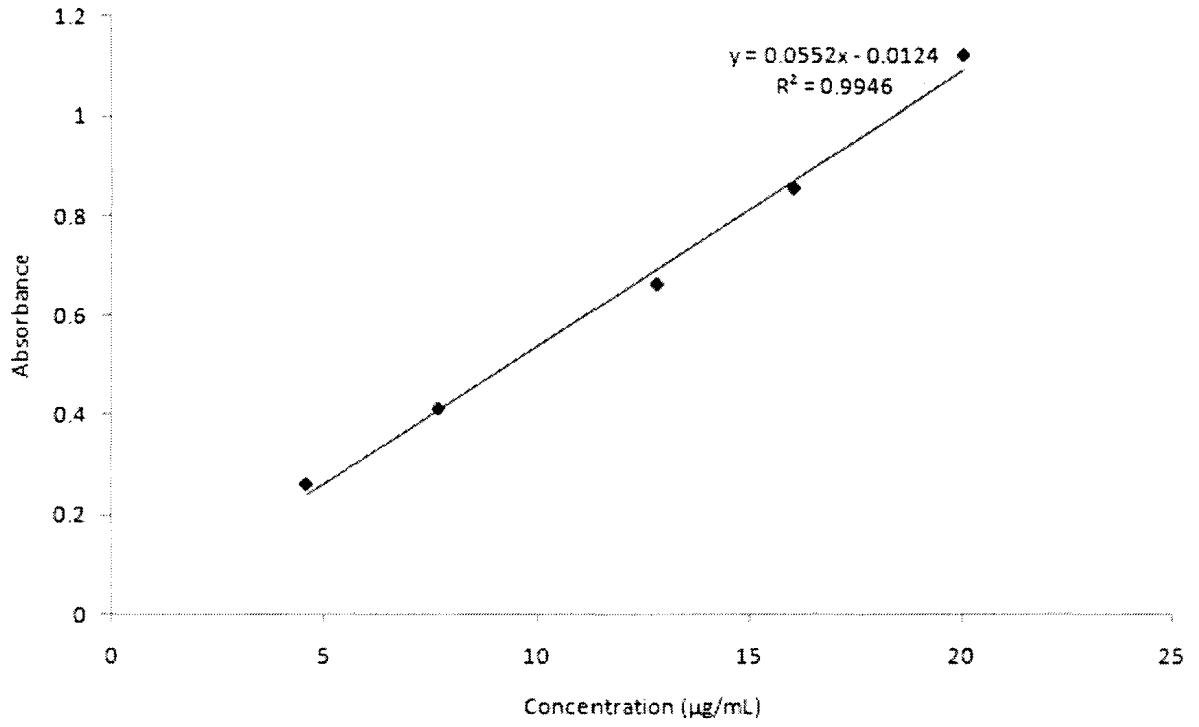

Figure B-3. Calibration curve of stavudine (λ = 266 nm) in PBS solution. The depicted results are mean values (*n* = *3*).

Table B-1. UV absorbance measurements and sample data used to determine the cumulative release (%) of acetaminophen from MIL-53(Fe) after each time interval (trial #1).

Time	Absorbance	Conc. (μg/mL)	Sample Conc. (μg/mL)	Starting Conc. (μg/mL)	Amount Released (μg)	Cumulative Release (μg)	Amount Remaining in Solution (μg)	Cumulative Release (%)
5 min	0.6569	8.03	32.13	0	482	482	418	45.8
15 min	0.9421	11.42	45.67	27.87	267	749	594	71.2
30 min	0.9051	10.98	43.91	39.58	65	814	571	77.4
45 min	0.7874	9.58	38.32	38.06	4	818	498	77.8
60 min	0.6797	8.30	33.21	33.21	0	818	432	77.8
90 min	0.5891	7.23	28.92	28.78	2	820	376	77.9
2 h	0.5079	6.27	25.06	25.06	0	820	326	77.9
3 h	0.4445	5.51	22.05	21.72	5	825	287	78.4
4 h	0.3867	4.83	19.31	19.11	3	828	251	78.7
1 d	0.4336	5.38	21.54	16.74	72	900	280	85.6
2 d	0.4448	5.52	22.07	18.67	51	951	287	90.4
3 d	0.4024	5.01	20.06	19.12	14	965	261	91.7
4 d	0.4051	5.05	20.18	17.38	42	1007	262	95.7
5 d	0.3821	4.77	19.09	17.49	24	1031	248	98.0
6 d	0.3326	4.19	16.75	16.55	3	1034	218	98.3
7 d	0.2856	3.63	14.51	14.51	0	1034	189	98.3

Table B-2. UV absorbance measurements and sample data used to determine the cumulative release (%) of acetaminophen from MIL-53(Fe) after each time interval (trial #2).

Time	Absorbance	Conc. (μg/mL)	Sample Conc. (μg/mL)	Starting Conc. (μg/mL)	Amount Released (μg)	Cumulative Release (μg)	Amount Remaining (μg)	Cumulative Release (%)
5 min	0.9393	11.38	45.53	0	683	683	592	66.6
15 min	0.8788	10.67	42.66	39.46	48	731	555	71.2
30 min	0.7997	9.73	38.91	36.97	29	760	506	74.1
45 min	0.7030	8.58	34.32	33.72	9	769	446	75.0
60 min	0.6248	7.65	30.61	29.74	13	782	398	76.2
90 min	0.5388	6.63	26.53	26.53	0	782	345	76.2
2 h	0.4699	5.81	23.26	22.99	4	786	302	76.6
3 h	0.4354	5.41	21.62	20.16	22	808	281	78.8
4 h	0.4140	5.15	20.61	18.74	28	836	268	81.5
1 d	0.4390	5.45	21.79	17.86	59	895	283	87.2
2 d	0.4213	5.24	20.95	18.89	31	926	272	90.3
3 d	0.4074	5.07	20.29	18.16	32	958	264	93.4
4 d	0.3672	4.60	18.39	17.59	12	970	239	94.5
5 d	0.3366	4.23	16.94	15.94	15	985	220	96.0
6 d	0.2947	3.74	14.94	14.68	4	989	194	96.4
7 d	0.2527	3.24	12.95	12.95	0	989	168	96.4

Table B-3. UV absorbance measurements and sample data used to determine the cumulative release (%) of progesterone from MIL-53(Fe) after each time interval (trial #1).

Time	Absorbance	Conc. (μg/mL)	Sample Conc. (μg/mL)	Starting Conc. (μg/mL)	Amount Released (μg)	Cumulative Release (μg)	Amount Remaining (μg)	Cumulative Release (%)
5 min	0.8155	13.85	55.40	0	831	831	720	79.4
15 min	0.7867	13.39	53.55	48.01	83	914	696	87.3
30 min	0.7162	12.25	49.01	46.41	39	953	637	91.0
45 min	0.6386	11.00	44.01	42.47	23	976	572	93.2
60 min	0.5568	9.68	38.74	38.14	9	985	504	94.1
90 min	0.4766	8.39	33.57	33.57	0	985	436	94.1
2 h	0.4113	7.34	29.36	29.10	4	989	382	94.5
3 h	0.3515	6.38	25.52	25.45	1	990	332	94.6
4 h	0.2987	5.53	22.11	22.11	0	990	287	94.6
1 d	0.2643	4.97	19.90	19.16	11	1001	259	95.6
2 d	0.2324	4.46	17.85	17.25	9	1010	232	96.5
3 d	0.2100	4.10	16.40	15.47	14	1024	213	97.8
4 d	0.1936	3.84	15.35	14.21	17	1041	199	99.4
5 d	0.1660	3.39	13.57	13.30	4	1045	176	99.8
6 d	0.1379	2.94	11.76	11.76	0	1045	153	99.8
7 d	0.1136	2.55	10.19	10.19	0	1045	132	99.8

Table B-4. UV absorbance measurements and sample data used to determine the cumulative release (%) of progesterone from MIL-53(Fe) after each time interval (trial #2).

Time	Absorbance	Conc. (μg/mL)	Sample Conc. (μg/mL)	Starting Conc. (μg/mL)	Amount Released (μg)	Cumulative Release (μg)	Amount Remaining (μg)	Cumulative Release (%)
5 min	0.8838	14.95	59.80	0	897	897	777	86.5
15 min	0.8024	13.64	54.56	51.83	41	938	709	90.5
30 min	0.7081	12.12	48.49	47.29	18	956	630	92.2
45 min	0.6140	10.61	42.42	42.02	6	962	551	92.8
60 min	0.5262	9.19	36.76	36.76	0	962	478	92.8
90 min	0.4532	8.02	32.06	31.86	3	965	417	93.1
2 h	0.3909	7.01	28.05	27.79	4	969	365	93.4
3 h	0.3329	6.08	24.31	24.31	0	969	316	93.4
4 h	0.2825	5.27	21.07	21.07	0	969	274	93.4
1 d	0.2638	4.97	19.86	18.26	24	993	258	95.8
2 d	0.2371	4.54	18.15	17.21	14	1007	236	97.1
3 d	0.2089	4.08	16.33	15.73	9	1016	212	98.0
4 d	0.1823	3.65	14.62	14.15	7	1023	190	98.6
5 d	0.1562	3.23	12.94	12.67	4	1027	168	99.0
6 d	0.1294	2.80	11.21	11.21	0	1027	146	99.0
7 d	0.1062	2.43	9.72	9.72	0	1027	126	99.0

Table B-5. UV absorbance measurements and sample data used to determine the cumulative release (%) of stavudine from MIL-53(Fe) after each time interval (trial #1).

Time	Absorbance	Conc. (μg/mL)	Sample Conc. (μg/mL)	Starting Conc. (μg/mL)	Amount Released (μg)	Cumulative Release (μg)	Amount Remaining (μg)	Cumulative Release (%)
5 min	0.6049	11.18	44.73	0	671	671	582	63.3
15 min	0.7167	12.26	49.04	38.77	154	825	637	77.8
30 min	0.6266	10.81	43.23	42.50	11	836	562	78.9
45 min	0.5609	9.75	39.00	37.47	23	859	507	81.0
60 min	0.4977	8.73	34.93	33.80	17	876	454	82.6
90 min	0.4347	7.72	30.88	30.28	9	885	401	83.5
2 h	0.3719	6.71	26.83	26.76	1	886	349	83.6
3 h	0.3236	5.93	23.72	23.25	7	893	308	84.2
4 h	0.2776	5.19	20.75	20.55	3	896	270	84.5
1 d	0.2750	5.15	20.59	17.99	39	935	268	88.2
2 d	0.2562	4.84	19.37	17.84	23	958	252	90.4
3 d	0.2606	4.91	19.66	16.79	43	1001	256	94.4
4 d	0.2416	4.61	18.44	17.04	21	1022	240	96.4
5 d	0.2128	4.14	16.58	15.98	9	1031	216	97.3
6 d	0.1795	3.61	14.43	14.37	1	1032	188	97.4
7 d	0.1496	3.13	12.51	12.51	0	1032	163	97.4

Table B-6. UV absorbance measurements and sample data used to determine the cumulative release (%) of progesterone from MIL-53(Fe) after each time interval (trial #2).

Time	Absorbance	Conc. (μg/mL)	Sample Conc. (μg/mL)	Starting Conc. (μg/mL)	Amount Released (μg)	Cumulative Release (μg)	Amount Remaining (μg)	Cumulative Release (%)
5 min	0.7190	13.25	53.00	0	795	795	689	75.6
15 min	0.7130	12.20	48.80	45.93	43	838	634	79.7
30 min	0.6451	11.11	44.43	42.29	32	870	578	82.7
45 min	0.5697	9.89	39.57	38.50	16	886	514	84.2
60 min	0.4930	8.66	34.63	34.29	5	891	450	84.7
90 min	0.4254	7.57	30.28	30.01	4	895	394	85.1
2 h	0.3721	6.71	26.84	26.24	9	904	349	85.9
3 h	0.3196	5.87	23.46	23.26	3	907	305	86.2
4 h	0.2794	5.22	20.87	20.33	8	915	271	87.0
1 d	0.2786	5.20	20.82	18.08	41	956	271	90.9
2 d	0.2686	5.04	20.18	18.04	32	988	262	93.9
3 d	0.2465	4.69	18.75	17.49	19	1007	244	95.7
4 d	0.2191	4.25	16.98	16.25	11	1018	221	96.8
5 d	0.1995	3.93	15.72	14.72	15	1033	204	98.2
6 d	0.1669	3.41	13.62	13.62	0	1033	177	98.2
7 d	0.1387	2.95	11.81	11.81	0	1033	153	98.2

Table B-7. UV absorbance measurements and sample data used to determine the cumulative release (%) of acetaminophen from MIL-101 after each time interval (trial #1).

Time	Absorbance	Conc. (μg/mL)	Sample Conc. (μg/mL)	Starting Conc. (μg/mL)	Amount Released (μg)	Cumulative Release (μg)	Amount Remaining (μg)	Cumulative Release (%)
5 min	1.0459	12.65	50.59	0	759	759	658	69.3
15 min	1.1648	14.06	56.23	43.87	185	944	731	86.1
30 min	1.0278	12.43	49.73	48.73	15	959	647	87.5
45 min	0.8774	10.65	42.60	43.13	0	959	562	87.5
60 min	0.7860	9.56	38.26	37.47	12	971	497	88.6
90 min	0.6872	8.39	33.57	33.13	7	978	437	89.2
2 h	0.6107	7.49	29.94	29.13	12	990	389	90.3
3 h	0.5430	6.68	26.73	25.93	12	1002	348	91.4
4 h	0.4808	5.94	23.78	23.20	9	1011	309	92.2
1 d	0.5201	6.41	25.64	20.60	76	1087	313	99.2
2 d	0.4466	5.54	22.15	22.04	2	1089	271	99.4
3 d	0.3644	4.56	18.25	19.08	0	1089	235	99.4
4 d	0.3108	3.93	15.71	16.55	0	1089	204	99.4

Table B-8. UV absorbance measurements and sample data used to determine the cumulative release (%) of acetaminophen from MIL-101 after each time interval (trial #2).

Time	Absorbance	Conc. (μg/mL)	Sample Conc. (μg/mL)	Starting Conc. (μg/mL)	Amount Released (μg)	Cumulative Release (μg)	Amount Remaining (μg)	Cumulative Release (%)
5 min	1.1182	13.51	54.02	-	810	810	702	79.1
15 min	1.1020	13.31	53.25	46.80	97	907	693	88.6
30 min	0.9921	12.01	48.04	46.20	28	935	625	91.3
45 min	0.8580	10.42	41.67	41.67	0	935	542	91.3
60 min	0.7531	9.17	36.70	36.13	9	944	478	92.2
90 min	0.6510	7.96	31.85	31.87	0	944	398	92.2
2 h	0.5795	7.12	28.46	26.53	13	957	370	93.5
3 h	0.5183	6.39	25.56	24.67	13	970	332	94.7
4 h	0.4735	5.86	23.43	22.13	20	990	305	96.7
1 d	0.4446	5.51	22.06	20.33	26	1016	287	99.2
2 d	0.3799	4.75	18.99	19.13	0	1016	249	99.2

Table B-9. UV absorbance measurements and sample data used to determine the cumulative release (%) of progesterone from MIL-101 after each time interval (trial #1).

Time	Absorbance	Conc. (μg/mL)	Sample Conc. (μg/mL)	Starting Conc. (μg/mL)	Amount Released (μg)	Cumulative Release (μg)	Amount Remaining (μg)	Cumulative Release (%)
5 min	0.6613	11.37	45.47	0	682	682	591	63.4
15 min	0.8156	13.85	55.40	39.40	240	922	720	85.7
30 min	0.7578	12.92	51.68	48.02	55	977	672	90.8
45 min	0.6591	11.33	45.33	44.79	8	985	589	91.5
60 min	0.5766	10.00	40.02	39.28	11	996	520	92.6
90 min	0.4980	8.74	34.95	34.68	4	1000	454	92.9
2 h	0.4391	7.79	31.15	30.29	13	1013	405	94.1
3 h	0.3973	7.12	28.47	27.00	22	1035	370	96.2
4 h	0.3519	6.38	25.54	24.67	13	1048	332	97.4
1 d	0.2990	5.53	22.13	22.13	0	1048	288	97.4
2 d	0.2532	4.80	19.18	19.18	0	1048	249	97.4

Table B-10. UV absorbance measurements and sample data used to determine the cumulative release (%) of progesterone from MIL-101 after each time interval (trial #2).

Time	Absorbance	Conc. (μg/mL)	Sample Conc. (μg/mL)	Starting Conc. (μg/mL)	Amount Released (μg)	Cumulative Release (μg)	Amount Remaining (μg)	Cumulative Release (%)
5 min	0.5133	8.98	35.93	0	539	539	467	0
15 min	0.7349	12.55	50.21	31.14	286	825	653	54.1
30 min	0.7562	12.90	51.58	43.51	121	946	671	82.7
45 min	0.6505	11.19	44.77	44.70	1	947	582	94.9
60 min	0.5578	9.70	38.80	38.80	0	947	504	95.0
90 min	0.4785	8.42	33.69	33.63	1	948	438	95.0
2 h	0.4170	7.43	29.73	29.20	8	956	387	95.1
3 h	0.3565	6.46	25.84	25.77	1	957	336	95.9
4 h	0.3113	5.73	22.93	22.39	8	965	298	96.0
1 d	0.2701	5.07	20.27	19.87	6	971	263	96.8
2 d	0.2416	4.61	18.43	17.57	13	984	240	97.4
3 d	0.2065	4.04	16.18	15.98	3	987	210	98.7
4 d	0.1730	3.50	14.02	14.02	0	987	182	99.0

Table B-11. UV absorbance measurements and sample data used to determine the cumulative release (%) of stavudine from MIL-101 after each time interval (trial #1).

Time	Absorbance	Conc. (μg/mL)	Sample Conc. (μg/mL)	Starting Conc. (μg/mL)	Amount Released (μg)	Cumulative Release (μg)	Amount Remaining (μg)	Cumulative Release (%)
5 min	0.6968	12.85	51.39	0	771	771	668	88.0
15 min	0.5800	10.73	42.93	44.53	0	771	582	88.0
30 min	0.5377	9.97	39.86	38.80	16	787	518	89.8
45 min	0.4374	8.15	32.60	34.53	0	787	453	89.8
60 min	0.4017	7.50	30.01	30.20	0	787	393	89.8
90 min	0.3612	6.77	27.07	26.20	13	800	352	91.3
2 h	0.2798	5.29	21.17	23.47	0	800	310	91.3
3 h	0.2787	5.27	21.09	20.67	6	806	274	92.0
4 h	0.2530	4.81	19.23	18.27	14	820	250	93.6
1 d	0.2200	4.21	16.84	16.67	3	823	219	93.9
2 d	0.2001	3.85	15.40	14.60	12	835	200	95.3
3 d	0.1884	3.64	14.55	13.33	18	853	189	97.4
4 d	0.1624	3.17	12.67	12.60	1	854	165	97.5
5 d	0.1420	2.80	11.19	11.00	3	857	146	97.8

Table B-12. UV absorbance measurements and sample data used to determine the cumulative release (%) of stavudine from MIL-101 after each time interval (trial #2).

Time	Absorbance	Conc. (μg/mL)	Sample Conc. (μg/mL)	Starting Conc. (μg/mL)	Amount Released (μg)	Cumulative Release (μg)	Amount Remaining (μg)	Cumulative Release (%)
5 min	0.5828	10.78	43.13	0	647	647	561	71.7
15 min	0.6310	10.88	43.52	37.38	92	739	566	81.9
30 min	0.5668	9.85	39.38	37.71	25	764	512	84.7
45 min	0.4894	8.60	34.40	34.13	4	768	447	85.1
60 min	0.4182	7.45	29.81	29.81	0	768	388	85.1
90 min	0.3648	6.59	26.37	25.84	8	776	343	86.0
2 h	0.3102	5.71	22.85	22.85	0	776	297	86.0
3 h	0.2701	5.07	20.27	19.81	7	783	264	86.8
4 h	0.2458	4.68	18.70	17.57	17	800	243	88.7
1 d	0.2433	4.64	18.54	16.21	35	835	241	92.6
2 d	0.2266	4.37	17.47	16.07	21	856	227	94.9
3 d	0.2039	4.00	16.01	15.14	13	869	208	96.3
4 d	0.1739	3.52	14.07	13.87	3	872	183	96.7
5 d	0.1448	3.05	12.20	12.20	0	872	159	96.7

Table B-13. UV absorbance measurements and sample data used to determine the cumulative release (%) of acetaminophen from SBA-15 after each time interval (trial #1).

Time	Absorbance	Conc. (μg/mL)	Sample Conc. (μg/mL)	Starting Conc. (μg/mL)	Amount Released (μg)	Cumulative Release (μg)	Amount Remaining (μg)	Cumulative Release (%)
5 min	0.9604	11.63	46.53	0	698	698	605	66.3
15 min	1.3087	15.77	63.06	40.33	341	1039	820	98.7
30 min	1.1554	13.95	55.79	54.65	17	1056	725	100.3
45 min	0.9987	12.09	48.35	48.35	0	1056	629	100.3
60 min	0.8628	10.48	41.90	41.90	0	1056	545	100.3
90 min	0.7450	9.08	36.32	36.32	0	1056	472	100.3
2 h	0.6430	7.87	31.47	31.47	0	1056	409	100.3
3 h	0.5546	6.82	27.28	27.28	0	1056	355	100.3
4 h	0.4779	5.91	23.64	23.64	0	1056	307	100.3

Table B-14. UV absorbance measurements and sample data used to determine the cumulative release (%) of acetaminophen from SBA-15 after each time interval (trial #2).

Time	Absorbance	Conc. (μg/mL)	Sample Conc. (μg/mL)	Starting Conc. (μg/mL)	Amount Released (μg)	Cumulative Release (μg)	Amount Remaining (μg)	Cumulative Release (%)
5 min	1.0967	13.25	53.00	0	795	795	689	76.8
15 min	1.2470	15.03	60.13	45.93	213	1008	782	97.4
30 min	1.0949	13.23	52.92	52.12	12	1020	688	98.6
45 min	0.9560	11.58	46.33	45.86	7	1027	602	99.2
60 min	0.8259	10.04	40.15	40.15	0	1027	522	99.2
90 min	0.7130	8.70	34.80	34.80	0	1027	452	99.2
2 h	0.6153	7.54	30.16	30.16	0	1027	392	99.2
3 h	0.5305	6.53	26.14	26.14	0	1027	340	99.2
4 h	0.4571	5.66	22.65	22.65	0	1027	294	99.2

Table B-15. UV absorbance measurements and sample data used to determine the cumulative release (%) of progesterone from SBA-15 after each time interval (trial #1).

Time	Absorbance	Conc. (μg/mL)	Sample Conc. (μg/mL)	Starting Conc. (μg/mL)	Amount Released (μg)	Cumulative Release (μg)	Amount Remaining (μg)	Cumulative Release (%)
5 min	0.3591	6.50	26.00	0	390	390	338	36.6
15 min	0.7089	12.13	48.53	22.53	390	780	631	73.1
30 min	0.7950	13.52	54.08	42.07	180	960	703	90.0
45 min	0.6714	11.53	46.12	46.87	0	960	611	90.0
60 min	0.6192	10.69	42.76	40.73	30	990	555	92.8
90 min	0.5416	9.44	37.76	37.00	11	1001	490	93.8
2 h	0.4887	8.59	34.35	32.67	25	1026	446	96.2
3 h	0.4223	7.52	30.07	29.73	5	1031	391	96.6
4 h	0.3616	6.54	26.16	26.07	1	1032	340	96.7
1 d	0.2980	5.52	22.07	22.67	0	1032	296	96.7

Table B-16. UV absorbance measurements and sample data used to determine the cumulative release (%) of progesterone from SBA-15 after each time interval (trial #2).

Time	Absorbance	Conc. (μg/mL)	Sample Conc. (μg/mL)	Starting Conc. (μg/mL)	Amount Released (μg)	Cumulative Release (μg)	Amount Remaining (μg)	Cumulative Release (%)
5 min	0.4553	8.05	32.20	0	483	483	419	44.5
15 min	0.8140	13.83	55.31	27.91	411	894	719	82.4
30 min	0.7968	13.55	54.20	47.93	94	988	705	91.1
45 min	0.7219	12.34	49.37	46.97	36	1024	642	94.4
60 min	0.6456	11.11	44.46	42.79	25	1049	578	96.7
90 min	0.5649	9.82	39.26	38.53	11	1060	510	97.7
2 h	0.4909	8.62	34.49	34.03	7	1067	448	98.3
3 h	0.4205	7.49	29.96	29.89	1	1068	389	98.4
4 h	0.3585	6.49	25.97	25.97	0	1068	338	98.4
1 d	0.3048	5.63	22.50	22.50	0	1068	293	98.4

Table B-17. UV absorbance measurements and sample data used to determine the cumulative release (%) of stavudine from SBA-15 after each time interval (trial #1).

Time	Absorbance	Conc. (μg/mL)	Sample Conc. (μg/mL)	Starting Conc. (μg/mL)	Amount Released (μg)	Cumulative Release (μg)	Amount Remaining in Solution (μg)	Cumulative Release (%)
5 min	0.4752	8.83	35.33	0	530	530	459	49.8
15 min	0.8707	14.74	58.96	30.62	425	955	766	89.7
30 min	0.7973	13.56	54.23	51.09	47	1002	705	94.1
45 min	0.6850	11.75	47.00	47.00	0	1002	611	94.1
60 min	0.5878	10.18	40.73	40.73	0	1002	530	94.1
90 min	0.5034	8.83	35.30	35.30	0	1002	459	94.1
2 h	0.4304	7.65	30.59	30.59	0	1002	398	94.1
3 h	0.3670	6.63	26.51	26.51	0	1002	345	94.1
4 h	0.3122	5.74	22.98	22.98	0	1002	299	94.1

Table B-18. UV absorbance measurements and sample data used to determine the cumulative release (%) of stavudine from SBA-15 after each time interval (trial #2).

Time	Absorbance	Conc. (μg/mL)	Sample Conc. (μg/mL)	Starting Conc. (μg/mL)	Amount Released (μg)	Cumulative Release (μg)	Amount Remaining (μg)	Cumulative Release (%)
5 min	0.5313	9.85	39.40	0	591	591	512	54.6
15 min	0.9088	15.35	61.41	34.15	409	1000	798	92.3
30 min	0.8335	14.14	56.56	53.22	50	1050	735	97.0
45 min	0.7236	12.37	49.48	49.02	7	1057	643	97.6
60 min	0.6212	10.72	42.89	42.89	0	1057	558	97.6
90 min	0.5324	9.29	37.17	37.17	0	1057	483	97.6
2 h	0.4555	8.05	32.21	32.21	0	1057	419	97.6
3 h	0.3888	6.98	27.92	27.92	0	1057	363	97.6
4 h	0.3310	6.05	24.19	24.19	0	1057	315	97.6